

Transport phenomena in nonitinerant magnets

INAUGURALDISSERTATION

zur

Erlangung der Würde eines Doktors der
Philosophie

vorgelegt der

Philosophisch-Naturwissenschaftlichen Fakultät
der Universität Basel

von

Kevin Alexander van Hoogdalem
aus 's-Gravenhage, Niederlande

Basel, 2013

Originaldokument gespeichert auf dem Dokumentenserver der Universität Basel
edoc.unibas.ch



Dieses Werk ist unter dem Vertrag „Creative Commons Namensnennung-Keine kommerzielle Nutzung-Keine Bearbeitung 2.5 Schweiz“ lizenziert. Die vollständige Lizenz kann unter

creativecommons.org/licences/by-nc-nd/2.5/ch
eingesehen werden.



Namensnennung-Keine kommerzielle Nutzung-Keine Bearbeitung 2.5 Schweiz

Sie dürfen:



das Werk vervielfältigen, verbreiten und öffentlich zugänglich machen

Zu den folgenden Bedingungen:



Namensnennung. Sie müssen den Namen des Autors/Rechteinhabers in der von ihm festgelegten Weise nennen (wodurch aber nicht der Eindruck entstehen darf, Sie oder die Nutzung des Werkes durch Sie würden entlohnt).



Keine kommerzielle Nutzung. Dieses Werk darf nicht für kommerzielle Zwecke verwendet werden.



Keine Bearbeitung. Dieses Werk darf nicht bearbeitet oder in anderer Weise verändert werden.

- Im Falle einer Verbreitung müssen Sie anderen die Lizenzbedingungen, unter welche dieses Werk fällt, mitteilen. Am Einfachsten ist es, einen Link auf diese Seite einzubinden.
- Jede der vorgenannten Bedingungen kann aufgehoben werden, sofern Sie die Einwilligung des Rechteinhabers dazu erhalten.
- Diese Lizenz lässt die Urheberpersönlichkeitsrechte unberührt.

Die gesetzlichen Schranken des Urheberrechts bleiben hiervon unberührt.

Die Commons Deed ist eine Zusammenfassung des Lizenzvertrags in allgemeinverständlicher Sprache: <http://creativecommons.org/licenses/by-nc-nd/2.5/ch/legalcode.de>

Haftungsausschluss:

Die Commons Deed ist kein Lizenzvertrag. Sie ist lediglich ein Referenztext, der den zugrundeliegenden Lizenzvertrag übersichtlich und in allgemeinverständlicher Sprache wiedergibt. Die Deed selbst entfaltet keine juristische Wirkung und erscheint im eigentlichen Lizenzvertrag nicht. Creative Commons ist keine Rechtsanwalts-gesellschaft und leistet keine Rechtsberatung. Die Weitergabe und Verlinkung des Commons Deeds führt zu keinem Mandatsverhältnis.

Genehmigt von der Philosophisch-Naturwissenschaftlichen
Fakultät auf Antrag von

Prof. Dr. Daniel Loss

Prof. Dr. Pascal Simon

Basel, den 16. Oktober 2012

Prof. Dr. J. Schibler
Dekan

Summary

Traditionally, the role of information carrier in spin- and electronic devices is taken by respectively the spin or the charge of the conduction electrons in the system. In recent years, however, there has been an increasing awareness that spin excitations in insulating magnets (either magnons or spinons) may offer an interesting alternative to this paradigm. One of the advantageous properties of these excitations is that they are not subject to Joule heating. Hence, the energy associated with the transport of a single unit of information carried by a magnon- or spinon current could be much lower in such insulating magnets. Additionally, the bosonic nature of the magnon quasi-particles may be advantageous.

Three crucial requirements for the successful implementation of spintronics in insulating magnets are the ability to create, detect, and control a magnon- or spinon current. The topic of creation and read-out of such currents in insulating magnets has been discussed elsewhere, in this thesis we will mainly focus on the third requirement, that of the ability to control magnon- and spinon currents.

In the first part of this thesis we aim to draw a parallel between spintronics in nonitinerant systems and traditional electronics. We do this by considering the question to which extent it is possible to create the analog of the different elements that are used in electronics for magnetic excitations in insulating magnets. To this end, we consider (in Ch. 2 and 3 respectively) rectification effects and finite-frequency transport in one-dimensional (1D) antiferromagnetic spin chains. We mainly focus our attention on the effects of impurities, which are modeled by local changes in the exchange interaction of the underlying Hamiltonian. Using methods from quantum field theory, which include renormalization group analysis and functional field integration, we determine the effect of such impurities on the transport properties of the spin chains. Our findings allow us to propose systems which behave as a diode and a capacitance for the magnetic excitations. In Ch. 4 we introduce a setup which behaves as a transistor for either magnons or spinons: a triangu-

lar molecular magnet, which is weakly exchange-coupled to nonitinerant spin reservoirs. We use the possibility to control the state of triangular molecular magnets by either electric or magnetic fields to affect tunneling of magnons or spinons between the two spin reservoirs.

The second part of this thesis is devoted to the study of thermal transport in two-dimensional (2D) nonitinerant ferromagnets with a noncollinear ground state magnetization. More specifically, our interest is in thermal Hall effects. Such effects can be used to control a magnetization current, and arise because the magnons (which carry the thermal current) experience a fictitious magnetic field due to the equilibrium magnetization texture. We consider the different magnetic textures that occur in ferromagnets with spin-orbit interaction, and discuss which of them give rise to a finite thermal Hall conductivity.

Acknowledgements

The work presented in this thesis would not have been possible without the support of several people.

First of all, I would like to thank my supervisor Daniel Loss for accepting me as a PhD student. His knowledge, insight, and the originality of his ideas have benefitted and motivated me throughout the last four years, and I will remember his enthusiasm and the trust he bestowed upon me warmly. Furthermore, I am grateful for his continued efforts to make the theoretical condensed matter group not only a stimulating research environment, but also a place where people feel at home.

I would also like to thank my collaborator Yaroslav Tserkovnyak for sharing with me his knowledge on a wide variety of subjects, as well as his contagious enthusiasm. I am grateful to Pascal Simon for being co-referee.

My time in Basel has been interesting and enjoyable, for which I have to thank the group members and regular visitors of the condensed matter theory group, many of whom I consider friends rather than colleagues. My thanks go out to Samuel Aldana, Daniel Becker, Massoud Borhani, Dan Bohr, Bernd Braunecker, Christoph Bruder, Stefano Chesi, Charles Doiron, Mathias Duckheim, Carlos Egues, Gerson Ferreira, Jan Fischer, Suhas Gangadharaiah, Adrian Hutter, Daniel Klauser, Jelena Klinovaja, Christoph Klöffel, Viktoriia Kornich, Verena Körting, Jörg Lehmann, Franziska Maier, Dmitrii Maslov, Tobias Meng, Andreas Nunnenkamp, Christoph Orth, Fabio Pedrocchi, Diego Rainis, Hugo Ribeiro, Maximilian Rink, Beat Röthlisberger, Arijit Saha, Manuel Schmidt, Thomas Schmidt, Peter Stano, Dimitrije Stepanenko, Vladimir M. Stojanovic, Grégory Strübi, Rakesh Tiwari, Björn Trauzettel, Mircea Trif, Luka Trifunovic, Filippo Troiani, Oleksandr Tsyplatyev, Andreas Wagner, Stefan Walter, Ying-Dan Wang, James Wootton, Robert Zak, Robert Zielke, and Alexander Zyuzin.

Finally, I would like to thank Martha and my family for their support.

Contents

Contents	ix
1 Introduction	1
1.1 History of magnetism	1
1.2 Spintronics	4
1.3 Theory of magnetic materials	6
1.4 Outline	9
I Spin transport in low-dimensional systems	
2 Rectification effects	13
2.1 Introduction	13
2.2 System and model	15
2.3 Ferromagnetic spin chains: spin wave formalism	17
2.4 AF spin chains: Luttinger liquid formalism	19
2.5 Renormalization group treatment	25
2.6 Enhanced anisotropy	27
2.7 Suppressed anisotropy	28
2.8 Estimate of rectification currents	31
2.9 Experimental realizations	35
2.10 Conclusions	37
3 Finite-frequency response	39
3.1 Introduction	39
3.2 System and model	40
3.3 Finite-frequency spin conductance	43
3.4 Results	46
3.5 Conclusions	49
4 Transistor behavior	51

4.1	Introduction	51
4.2	System	53
4.3	Transition rates and spin current	56
4.4	Transistor behavior	62
4.5	Experimental realizations	63
4.6	Discussions	67
4.7	Conclusions	68
II Thermal transport in textured ferromagnets		
5	Thermal Hall effects	71
5.1	Introduction	71
5.2	Magnons in the presence of magnetic texture	73
5.3	Textured ground states	76
5.4	Thermal Hall conductivity of the skyrmion lattice	80
5.5	Conclusions	86
Appendix		
A	Determining Luttinger Liquid parameters from the non-linear sigma model.	91
B	Calculation of the magnetization current in the Keldysh formalism	93
C	Correlators	97
Bibliography		99

Introduction

We begin this chapter by giving a brief historic introduction to magnetism. Starting with Thales of Miletus, we address some of the most important persons and milestones in its history. Next, we give an introduction to spintronics, the field of spin-based electronics. Specifically, we focus on spintronics in nonitinerant magnets. Lastly, we give some theoretical background information on the most important models used in this thesis.

1.1 History of magnetism

The history of magnetism is a long and rich one. Probably the first written reference to a magnetic phenomenon dates back to the sixth century BC, and is due to Thales of Miletus. [1] Thales was an early Greek philosopher, who described the attraction between lodestone and iron.

The most interesting myth regarding the origin of the name magnet is due to the Roman scholar Gaius Plinius Secundus, or Pliny the Elder. [2] According to the story, there was once a Greek shepherd named Magnes, whose iron soles (or staff, depending on who tells the story) on many an occasion became stuck on the rocks in his native land. The rocks, naturally, were rich in lodestone. An explanation that is possibly closer to the truth, is that the name finds its origin in the Magnesia region, a place where naturally magnetic ore is abundant.

Already around the time of the start of the Gregorian calendar, there were attempts to describe magnetic phenomena on a more or less scien-

tific basis. One famous work is due to Lucretius. His poem 'De Rerum Natura' (On the Nature of Things) was inspired by the work of Epicurus, who was himself a follower of Democritus. The latter is well-known as the joint inventor of an atomic theory for the universe, together with his mentor Leucippus. Hence, Lucretius' attempt to describe the action of a magnet on iron relies on atomic theory: [2]

First, from the Magnet num'rous Parts arise.
And swiftly move; the Stone gives vast supplies;
Which, springing still in Constant Stream, displace
The neighb'ring air and make an empty Space;
So when the Steel comes there, some Parts begin
To leaps on through the Void and enter in...
The steel will move to seek the Stone's embrace,
Or up or down, or t'any other place
Which way soever lies the Empty Space.

After the initial attempts of the Roman scholars to explain magnetism, things quieted down as the dark ages came and went. The next milestone in the field of magnetism (setting aside the introduction of the compass) occurred only around 1600, and can be ascribed to William Gilbert, [2] an English physician, physicist and natural philosopher, who lived from 1544 to 1603. Gilbert conducted many experiments on both electricity and magnetism, perhaps the most famous of which were on his terrella: a small magnetized ball, which acts as a model for the earth. From his experiments, he concluded that the earth itself must be a magnet. These, and many other of his findings, were published in his magnum opus, 'De Magnete', in 1600. [3] Maybe even more important than his discoveries themselves, was the way in which he proceeded to make them. Unlike many natural philosophers before him, who were content to take known knowledge and try to expand the knowledge by philosophical means, he tried to expand the known knowledge by systematic experimental means. In this respect, Gilbert was genuinely a child of his time.

Around the start of the nineteenth century, the development of the theory of electromagnetism as we know it today started. [4] In 1819, the Danish scientist Hans Christian Ørsted discovered that a wire that carries an electric current deflects a nearby magnetic compass, thereby establishing that an electric current produces a magnetic field. Shortly thereafter, in 1820, André-Marie Ampère extended Ørsted's work by performing experiments that gave rise to his discovery of Ampère's law, which relates the line integral of the magnetic field around a surface to the current

through that surface. At roughly the same time, Jean-Baptiste Biot and Félix Savart discovered their Biot-Savart law, which gives the magnetic field for a given current distribution.

Up to this point, the experiments were on static phenomena. This changed when Faraday discovered electromagnetic induction in 1831: a magnetic field that is changing in time gives rise to an electric field. By now, we are firmly in the realm of the central set of equations in electrodynamics: Maxwell's equations. This set of 4 vector equations (Ampère's law with Maxwell's correction, Gauss' law, Gauss' law of magnetism, and Faraday's law), together with the Lorentz force law and Newton's second law fully describes the behavior of a charged particle in a classical electromagnetic field. [4]

Even though Maxwell's equations fully describe the classical behavior of charged particles in an electromagnetic field, they do not give an explanation for the existence of magnetic ordering in solids. In other words, they do not explain the ordering of the net magnetic moments of the constituents of a solid, be they atoms or ions. In fact, according to the Bohr-van Leeuwen theorem, [2] the expectation value of the magnetization of a collection of classical non-relativistic charged particles is identically zero at any finite temperature. Instead, the explanation of magnetic ordering requires quantum mechanics. The magnetic moment of atoms or ions can originate both from the spin of the electrons as well as from their orbital motion. When two electrons have overlapping wave functions, their magnetic moments are coupled due to exchange interaction. The origin of exchange interaction lies in the fact that Pauli's exclusion principle puts strong constraints on the quantum numbers (and hence on the magnetic moment) of overlapping wave functions. We will explain the origin of exchange interaction in more detail in Sec. 1.3.

Applications of magnetism

Today, magnetic phenomena have found a plethora of applications in many branches of society. We have already mentioned what was arguably the first technological invention which involved magnetism, the compass. This device was especially crucial for the development of maritime navigation. Among the most important modern applications of magnetism are those in medicine (for instance in Magnetic Resonance Imaging) and information storage (where the most famous example is Magnetoresistive Random-Access Memory). This thesis, however, focuses on a different application of magnetism, namely spintronics.

1.2 Spintronics

Spintronics [5] is the field of spin-based electronics. Unlike in traditional electronics, where information is carried by charge, in spintronics the spin degree of freedom is taken as the carrier of information. Spintronics in metallic devices has its origin in 1988, when the giant magnetoresistance (GMR) effect was discovered independently by two different research groups. [6, 7] In 2007, the Noble prize in physics was awarded to Albert Fert and Peter Grünberg for this discovery. The GMR effect is observed in multilayer materials consisting of alternating ferromagnetic and non-magnetic metallic layers. A large decrease in electric conductance is measured when the alternating ferromagnetic layers are switched from a parallel- to an anti-parallel orientation. This effect can be understood by considering the fact that the electric current is made up of two contributions, a current of spin-up electrons and one of spin-down electrons, both of which have a magnetization-dependent conductance. Present-day magnetic storage devices (MRAMs) are based on the TMR effect, an effect closely related to the GMR effect.

Spintronics in semiconductors can be traced back to the proposal by Datta and Das for a spin field-effect transistor. [8] The use of semiconductors offers several advantages compared to metallic devices. [9, 10] Perhaps most notable is the fact that strong spin-orbit interaction in semiconductors in principle opens up possibilities of electric control of spintronic devices. [11] Furthermore, it has been shown to be possible to electrically control the Curie temperature [12] and coercive field [13] of ferromagnetic semiconductors. Lastly, the sheer enormity of the semiconductor electronics industry can be seen as an incentive to consider spintronics in semiconducting materials.

From a practical point of view, the wide-spread interest in spintronic devices arises from the fact that they are considered to have certain favorable properties compared to electronic devices. Indeed, one of the main issues in modern electronics is that as devices get ever smaller the removal of waste energy generated by Joule heating (which is in turn caused by the scattering of the information carrying conduction electrons) becomes problematic. In principle, one of the main potential advantages of spin-based devices in comparison to their charge-based counterparts is the anticipated lower energy dissipation associated with performing logical operations and transporting the information carriers. However, this advantage is strongly reduced by the fact that schemes for spin-based devices in metallic- and semiconducting materials rely on spin currents that are generated as a by-product of associated charge cur-

rents. [5, 9, 10]

Spintronics in nonitinerant (insulating) materials does not suffer from this deficiency. Indeed, there is virtually no transport of charge in nonitinerant materials at all. Nevertheless, since the spin states of the different constituents are coupled via exchange interaction, information about the spin state can still propagate through the system. As a consequence, magnetization can be transported by magnons (spin waves) or spinons (domain walls), without any transport of charge, in such systems. Since charge transport is absent in such materials, the energy that is dissipated in the transport of a single information carrier (a spin) in a nonitinerant system can be much lower [14] than in both itinerant electronic- and spintronic devices. [15, 16] Furthermore, it has been theoretically shown that the energy required for a single logic operation can be low in a spin-based device. [17] We mention here also the fact that this type of ballistic transport in magnetic systems is not the only kind of nearly dissipationless spin transport. Other systems which have received wide attention recently are topological insulators, [18] where in particular edge states in a quantum spin Hall insulator have been predicted to be dissipationless. [19] For an overview of other possibilities see a recent review by Sonin. [20]

Clearly, energy considerations are not the only factor that play a role in the determination of the feasibility of spintronics in nonitinerant materials. Other important considerations are the working principle and operating speed of potential devices, and the possibility of creation, control, and read-out of the signals used in these systems. Spin pumping has been proposed as a method to create a pure spin current in nonitinerant systems. [21] Creation of a magnon current has been shown to be possible by means of the spin Seebeck effect, [22] and with high spatial accuracy by means of laser-controlled local temperature gradients. [23] The resulting spin current can be measured utilizing the inverse spin Hall effect. [24, 25] It has also been shown that, using the spin Hall effect, it is possible to convert an electric signal in a metal into a spin wave, which can then be transmitted into an insulator. [24]

Logic schemes that are based on interference of spin waves in insulating magnets have been proposed. [26, 27] In these schemes, the dispersion relation of the spin waves can be controlled either by magnetic fields, magnetic textures, [28, 29] electric fields due to the induced Aharonov-Casher phase [30] or in multiferroic materials, [31, 32] or spin-orbit coupling. [33]

Likewise, much of the work in this thesis is motivated by the wish to successfully implement spintronics using spinons and magnons in non-

itinerant magnets. In the first part of this thesis, in Ch. 2, 3, and 4, we introduce systems which behave as the spintronic elements which mimic the working of some of the most important elements used in conventional electronics: the diode, the capacitance, and the transistor. Specifically, the transistor in Ch. 4 allows to perform arbitrary logic operations using magnetic excitations in insulating magnets. In the second part of this thesis, in Ch. 5, we study thermal Hall effects in nonitinerant ferromagnets. From a practical point of view, such effects are interesting because they allow one to control spin currents.

1.3 Theory of magnetic materials

In the first part of this thesis we will often consider insulating antiferromagnetic 1D spin-1/2 systems. We will see that such systems must be analyzed using a fully quantum mechanical description, which is most conveniently based on the Heisenberg Hamiltonian. In contrast, when considering thermal Hall effects in Ch. 5, we will be interested in describing bulk ferromagnetic systems with a macroscopic magnetization $\mathbf{M}(\mathbf{r})$. In this case, since the macroscopic magnetization is a classical object, a phenomenological description suffices. To gain some more insight into these different models, we will discuss the origin of the Heisenberg model and the phenomenological description here.

The Heisenberg Hamiltonian

In Ch. 2, 3, and 4 we will typically use the anisotropic Heisenberg Hamiltonian as the starting point of our analysis of transport phenomena in 1D insulating magnets

$$H = \sum_{\langle ij \rangle} J_{ij} [S_i^x S_j^x + S_i^y S_j^y + \Delta_{ij} S_i^z S_j^z]. \quad (1.1)$$

Here, the summation is over nearest neighbors, and we avoid double counting of the bonds. Furthermore, S_i^α is the α -component of the spin-1/2 operator at position \mathbf{r}_i , with $\alpha = x, y, z$. The different components of the spin operator satisfy the usual commutation relations

$$[S_j^\alpha, S_j^\beta] = i\hbar \epsilon_{\alpha\beta\gamma} S_j^\gamma, \quad (1.2)$$

and spin operators at different positions commute. Furthermore, J_{ij} denotes the strength of the exchange interaction between the two nearest

neighbors at \mathbf{r}_i and \mathbf{r}_j . For constant $J_{ij} < 0$ the system is ferromagnetic (FM), meaning that neighboring spins wish to align in a parallel manner; For constant $J_{ij} > 0$ the system is antiferromagnetic (AF), and neighboring spins tend to antiparallel alignment. The magnetic properties of the system described by Eq. (1.1) depend strongly on the value of the anisotropy Δ_{ij} . For constant anisotropy $\Delta_{ij} = \Delta > 1$, the system has an easy axis along the z axis, so that any magnetic order will preferably be along this axis. In the limit $\Delta \gg 1$ the system is described by the famous Ising model. For $0 < \Delta < 1$, the magnetization is preferably in plane, since the system has the xy plane as its easy plane. This regime is often called the xy -limit. For $\Delta = 1$, Eq. (1.1) describes the rotationally invariant isotropic Heisenberg Hamiltonian. Even though we use Eq. (1.1) as the starting point of our calculations, a tremendous amount of work has gone into the justification of this equation over the last decades. We will therefore devote this section to giving a very brief introduction to the origin of Eq. (1.1) for insulating magnets.

Exchange interaction in insulating materials can be explained by the superexchange mechanism. First proposed by Anderson in 1959, [34] this mechanism also gives a microscopic explanation for the fact that many insulating materials can be described by the AF isotropic Heisenberg Hamiltonian. Superexchange processes are important in magnets in which direct exchange is suppressed due to the limited overlap of the wave functions of the localized electrons on the magnetic ions. [35] Instead, interaction between two magnetic ions is mediated by a non-magnetic ion. To explain superexchange, Anderson considered the question which spin-dependent interactions can originate from electronic interactions between different localized d - or f -shell electrons in an insulator (the wave functions are adapted to the underlying lattice, and hence contain an admixture of the electron wave function on the non-magnetic ions). His most important observation was that the system can gain a small amount of energy due to virtual hopping of localized electrons between the two neighboring magnetic ions. Due to the Pauli exclusion principle, this hopping can only take place when the unpaired electrons on the two neighboring ions have opposite spin. Hence, the resulting isotropic spin-interaction is of antiferromagnetic character. His observation that such superexchange processes determine the magnetic properties of insulators explains the fact that most known insulating magnets are of an antiferromagnetic nature.

One possible origin of anisotropy in the Heisenberg Hamiltonian is spin-orbit interaction. As we will see, the presence of this interaction can lead to the so-called Dzyaloshinskii-Moriya (DM) interaction term. This

term has to be added to the isotropic Heisenberg Hamiltonian

$$H_{\text{DM}} = \sum_{\langle ij \rangle} J'_{ij} \mathbf{S}_i \cdot \mathbf{S}_j + \mathbf{D}_{ij} \cdot (\mathbf{S}_i \times \mathbf{S}_j). \quad (1.3)$$

The fact that the DM interaction term has to occur generally in the Hamiltonian of magnets that lack inversion symmetry was first realized by Dzyaloshinskii, [36] who used a phenomenological approach to derive its form. The microscopic explanation was given by Moriya [37] and, as we mentioned before, is based on the addition of spin-orbit interaction to Anderson's model. The mapping of Eq. (1.3) on the anisotropic model is done by performing a rotation in spin space. Assuming that $\mathbf{D}_{ij} = D\hat{z}$ and $J'_{ij} = J'$, the rotation is implemented by rewriting Eq. (1.3) in terms of the new operators

$$\begin{aligned} \tilde{S}_j^+ &= e^{i\theta j} S_j^+, \\ \tilde{S}_j^- &= e^{-i\theta j} S_j^-, \\ \tilde{S}_j^z &= S_j^z. \end{aligned} \quad (1.4)$$

Here, $\theta = \text{atan}(D/J')$, and the spin-ladder operators are defined as $S_j^+ = (S_j^x + iS_j^y)$ and $S_j^- = (S_j^x - iS_j^y)$. With these definitions, the Hamiltonian in terms of the new spin operators (now written without tilde) becomes Eq. (1.1) with parameters $J = \sqrt{J'^2 + D^2}$ and $\Delta = J'/\sqrt{J'^2 + D^2}$.

Another possible source of anisotropy is magnetic dipole-dipole interaction. [35] To see how this interaction can lead to anisotropy, let us consider the interaction between two magnetic dipoles with respective magnetic moments $\mathbf{m}_1 = g\mu_B \mathbf{S}_1$ (located at the origin) and $\mathbf{m}_2 = g\mu_B \mathbf{S}_2$ (located at position \mathbf{r}). The magnetic field at the position \mathbf{r} due to the dipole moment \mathbf{m}_1 is

$$\mathbf{B}_{\text{dip}}(\mathbf{r}) = \frac{\mu_0}{4\pi} \frac{3(\mathbf{m}_1 \cdot \hat{\mathbf{r}})\hat{\mathbf{r}} - \mathbf{m}_1}{r^3}. \quad (1.5)$$

Here, $\mu_0 = 4\pi \cdot 10^{-7} \text{ N A}^{-2}$, is the permeability of vacuum. Also, $\hat{\mathbf{r}} = \mathbf{r}/r$, with $r = |\mathbf{r}|$. Since the energy of a magnetic dipole in a magnetic field is given by $U = -\mathbf{m} \cdot \mathbf{B}$, the interaction energy depends on the angle between \mathbf{r} and the two magnetic moments. For instance, when $\hat{\mathbf{r}} = \hat{\mathbf{z}}$, the dipole-dipole interaction leads to an additional term $\propto S_1^z S_2^z$. We note that, even though the magnitude of the dipole-dipole interaction term is typically much smaller than that of the exchange interaction, the latter decays exponentially with distance, whereas the former decays as $1/r^3$. Therefore, dipole-dipole interactions can become important for materials with relatively large interatomic spacing.

Phenomenologic description

The Heisenberg model is inherently a quantum mechanical model. This is due to the fact that the individual magnetic moments are quantum mechanical objects. However, when one is interested in describing the macroscopic magnetization $\mathbf{M}(\mathbf{r})$ of a material, the quantum mechanical nature of the individual magnetic moments is irrelevant. In this scenario, one can work with a phenomenological description. The description we will introduce here is valid for ferromagnets, although similar models exist for antiferromagnetic materials.

To illustrate the mechanism, we will first consider ferromagnets with isotropic exchange interaction. At temperatures far below the Curie temperature, the free energy of such an isotropic ferromagnet is minimized through the alignment of all magnetic moments, such that the equilibrium magnetization is uniform. This alignment occurs in an arbitrary direction, and is an example of the spontaneous breaking of a continuous symmetry, in this case the spin-rotational symmetry. The classical gapless low-energy excitations of the system are called spin waves. These correspond to long-wavelength rotations of the magnetization $\mathbf{M}(\mathbf{r})$ around its equilibrium value, and are the Goldstone modes related to the breaking of the spin-rotational invariance of the Hamiltonian. Indeed, due to this symmetry, such rotations with an infinite wavelength cannot require any energy. Furthermore, it can easily be shown that when the deviation from the equilibrium magnetization is small, the magnetization of the spin waves is perpendicular to the equilibrium magnetization, and their time-evolution can be described by the Landau-Lifshitz-Gilbert equation. [38]

1.4 Outline

This work is organized as follows. In the first part of this thesis, we focus mainly on transport of magnetic excitations in low-dimensional non-itinerant systems. In Ch. 2 we study rectification effects in both ferromagnetic and antiferromagnetic insulating magnets. We find a variety of possible realizations of systems that display a nonzero rectification current. In Ch. 3 we analyze finite-frequency spin transport in nonitinerant 1D spin chains. We propose a system that behaves as a capacitor for the spin degree of freedom. In Ch. 4 we consider a magnon- and spinon-transistor, which uses the possibility to control the state of triangular molecular magnets by either electric or magnetic fields to affect

tunneling of magnons or spinons between two spin reservoirs.

In the second part of this thesis we consider thermal transport in textured ferromagnets. We investigate how fictitious magnetic fields due to a noncollinear equilibrium magnetic texture (the texture itself is caused by spin-orbit interaction) lead to thermal Hall effects in 2D insulating ferromagnets. We consider the different ground states in the phase diagram of a 2D ferromagnet with spin-orbit interaction: the spiral state and the skyrmion lattice. We find that thermal Hall effects can occur in certain domain walls as well as the skyrmion lattice.

Part I

Spin transport in low-dimensional systems

CHAPTER 2

Rectification effects

Adapted from:
K. A. van Hoogdalem and D. Loss,
“Rectification of spin currents in spin chains”,
Phys. Rev. B **84**, 024402 (2011).

In this chapter, we study magnetization transport in nonitinerant 1D quantum spin chains. Motivated by possible applications in spintronics, we consider rectification effects in both ferromagnetic and antiferromagnetic systems. We find that the crucial ingredients in designing a system that displays a nonzero rectification current are an anisotropy in the exchange interaction of the spin chain combined with an offset magnetic field. For both ferromagnetic and antiferromagnetic systems we can exploit the gap in the excitation spectrum that is created by a bulk anisotropy to obtain a measurable rectification effect at realistic magnetic fields. For antiferromagnetic systems we also find that we can achieve a similar effect by introducing a magnetic impurity, obtained by altering two neighboring bonds in the spin Hamiltonian.

2.1 Introduction

The focus of the present chapter lies on transport of spin excitations in nonitinerant 1D quantum systems (spin chains). More specifically, we investigate rectification effects in such spin systems. Our motivation to do so lies therein that such effects form the basis for a device crucial to spin-

and electronics, the diode. In charge transport, rectification effects in mesoscopic systems have received considerable attention in recent years, both in 1D [39, 40, 41, 42] and higher dimensional systems. [43, 44, 45] However, these studies have so far been limited to the itinerant electronic case. Here, we consider insulating spin chains (without itinerant charge carriers) and study the analog of such rectification effects in the transport of magnetization, see Fig. 2.1.

The magnetic systems we consider are assumed to have an anisotropy Δ in the z direction in the exchange interaction between neighboring spins in the spin chain. Together with an offset magnetic field applied to the entire system, also in the z direction, this anisotropy will allow us to design systems that display a nonzero rectification effect. We consider both ferro- and antiferromagnetic systems, using respectively a spin wave and a Luttinger liquid description. For both types of magnetic order we find that an enhanced exchange interaction in the z direction gives rise to the opening of a gap in the excitation spectrum of the spin chain. We can use the offset magnetic field to tune the system to just below the lower edge of the gap, so that we get the asymmetry in the magnetization current between positive and negative magnetic field gradients ΔB required to achieve a nonzero rectification current. We find here that larger values of the exchange interaction J or the exchange anisotropy Δ lead to a larger gap, and hence require stronger magnetic fields.

For the case of antiferromagnetic order we also discuss the case of suppressed exchange interaction in the z direction. As it turns out, in this case we need an extra ingredient to achieve a sizable rectification effect. Here the extra is a 'site impurity', a local change in the exchange anisotropy, which models the substitution of a single atom in the spin chain. We find that, in the presence of the offset magnetic field, the leading term in the perturbation caused by such an impurity flows - in a renormalization group sense- to strong coupling for low energies. We can therefore, again in combination with the offset magnetic field, use it to achieve the rectification effect. In the regime where our calculations are valid, we find that the rectification current is quadratic in the strength of the impurity, and behaves as a negative power of $(\Delta B/J)$. The dependence of the rectification current on the anisotropy Δ is more complicated, and described in detail in section 2.8.

This chapter is organized as follows. In Section 2.2 we introduce our model, in Section 2.3 we discuss the rectification effect for ferromagnetic systems using the spin wave formalism. In Section 2.4 we map the antiferromagnetic (AF) Heisenberg Hamiltonian on the Luttinger Liquid model and describe the different perturbations resulting from the

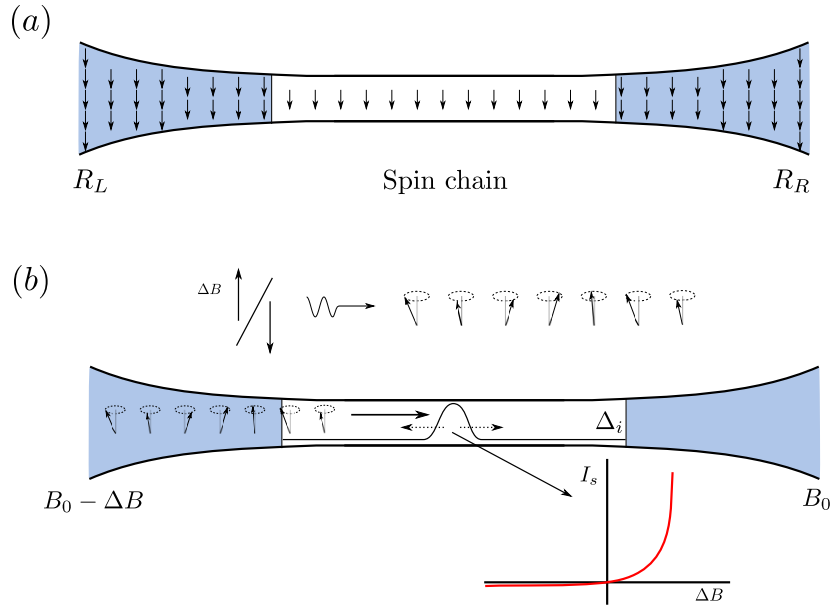


Figure 2.1: (a) Schematic view of the nonitinerant spin system. The 1D spin chain is adiabatically connected (see text) to two spin reservoirs. (b) A magnetic field gradient ΔB gives rise to transport of magnetization through the spin chain, *e.g.* via spin waves. Depending on the anisotropy in the exchange interaction Δ_i in the spin chain [see Eq. (2.1)], part of the magnetization current can be reflected. In a rectifying system, the magnitude of the magnetization current through the system depends on the sign of ΔB .

anisotropic exchange anisotropy in the presence of the offset magnetic field. We then continue in Section 2.5 with a renormalization group analysis to find the most relevant perturbations. In Section 2.6 we focus on the case of enhanced exchange anisotropy and find the resulting rectification effect. Section 2.7 contains the analysis for a suppressed exchange anisotropy in combination with the site impurity, and in Section 2.8 we give numerical estimates of the rectification effect for the latter system. Finally, in Sec. 2.9 we will discuss some experimental realization of quasi-1D insulating magnets.

2.2 System and model

The system we consider consists of a 1D spin chain of length L , adiabatically connected (see below) to two three-dimensional (3D) spin reser-

voirs. This system is described by the anisotropic Heisenberg Hamiltonian

$$H = \sum_{\langle ij \rangle} J_{ij} [S_i^x S_j^x + S_i^y S_j^y + \Delta_{ij} S_i^z S_j^z] + g\mu_B \sum_i B_i S_i^z. \quad (2.1)$$

Here $\langle ij \rangle$ denotes summation over nearest neighbors, and we count each bond between nearest neighbors only once. S_i^α is the α -component of the spin operator at position \mathbf{r}_i . J_{ij} denotes the exchange coupling between the two nearest neighbors at \mathbf{r}_i and \mathbf{r}_j . The non-negative variable Δ_{ij} is the anisotropy in the exchange coupling. Regarding the ground state of the spin chain, assuming Δ_{ij} to be constant, we can distinguish two different classes of ground states in the absence of an external magnetic field, depending on the sign of the exchange coupling J_{ij} . For constant $J_{ij} < 0$ the spin chain has a ferromagnetic ground state and we can describe its low-energy properties within the spin wave formalism. For constant $J_{ij} > 0$ the ground state is antiferromagnetic, and, in principle, we can determine the full excitation spectrum using Bethe-Ansatz methods. [46] However, given the complexity of the resulting solution it is convenient to use a different approach and describe the system and its low-lying excitations using inhomogeneous Luttinger Liquid theory, which is what we will do in this chapter.

We will study two different scenarios for the exchange interaction in the spin chain. In the first scenario we assume

$$\Delta_{ij} = \Delta > 1. \quad (2.2)$$

In general, such a constant anisotropy in the spin chain will open a gap in the excitation spectrum, which we can use to design a system that displays a nonzero rectification effect. Furthermore, it will turn out that when the constant Δ satisfies $0 < \Delta < 1$ we need a spatially varying Δ_{ij} to achieve a sizable rectification effect. Therefore, in the second scenario we will consider a site impurity at position \mathbf{r}_{i_0} . This perturbation, in which two adjacent bonds are altered, describes the replacement of a single atom in the spin chain. It can be modeled as

$$\Delta_{ij} = \Delta + \Delta' \delta_{i,j-1} (\delta_{i,i_0} + \delta_{i,i_0+1}) \quad \text{and} \quad \Delta < 1. \quad (2.3)$$

Here $\delta_{i,j}$ is the Kronecker delta function.

The last term in the Hamiltonian (2.1) is the Zeeman coupling caused by an external, possibly spatially varying, magnetic field $\mathbf{B}_i = B_i \mathbf{z}$ (where \mathbf{z} is a unit vector). This term defines the z axis as the quantization axis of the spin. In all the cases that we will consider the total magnetic

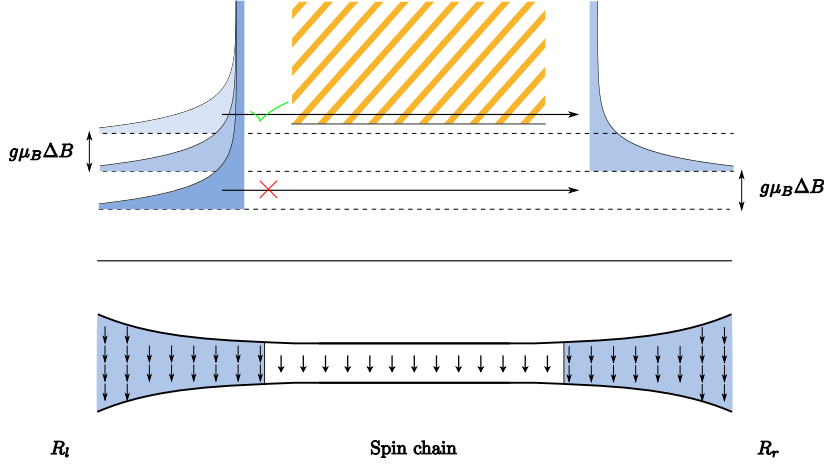


Figure 2.2: Schematic view of the system under consideration (bottom) and the band structure for the ferromagnetic exchange interaction (top). The colored areas on the left and right in the top picture depict the filled states in the reservoirs. The position of the bottom of the band in the left reservoir depends on ΔB . The striped area in the middle denotes the band of allowed states in the spin chain. It is seen that magnetization transport through the spin chain can be large for $\Delta B < 0$, but only small for $\Delta B > 0$

field B_i can be split into a constant part and a spatially varying part, $B_i = B_0 + \Delta B_i$. Here the constant offset magnetic field $B_0 > 0$ is applied to the spin chain and the two reservoirs. ΔB_i is constant and equal to $-\Delta B$ in the left reservoir and goes to zero in the contact region between the left reservoir and the spin chain. The extra minus-sign has been included to ensure that a positive ΔB yields a positive magnetization current. We now define a rectifying system as a system in which the magnetization current $I_m(\Delta B)$ satisfies $I_m(\Delta B) \neq -I_m(-\Delta B)$, see also Figure 2.1. To quantify the amount of rectification, we use the rectification current $I_r(\Delta B)$, defined as

$$I_r(\Delta B) = \frac{I_m(\Delta B) + I_m(-\Delta B)}{2}. \quad (2.4)$$

2.3 Ferromagnetic spin chains: spin wave formalism

To illustrate the mechanism behind the rectification effect we first consider a ferromagnetic spin chain with constant anisotropic exchange in-

interaction in the z direction [$J_{ij} = J < 0$ and $\Delta_{ij} = \Delta > 1$ in Eq. (2.1)]. The spin chain is adiabatically connected (see below) to two 3D ferromagnetic reservoirs R_L and R_R (see Fig. 2.1) and we assume initially that only the constant magnetic field B_0 is present. For temperatures $T \ll g\mu_B/k_B$ the density of spin-excitations is low, which allows us to use the Holstein-Primakoff transformation to map the Heisenberg Hamiltonian on a set of independent harmonic oscillators. [2] In the presence of a constant magnetic field B_0 and a nonzero anisotropy Δ the excitation spectrum of the magnons, the bosonic excitations of the system, has the following form

$$\hbar\omega_k = g\mu_B B_0 + 2(\Delta - 1)|J|s + |J|s(ka)^2, \quad (2.5)$$

with a the distance between nearest-neighbor spins and s the magnitude of a single spin. The magnons have magnetic moment $-|g|\mu_B \mathbf{z}$. The magnon distribution is given by the Bose-Einstein distribution $n_B(\omega_k)$. In order for the spin chain and reservoirs to be adiabatically connected, the length of the transition region L_t between spin chain and reservoir must be much larger than the typical wavelength of the excitations. From Eq. 2.5 we can now see that for ferromagnets this requirement becomes $L_t \gg 2\pi\sqrt{Js/g\mu_B B_0}a$ (we ignore the anisotropy in this estimate). For $Js = 10k_B J$, $B_0 = 0.5$ T the requirement amounts to $L_t \gg 25a$.

From Eq. (2.5) it follows that magnons in the spin chain require a minimum energy of $g\mu_B B_0 + 2(\Delta - 1)Js$, whereas the magnons in the reservoirs (assuming that $\Delta = 1$ in the reservoirs) have a minimum energy of $g\mu_B B_0$. The effect of applying a magnetic field $-\Delta B$ to the left reservoir is to create the non-equilibrium situation in which the distribution of magnons in the left reservoir is shifted by an amount $-g\mu_B \Delta B$. From Fig. 2.2 it is seen that shifting the magnon spectrum up ($\Delta B < 0$) allows the magnons from R_L to be transported through the spin chain. Because of the asymmetry of the distributions in R_L and R_R a large magnetization current will flow in this situation. When we shift the spectrum in R_L down ($\Delta B > 0$), the magnetization current is blocked by the gap in the excitation spectrum of the spin chain, hence only a small magnetization current will flow in the opposite direction. To determine the rectification current we use the Landauer-Büttiker approach [47] to calculate the magnetization current through the chain. The total magnetization current is given by $I_m = I_{L \rightarrow R} - I_{R \rightarrow L}$, where

$$I_{L \rightarrow R}(\Delta B) = -g\mu_B \int_{k_{\min,L}}^{k_{\max,L}} \frac{dk}{2\pi} n_B(\omega_k) v(k) T(k), \quad (2.6)$$

and $I_{R \rightarrow L}$ is defined analogously. The ΔB -dependence will be shown to be in the limits of integration. Here $v(k)$ is the group velocity of the

magnons, $v(k) = \partial\omega_k/\partial k$, and $T(k)$ is the transmission coefficient of the spin chain. For this system the transmission coefficient $T(k) = 1$ as long as the magnons are not blocked by the gap in the excitation spectrum of the spin chain. In the absence of ΔB the magnon spectrum in the reservoirs reaches the upper edge of the gap in the spectrum at wave vector $k_0 = \sqrt{2(\Delta - 1)/a^2}$. We can incorporate the shift in the magnon spectrum in the left reservoir by changing the lower boundary in the integral for the magnetization current to $k_{\min} = \max\{0, k_L\}$, where we defined $k_L = \text{Re}[\sqrt{k_0^2 + \xi\Delta B}]$ and $\xi \equiv g\mu_B/(Jsa^2)$. For temperatures T such that $T \ll sJ/k_B$, so that we can set the upper boundary to infinity, we then have the limits of integration $(\max\{0, k_L\}, \infty)$ for the current from R_L to R_R . For $I_{R \rightarrow L}$ we have the limits $(\max\{k_0, k_R\}, \infty)$, where $k_R = \text{Re}[\sqrt{-\xi\Delta B}]$. The resulting magnetization current is then

$$I_m(\Delta B) = -\frac{g\mu_B}{h} \int_{\max\{0, k_L\}}^{\max\{k_0, k_R\}} dk \frac{2\alpha k}{e^{\beta(\alpha k^2 + g\mu_B B_0)} - 1}, \quad (2.7)$$

where $\alpha \equiv sa^2J$. The magnetization current has been plotted in Fig. 2.3 for reasonable material parameters.

2.4 AF spin chains: Luttinger liquid formalism

We now consider the case of an antiferromagnetic spin chain consisting of spins-1/2 which is adiabatically connected (for the antiferromagnetic system this means $L_t \gg 2\pi k_F^{-1} = 4a$, see below) to two 3D antiferromagnetic reservoirs. We will show that it is possible to map both the spin chain and the two reservoirs on the Luttinger Liquid model.

We start with the description of the spin chain and come back to the description of the reservoirs at the end of this section. To model the spin chain [48] we use that in one dimension we can apply the Jordan-Wigner transformation to map the spin operators onto fermionic operators: $S_i^+ \rightarrow c_i^\dagger e^{i\pi \sum_{j=-\infty}^{i-1} c_j^\dagger c_j}$ and $S_i^z \rightarrow c_i^\dagger c_i - 1/2$. This allows us to rewrite the part of Hamiltonian (2.1) that describes the spin chain as the fermionic Hamiltonian

$$\begin{aligned} H &= \sum_i \frac{J}{2} \left(c_{i+1}^\dagger c_i + c_i^\dagger c_{i+1} \right) + g\mu_B \sum_i B_i \left(c_i^\dagger c_i - 1/2 \right) + \\ &\quad + \sum_i J\Delta_i \left(c_{i+1}^\dagger c_{i+1} - 1/2 \right) \left(c_i^\dagger c_i - 1/2 \right) \\ &\equiv H_0 + H_B + H_z. \end{aligned} \quad (2.8)$$

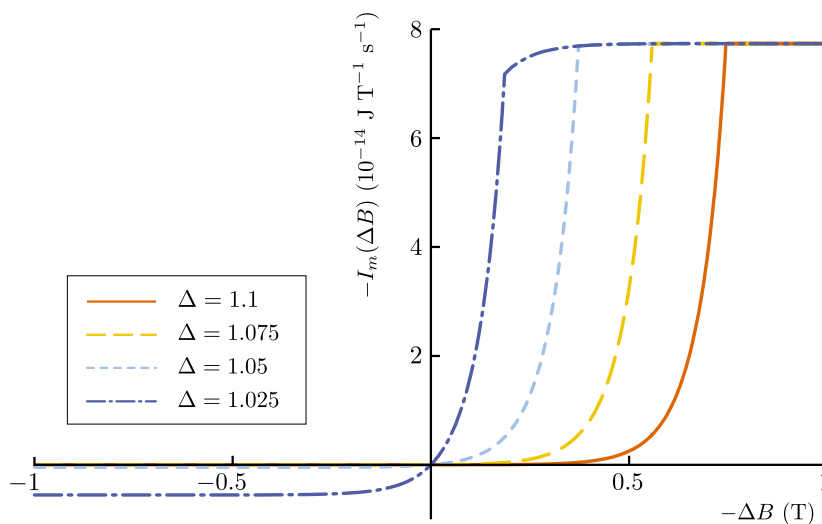


Figure 2.3: Magnetization current as function of applied magnetic field for the parameters $J = 10k_B J$, $s = 1$, $g = 2$, $B_0 = 0.1$ T, $T = 100$ mK, and $a = 10$ nm. The magnetization currents for different anisotropies all saturate at the same positive value, this is the point where all the magnons incoming from the left reservoir are transmitted. This maximum current is on the order of 10^9 magnons per second. Since the typical magnon velocity $\bar{v} = Ja^2k_0/\hbar$ is on the order of 10^3 m s $^{-1}$, and assuming length $L \approx 1$ μ m for the spin chain, this is indeed within the single magnon regime.

We initially assume that the magnetic field satisfies $g\mu_B B \ll J$ and that $\Delta \ll 1$, so that we can use perturbation theory to describe $H_B + H_z$. We will ultimately want a description of the system by its bosonic action.

Considering first H_0 , and restricting the Hamiltonian to low-energy excitations, we can take the continuum limit and linearize the excitation spectrum around the Fermi wave vector $k_F = \pi/(2a)$, where a is again the lattice spacing, to arrive at an effective (1 + 1)-dimensional field theory involving left- and right-moving fermionic excitations. To this purpose we replace $c_i^\dagger \rightarrow a^{1/2}\psi^\dagger(x)$, $\sum_i a \rightarrow \int dx$ and $\Delta_i \rightarrow \Delta(x)$. Here $x = ia$. After introducing left- and right-moving fermions, $\psi^\dagger(x) = \psi_L^\dagger(x) + \psi_R^\dagger(x)$, we carry out a bosonization procedure [49, 50] using the following operators

$$\psi_r^\dagger(x) = \frac{1}{\sqrt{2\pi a}} e^{-\epsilon_r k_r x} e^{i[\epsilon_r \phi(x) - \theta(x)]}. \quad (2.9)$$

Here $r = L, R$, $\epsilon_r = \mp 1$, and k_r is the Fermi wave vector for r -moving

particles (see below). $\phi(x)$ is the bosonic field related to the density fluctuations in the system as $\partial_x \phi(x) = -\pi [\rho_R(x) + \rho_L(x)]$. Here, $\theta(x)$ is the conjugate field of $\phi(x)$. It satisfies $[\phi(x), \partial_{x'} \theta(x')] = i\pi \delta(x - x')$. We have left out the Klein operators in the fermionic creation operators, since they cancel in the subsequent perturbation theory. Using the aforementioned operations we can transform the Hamiltonian H_0 into the quadratic action

$$S_0[\phi] = \frac{\hbar}{2\pi K} \int d^2 r \left[u (\partial_x \phi(\mathbf{r}))^2 - \frac{1}{u} (\partial_t \phi(\mathbf{r}))^2 \right]. \quad (2.10)$$

In this chapter we use the notation $\mathbf{r} = (x, t)^T$. For the free action $u = Ja/\hbar$ and $K = 1$. These parameters will change due to the presence of the H_B - and H_z -terms.

The effect of the inclusion of the magnetic field term H_B is twofold: in the absence of any backscattering and umklapp scattering the field, which is applied to the left reservoir, will introduce different densities of left- and right-moving excitations in the spin chain. The effect of this is to change the Fermi wave vectors in Eq. (2.9) for the respective particles to: $k_R = \pi/(2a) + \frac{K}{u\hbar} g\mu_B (B_0 - \Delta B)$ and $k_L = \pi/(2a) + \frac{K}{u\hbar} g\mu_B B_0$. This does not affect the bosonized form of H_0 , but will have an effect on the bosonized form of H_z . Furthermore, the spatial dependence of the magnetic field makes that the spin chain is now described by $S[\phi] = S_0[\phi] + S_B[\phi]$, where

$$S_B[\phi] = -\frac{g\mu_B}{\pi} \int d^2 r \phi(\mathbf{r}) \partial_x B(\mathbf{r}). \quad (2.11)$$

We use the specific form of the magnetic field

$$\partial_x B(\mathbf{r}) = \Delta B \delta(x - L/2). \quad (2.12)$$

This corresponds to the magnetic field described in Section 2.2.

Next, we derive the bosonic representation of the H_z -term. [51, 52] In the continuum limit the z component of the spin operator is given by the normal ordered expression

$$S^z(x) = : \psi_R^\dagger(x) \psi_R(x) + \psi_L^\dagger(x) \psi_L(x) + \psi_R^\dagger(x) \psi_L(x) + \psi_L^\dagger(x) \psi_R(x) :. \quad (2.13)$$

The interaction term H_z contains terms that transfer approximately 0, $2k_F$ or $4k_F$ momentum. Around half-filling and for a constant anisotropy in the exchange interaction, as is the case in Eq. (2.2), conservation of momentum requires that the only terms that can survive are the ones

that transfer approximately 0 or $4k_F$ momentum, the $2k_F$ -terms are suppressed by rapidly oscillating $\exp(\pm 2ik_F x)$ terms. The terms that transfer small momentum give rise to terms proportional to $(\partial_x \phi(\mathbf{r}))^2$, and hence change the parameters u, K in Eq. (2.10). It is not possible to determine the exact values from the linearized theory, they can however be determined from the Bethe-Ansatz solution. [53] Important here is that for $\Delta \leq 1$ we have $K \geq 1/2$. The $4k_F$ -term (umklapp scattering term) becomes

$$S_{\text{US}}[\phi] = \frac{aJ}{(2\pi a)^2} \int d^2 r \Delta(x) \cos [4\phi(\mathbf{r}) - 4\rho x], \quad (2.14)$$

where $\rho \equiv \frac{K}{u\hbar} g\mu_B (B_0 - \Delta B/2)$. We have neglected a constant term $\propto \rho a$ inside the cosine.

If a spatially varying anisotropy is present, as in Eq. (2.3), the $2k_F$ -backscattering terms do not necessarily vanish in regions where $\Delta(x)$ varies on a scale of order a . The bosonization of the $2k_F$ -terms then requires some care. If we naively use the continuum form of Eq. (2.8), this term contains infinities after the bosonization. Therefore, it has to be normal ordered, [49] which we can do using Wick's theorem and the contraction

$$\overline{\psi_r(x)\psi_{r'}^\dagger(x+a)} = -\epsilon_r \frac{e^{-irk_r a}}{2\pi a i} \delta_{r,r'}. \quad (2.15)$$

Since the $S_i^z S_{i+1}^z$ -term contains four-fermion operators the normal ordering will yield not only additional constants, but also two-fermion operators, as can for instance be seen from the typical term $\psi_R^\dagger(x)\psi_R(x)\psi_R^\dagger(x+a)\psi_L(x+a)$, which becomes

$$: \psi_R^\dagger(x)\psi_R(x)\psi_R^\dagger(x+a)\psi_L(x+a) : - \frac{e^{-ik_R a}}{2\pi a i} : \psi_R^\dagger(x)\psi_L(x+a) : . \quad (2.16)$$

There are four such two-fermion operators. Together they give rise to the backscattering term

$$S_{\text{BS}}[\phi] = -\frac{2aJ}{(2\pi a)^2} \int d^2 r (-1)^{x/a} \Delta(x) \times \{ \sin [2\phi(\mathbf{r}) - 2\rho x] + \sin [2\phi(\mathbf{r}) - 2\rho(x+a)] \}. \quad (2.17)$$

The completely normal-ordered term becomes

$$S_{\text{BSN}}[\phi] = \frac{8aJ}{(2\pi a)^2} \int d^2 r (-1)^{x/a} \Delta(x) [a\partial_x \phi(\mathbf{r})]^2 \times \{ \sin [2\phi(\mathbf{r}) - 2\rho x] + \sin [2\phi(\mathbf{r}) - 2\rho(x+a)] \}. \quad (2.18)$$

The latter can be seen by expanding the normal ordered term around x and invoking the Pauli exclusion principle. Due to the presence of the $[a\partial_x\phi(\mathbf{r})]^2$ -term we can always neglect this contribution. The total action describing the spin chain is then given by

$$S[\phi] = S_0[\phi] + S_B[\phi] + S_{US}[\phi] + S_{BS}[\phi]. \quad (2.19)$$

Now we can distinguish between the two scenarios in Eq. (2.2) and Eq. (2.3). For the constant anisotropy in Eq. (2.2) the $S_{BS}[\phi]$ and $S_{BSN}[\phi]$ terms vanish as they are proportional to the rapidly oscillating $(-1)^{x/a}$. Hence only the bulk umklapp scattering term, given by

$$S_{BUS}[\phi] = \frac{\lambda_1}{(2\pi a)^2} \int dxdt \cos [4\phi(\mathbf{r}) - 4\rho x], \quad (2.20)$$

remains. Here $\lambda_1 \equiv aJ\Delta$. The spin chain in Eq. (2.2) is thus described by the action $S_0[\phi] + S_{BUS}[\phi] + S_B[\phi]$. As we will discuss in the next section, the bulk umklapp scattering term renormalizes as $2 - 4K$, hence it is irrelevant for $K > 1/2$ ($\Delta < 1$) and relevant for $K < 1/2$ ($\Delta > 1$). If this term is relevant, as it is for the parameters in Eq. (2.2), it opens a gap in the excitation spectrum of the spin chain, which, as we will show in Section 2.6, can be used to achieve the rectification effect in a similar way as for the ferromagnetic system in Section 2.3. To wit, if we tune B_0 such that it lies just below the upper edge of the gap, for $\Delta B > 0$ there can be no magnetization transport, since there are no states available for transport in the chain, whereas for $\Delta B < 0$ the states above the edge of the gap are accessible, and transport is made possible.

Next we discuss the case with spatially varying exchange anisotropy, Eq. (2.3). We start out by noting that, since the bulk umklapp scattering term is irrelevant for this scenario, the spin chain is not in a gapped state in equilibrium. The effect of the applied magnetic field is then to move the spin chain away from half-filling. As we will show later, in the current scenario this doping is required in order to achieve a nonzero rectification current. In the case of Eq. (2.3) the backscattering term vanishes everywhere, except in the region where $\Delta(x)$ itself varies on a short length scale. For the specific form of the anisotropy of Eq. (2.3), the action resulting from the site impurity is

$$\begin{aligned} S_{BS}[\phi] = & -\frac{a2J\Delta'}{(2\pi)^2} \int dt\partial_x \left\{ \sin \left[2\phi(x_0, t) - 2\rho(x_0 - \frac{a}{2}) \right] + \right. \\ & \left. + \sin \left[2\phi(x_0, t) - 2\rho(x_0 + \frac{a}{2}) \right] \right\}. \end{aligned} \quad (2.21)$$

Where, here and elsewhere, $\partial_x f(x_0, t)$ should be read as $\partial_x f(x, t)|_{x=x_0}$. Adding to this term the local umklapp scattering term caused by the site impurity, the total action coming from this impurity becomes

$$S_I[\phi] = \frac{1}{\pi^2 a} \int dt \left\{ \frac{1}{4} [\lambda_2^a \cos 4\phi(x_0, t) + \lambda_2^b \sin 4\phi(x_0, t)] + \right. \\ \left. + \sigma [\lambda_3^a \cos 2\phi(x_0, t) + \lambda_3^b \sin 2\phi(x_0, t)] + \right. \\ \left. + a [\lambda_4^a \partial_x \phi(x_0, t) \cos 2\phi(x_0, t) + \lambda_4^b \partial_x \phi(x_0, t) \sin 2\phi(x_0, t)] \right\}. \quad (2.22)$$

This expression contains terms caused by umklapp scattering (proportional to $\lambda_2^{a,b}$), terms that may be called offset-induced backscattering terms (proportional to $\lambda_3^{a,b}$), and terms that describe combined forward- and backscattering (proportional to $\lambda_4^{a,b}$). In the expression for the action $S_I[\phi]$ we have defined

$$\sigma \equiv \rho a = \frac{Ka}{u\hbar} g\mu_B (B_0 - \Delta B/2) = K [g\mu_B (B_0 - \Delta B/2) / (\hbar\omega_c)]. \quad (2.23)$$

Here we have identified the UV-cutoff of the theory ω_c with u/a . Furthermore the prefactors are given by

$$\begin{aligned} \lambda_2^a &= 2\lambda \left[\cos 4\rho \left(x_0 - \frac{a}{2} \right) + \cos 4\rho \left(x_0 + \frac{a}{2} \right) \right], \\ \lambda_2^b &= 2\lambda \left[\sin 4\rho \left(x_0 - \frac{a}{2} \right) + \sin 4\rho \left(x_0 + \frac{a}{2} \right) \right], \\ \lambda_3^a &= \lambda(-1)^{\frac{x_0}{a}} \left[\cos 2\rho \left(x_0 - \frac{a}{2} \right) + \cos 2\rho \left(x_0 + \frac{a}{2} \right) \right], \\ \lambda_3^b &= \lambda(-1)^{\frac{x_0}{a}} \left[\sin 2\rho \left(x_0 - \frac{a}{2} \right) + \sin 2\rho \left(x_0 + \frac{a}{2} \right) \right]. \end{aligned} \quad (2.24)$$

Where $\lambda = aJ\Delta'$. Lastly, $\lambda_4^{a,b} = -\lambda_3^{a,b}$. In this scenario the spin chain is thus described by $S_0[\phi] + S_{\text{BUS}}[\phi] + S_I[\phi] + S_B[\phi]$.

Finally we return to the description of the spin reservoirs. As we show in detail in Appendix A, we can describe the low-energy excitations of the reservoirs by the quadratic Luttinger Liquid action, Eq. (2.10). The effective Luttinger Liquid parameters u_r, K_r of the 3-dimensional reservoirs can be determined by mapping its dynamic susceptibility onto that of a Luttinger Liquid, using the non-linear sigma model, resulting in

$$u_r = \sqrt{3}Ja/\hbar \quad K_r = \pi/(4\sqrt{3}). \quad (2.25)$$

This means that we can describe the reservoirs by letting $u \rightarrow u(x)$ and $K \rightarrow K(x)$ in Eq. (2.10), where

$$u(x), K(x) = \begin{cases} u, K & \text{for } x \in (-L/2, L/2) \\ u_r, K_r & \text{for } x \notin (-L/2, L/2) \end{cases}. \quad (2.26)$$

2.5 Renormalization group treatment

We start the analysis of the antiferromagnetic spin chain by studying the scaling behavior of the spin chain. The results of this analysis allow us to determine which perturbations will be most relevant in the low energy sector. We perform the renormalization group (RG) calculation in momentum space, [48] assuming there is a hard natural momentum-cutoff Λ_0 in the system. In the RG procedure the cutoff $\Lambda(l) = \Lambda_0 e^{-l}$ is decreased from $\Lambda(l)$ to $\Lambda(l + dl)$. For the RG procedure we consider the partition function written in terms of the action in imaginary time. As is customary, we split the field $\phi(\mathbf{r})$ contained in this action up in a fast and a slow part, $\phi(\mathbf{r}) = \phi^>(\mathbf{r}) + \phi^<(\mathbf{r})$. The fast part contains Fourier components with momentum between $\Lambda(l + dl)$ and $\Lambda(l)$, and the slow part the components with momentum less than $\Lambda(l + dl)$. The RG-procedure then consists of integrating out the fast modes, and subsequently restoring the original cutoff in the action, in order to find an effective low-energy action with the same couplings, but different coupling constants. This allows us to find the relevant (increasing in magnitude under a decrease of the cutoff) and irrelevant (decreasing in magnitude under a decrease of the cutoff) couplings. For completeness, we mention the renormalization equations for the constant anisotropy Δ (see Ref. [48])

$$\begin{aligned}\frac{dK}{dl} &= -\frac{8\lambda_1^2}{(2\pi\hbar)^2} \frac{1}{u^2} K C_K, \\ \frac{du}{dl} &= \frac{8\lambda_1^2 K^2}{(2\pi)^3 \hbar^2} \frac{1}{u} C_u, \\ \frac{d\rho}{dl} &= \rho, \\ \frac{d\lambda_1}{dl} &= (2 - 4K) \lambda_1.\end{aligned}\tag{2.27}$$

We have omitted several instances of Λa , which is a number of order 1. The different constants are given by (here $\bar{\mathbf{r}} = \Lambda(x, u\tau)^T$ is dimensionless)

$$\begin{aligned}C_K &= \frac{1}{2} \int d^2\bar{\mathbf{r}} \cos[4\rho x] \bar{\mathbf{r}}^2 J_0(\bar{\mathbf{r}}) e^{-8KF_1(\bar{\mathbf{r}})}, \\ C_u &= -\frac{1}{2} \int d^2\bar{\mathbf{r}} (\bar{x}^2 - u^2\bar{\tau}^2) \cos[4\rho x] J_0(\bar{\mathbf{r}}) e^{-8KF_1(\bar{\mathbf{r}})}.\end{aligned}\tag{2.28}$$

Here $J_0(\bar{\mathbf{r}})$ is the zeroth-order Bessel function and $F_1(\bar{\mathbf{r}}) = \int_0^1 dq (1 - J_0(q\bar{\mathbf{r}})) q^{-1}$. Both integrals converge and are of order 1. From the last RG-

equation it follows that for $K < 1/2$, which as we have seen before corresponds to $\Delta > 1$, the perturbation caused by the bulk umklapp scattering grows under renormalization. This corresponds to the opening of a gap in the excitation spectrum of the spin chain. The magnitude M of this gap has been calculated analytically using Bethe-Ansatz methods, [54] and is given by

$$\frac{M}{J} = \frac{\pi \sinh \nu}{\nu} \sum_{n=-\infty}^{\infty} \frac{1}{\cosh [(2n+1)\pi^2/2\nu]}, \quad (2.29)$$

where $\nu = \text{acosh} \Delta$. For $\Delta \gtrsim 1$ this gap is exponentially small, and is given by $M \approx 4\pi J \exp[-\pi^2/(2[2(\Delta-1)]^{1/2})]$. For $\Delta \rightarrow \infty$ the gap becomes $M \approx J[\Delta - 2]$.

If we now assume to be in the regime where $K > 1/2$ and add the site impurity described by $S_I[\phi]$, we get the following additional equations

$$\begin{aligned} \frac{d\lambda_2^{a/b}}{dl} &= (1 - 4K) \lambda_2^{a/b} - \Gamma_{44}^{a/b} C_1 - \Gamma_{33}^{a/b} C_\beta, \\ \frac{d\lambda_3^{a/b}}{dl} &= (1 - K) \lambda_3^{a/b} - \Gamma_{23}^{a/b} C_\alpha - \Lambda_{3\mp}^{b/a} C_c \pm \Lambda_{4\pm}^{b/a} C_s, \\ \frac{d\lambda_4^{a/b}}{dl} &= (1 - K) \lambda_4^{a/b} - \Gamma_{24}^{a/b} C_\alpha - \Lambda_{4\pm}^{b/a} C_c. \end{aligned} \quad (2.30)$$

Where we have defined the second order terms $\Gamma_{nm}^{a/b} = \lambda_n^a \lambda_m^{a/b} + \lambda_n^b \lambda_m^{b/a}$ and $\Lambda_{n\eta}^{a/b} = \left(\eta \lambda_n^{a/b} \sin 4\rho x_0 + \lambda_n^{b/a} \cos 4\rho x_0 \right) \lambda_1$. Here $\eta = \pm$. The different constants used here are given by

$$\begin{aligned} C_1 &= \frac{1}{2\pi^3 \hbar u} \int d\bar{\tau} \frac{J_1(\bar{\tau})}{\bar{\tau}} e^{-2KF_1(\bar{\tau})}, \\ C_\alpha &= \frac{K}{\pi^2 \hbar u} \int d\bar{\tau} J_0(\bar{\tau}) e^{-3KF_1(\bar{\tau})}, \\ C_\beta &= \frac{8K\sigma^2}{\pi^2 \hbar u} \int d^2\bar{r} J_0(\bar{r}) e^{-2KF_1(\bar{r})}, \\ C_c &= \frac{K}{2\pi^2 \hbar u} \int d^2\bar{r} \cos [4(\rho/\Lambda)\bar{x}] J_0(\bar{r}) e^{-3KF_1(\bar{r})}, \\ C_s &= \frac{K^2}{\sigma\pi^2 \hbar u} \int d^2\bar{r} \frac{\bar{x}}{\bar{r}} \sin [4(\rho/\Lambda)\bar{x}] J_0(\bar{r}) e^{-3KF_1(\bar{r})}. \end{aligned} \quad (2.31)$$

Again, all integrals converge and are of order 1. From the form of the equations it follows that we can ignore contributions that are of second

order in the couplings, and we see that the most relevant couplings are the $\lambda_3^{a,b}$ - and $\lambda_4^{a,b}$ -terms, which to first order scale as $1 - K$. For $K \in (1/2, 1)$, the regime in which we operate in the case of Eq. (2.3), these terms thus grow in magnitude under a decrease of the cutoff. Because of the extra $\partial_x \phi(x_0, t)$ proportionality in the $\lambda_4^{a,b}$ -terms, one would expect the effect of these terms on the magnetization current to be smaller than that of the $\lambda_3^{a,b}$ -terms. However, since the $\lambda_3^{a,b}$ -terms have an additional σ in front of them, in the regime $B_0 \approx \Delta B/2$ these are suppressed, so that they could become comparable to the $\lambda_4^{a,b}$ -terms. Therefore we will consider the effect of both types of coupling when calculating the magnetization current for the system with anisotropy in the exchange interaction as in Eq. (2.3) in Section 2.7.

2.6 Enhanced anisotropy

As we have shown in Section 2.5, the enhanced exchange anisotropy of Eq. (2.2) gives rise to a bulk umklapp scattering term in the action of the spin chain, and the chain is described by the sine-Gordon model. [48] This model has been studied extensively, and is known to give rise to two possible phases depending on the value of the chemical potential $g\mu_B B$: for values of the chemical potential lower than the gap M the system is a Mott-insulator; when the chemical potential is increased to values above the gap, the system undergoes a commensurate-incommensurate transition and becomes conducting.

To simplify the sine-Gordon model we replace $\phi_M(\mathbf{r}) = 2\phi(\mathbf{r})$ and, in order to keep the commutation relation between the two fields unchanged, $\theta_M(\mathbf{r}) = \theta(\mathbf{r})/2$. The umklapp scattering term then reduces to a backscattering term (a two-particle operator), and the effective Luttinger parameter becomes $4K$. The fermionic form of the resulting new action is known as the massive Thirring model. At the Luther-Emery point, $K = 1/4$, (Ref. [55]) the new fermions whose action is given by the massive Thirring model are non-interacting, and we can diagonalize the quadratic part of the action by a Bogoliubov transformation, which gives rise to two separate bands of fermionic excitations with dispersion $\epsilon_{\pm}(k) = \pm\sqrt{(uk)^2 + M^2}$. If $K \neq 1/4$ there are residual four-fermion interactions present. However, it can be shown [56] that, independent of the initial interactions, near the C-IC transition the strength of these interactions vanishes faster than the density of the fermions, so that the interactions become negligible. The new free fermions are not the original fermions, instead they correspond to solitonic excitations of the origi-

nal action. These solitons have fractional magnetic moment $-g\mu_B/2$. We finally can relinearize the excitation spectrum around the point M to arrive at a new Luttinger Liquid in terms of the fields $\phi_M(\mathbf{r})$, $\theta_M(\mathbf{r})$ with parameter $K_M = 4K$.

To calculate the DC magnetization current through the system we use [30] that in linear response theory the DC magnetization current is given by $I_m = G\Delta B$, where the conductance G is given by

$$G = -i \frac{(g\mu_B)^2}{\pi^2 \hbar} \lim_{\omega \rightarrow 0} [\omega G_{\phi\phi}(x, x', \omega_n)|_{i\omega_n \rightarrow \omega + i\epsilon}], \quad (2.32)$$

and $G_{\phi\phi}(x, x', \omega_n)$ is the time-ordered Green's function in imaginary time

$$G_{\phi\phi}(x, x', \omega_n) = \int_0^\beta d\tau e^{i\omega_n \tau} \langle T_\tau \phi(x, \tau) \phi(x', 0) \rangle_{S_0}. \quad (2.33)$$

Here ω_n is the Matsubara frequency. At zero temperature, and assuming infinitesimal dissipation in the reservoirs, the $\omega \rightarrow 0$ limit of this Green's function can be determined for the inhomogeneous system including the two reservoirs, [57] and is given by $K_r/(2|\omega_n|)$. The effect of the entire mapping of the original sine-Gordon model onto the new free Luttinger Liquid can be captured here by replacing $g\mu_B \rightarrow g\mu_B/2$ and $K_r \rightarrow 4K_r$, so that the conductance in the conducting phase is $G = K_r(g\mu_B)^2/h$. Following Ref. [58] we conclude that excitations that are injected at energies above the Mott gap are transported through the chain, giving rise to the aforementioned conductance, whereas excitations injected at chemical potential lower than the gap are fully reflected. Assuming that $g\mu_B B_0 \approx M$, this gives rise to the magnetization current

$$I_m(\Delta B) = K_r \frac{(g\mu_B)^2}{h} \Delta B \Theta(-\Delta B). \quad (2.34)$$

Where $\Theta(-\Delta B)$ is the unit step function. Since magnetization transport is absent for $\Delta B > 0$, we have $I_r(\Delta B) = I_m(\Delta B)/2$. In these calculations we assumed that the length of the spin chain $L \rightarrow \infty$, so that we can neglect tunneling of solitons, and we have assumed zero temperature. Finite size and temperatures are known to give corrections to the conductance. [59, 60]

2.7 Suppressed anisotropy

To determine the rectification current resulting from the anisotropy as given in Eq. (2.3) we need to calculate the magnetization current through

the system given the action $S[\phi] = S_0[\phi] + S_I[\phi] + S_B[\phi]$. For simplicity we assume here that the impurity is located at $x_0 = 0$. We ignore the bulk umklapp scattering term, since we have shown in Section 2.5 that the contribution of this term is irrelevant for the parameters used here. From the RG analysis it also followed that the most important terms are the offset-induced backscattering terms and that in regions where $B_0 \approx \Delta B/2$ the effect of the terms describing combined forward- and backscattering and the offset-induced backscattering terms can become comparable, due to the extra σ in front of the latter terms. Therefore we need to calculate the magnetization current due to both types of contribution. We will show that the rectification effect appears in the contributions to the magnetization current that are second order in the coupling constants.

We calculate the magnetization current using the Keldysh technique. [61] We assume that at $t = -\infty$ the system is described by the action $S_0[\phi] + S_B[\phi]$, and that the perturbation $S_I[\phi]$ is turned on adiabatically. From conservation of spin it follows that the expression for the magnetization current in the Luttinger Liquid is given by $I_m(\mathbf{r}) = -(g\mu_B/\pi)\partial_t\phi(\mathbf{r})$. The magnetization current can then be calculated as [62]

$$I_m = -\frac{g\mu_B}{\pi}\partial_t\frac{1}{2}\sum_{\eta=\pm}\langle\phi^\eta(\mathbf{r})\rangle_S = \frac{g\mu_B^i}{\pi}\partial_t\left(\frac{\delta Z[J(\mathbf{r})]}{\delta J(\mathbf{r})}\right). \quad (2.35)$$

Here, $\langle\phi^\pm(\mathbf{r})\rangle_S$ is the average of the field $\phi(\mathbf{r})$ over the Keldysh contour with respect to the action $S[\phi]$. The \pm denotes that the field is located on the positive respectively negative branch of the contour. The right hand side contains the functional derivative of the partition function of the system with respect to the generating functional $J(\mathbf{r})$, which is given in Eq. (B.2). The details of the calculation are given in appendix B, here we summarize the results. We find that there are two fundamentally different contributions to the magnetization current

$$I_m(\Delta B) = I_0(\Delta B) + I_{BS}(\Delta B). \quad (2.36)$$

Here, $I_0(\Delta B)$ is the magnetization current through the systems in the absence of $S_I[\phi]$, given by the well-known expression

$$I_0(\Delta B) = K_r\frac{(g\mu_B)^2}{h}\Delta B, \quad (2.37)$$

and $I_{BS}(\Delta B)$ described (negative) contributions to the magnetization current due to $S_I[\phi]$, which we will derive next.

The contribution to the magnetization current that arises as the result of the contribution $\sigma(\lambda_3^a/\pi^2) \cos[2\phi(0, t)]$ (which describes offset-induced backscattering) is given by

$$I_{3a}(\Delta B) = \frac{g\mu_B\sigma^2 (\lambda_{3,R}^a)^2}{\pi^4} \frac{1}{a_s} K_r A_0(\Delta B), \quad (2.38)$$

where

$$A_0(\Delta B) = -\frac{K4^K\pi}{\Gamma(1+2K)} \gamma_R |\gamma_R|^{-2+2K} e^{-2|\gamma_R|}. \quad (2.39)$$

Here we introduced the dimensionless parameters $\lambda_{3,R}^a = \lambda_3^a/(\hbar\omega_c)$ and $\gamma_R = K_r g\mu_B \Delta B/(\hbar\omega_c)$. As before, ω_c denotes the UV-cutoff of our theory, given by $\omega_c = u/a$. In Section 2.5 it was determined that the backscattering term scales as $1 - K$ under renormalization. To improve our result we should therefore not use the bare coupling $\lambda_{3,R}^a$, but instead the renormalized coupling. Since we assumed an infinitely long chain, and consider zero temperature, the renormalization group procedure is stopped on the energy scale determined by the magnetic field, $g\mu_B \Delta B$. We can account for this by replacing $\lambda_{3,R}^a \rightarrow |g\mu_B \Delta B/(\hbar\omega_c)|^{-1+K} \lambda_{3,R}^a$. At this point we have determined the magnetization current resulting from the backscattering term. By repeating the previous calculation with both the λ_3^a - and the λ_3^b -proportional terms included it is easily seen that the $(\lambda_3^b)^2$ -proportional contribution to the magnetization current is also given by Eq. (2.38), with $(\lambda_{3,R}^a)^2$ replaced by $(\lambda_{3,R}^b)^2$. The two cross terms proportional to $\lambda_3^a \lambda_3^b$ do not contribute to the magnetization current, since they cancel each other.

The calculation of the contribution to the magnetization current due to a term $\frac{a\lambda_4^a}{\pi^2} \partial_x \phi(0, t) \cos 2\phi(0, t)$ that describe combined forward- and backscattering proceeds along the same lines, we refer again to appendix B for the details. The resulting contribution to the magnetization current is given by

$$I_{4a}(\Delta B) = \frac{g\mu_B (\lambda_{4,R}^a)^2}{\pi^4} \frac{1}{a_s} K_r A_1(\Delta B), \quad (2.40)$$

where

$$A_1(\Delta B) = -\frac{4^K\pi}{\Gamma(2+2K)} \gamma_R |\gamma_R|^{2K} e^{-2|\gamma_R|}. \quad (2.41)$$

Again, according to the RG analysis, we have to replace the bare coupling with its renormalized value, in this case: $\lambda_{4,R}^a \rightarrow |g\mu_B \Delta B/(\hbar\omega_c)|^{-1+K} \lambda_{4,R}^a$. Like with the backscattering-terms, we can easily determine the effect of the λ_4^a - and λ_4^b -terms combined. The magnetization current proportional

to $(\lambda_4^b)^2$ is given by Eq. (2.40) with $(\lambda_{4,R}^a)^2$ replaced by $(\lambda_{4,R}^b)^2$, and the two cross-terms cancel each other.

Finally, we need to consider the cross terms between the λ_3 - and λ_4 -terms, such as for instance $\lambda_3^a \lambda_4^b$. Using the results from appendix C it is easily seen that these always vanish, since they are all proportional to

$$\left\langle T_c \partial_x \phi^\eta(0, t) e^{\pm 2i[\phi^\eta(0, t) - \phi^{\eta'}(0, t')]} \right\rangle = 0. \quad (2.42)$$

The total backscattered current is then given by

$$I_{\text{BS}}(\Delta B) = \frac{g\mu_B}{\pi^4} \frac{K_r}{a_s} \left\{ \sigma^2 \lambda_{3,\text{eff}}^2 A_0(\Delta B) + \lambda_{4,\text{eff}}^2 A_1(\Delta B) \right\}, \quad (2.43)$$

where $\lambda_{i,\text{eff}} = [(\lambda_{i,R}^a)^2 + (\lambda_{i,R}^b)^2]^{1/2}$.

Eq. (2.43) is the main result of this section. From the explicit form of $A_0(\Delta B)$ and $A_1(\Delta B)$ (see Eq. (2.39) and (2.41)) it is clear that the impurity flows to strong coupling for low ΔB away from half-filling, as was expected from the RG analysis. We note that, since both $A_0(\Delta B)$ and $A_1(\Delta B)$ are odd in ΔB , one could naively think that the impurity does not contribute to the rectification current, which requires the magnetization current to have a component that is even in ΔB . However, from the explicit form of the $\lambda_{i,\text{eff}}$ (see Eq. (2.24) for the bare couplings) it follows that these couplings also contain parts that are proportional to ΔB . Furthermore, the part of the magnetization current that is proportional to $A_0(\Delta B)$ is proportional to σ^2 , which also contains a ΔB . Physically, these terms are caused by the fact that an incoming excitation sees a slightly different impurity depending on the energy with which it comes in. The magnetization current Eq. (2.43) therefore has components even in ΔB , which contribute to the rectification current. We are now also in a position to explain why it is needed to move the system away from half-filling in order to obtain a nonzero rectification current. If we set $B_0 = 0$ in Eq. (2.24), it turns out that the $\lambda_{i,\text{eff}}$'s and σ contain only terms that are even in ΔB , so that the magnetization current is odd in ΔB . In contrast, when $B_0 \neq 0$, we create terms in the $\lambda_{i,\text{eff}}$'s and σ that are odd in ΔB , thereby causing a nonzero rectification current.

2.8 Estimate of rectification currents

In this section we will give numerical estimates of the rectification current for realistic experimental parameters. Experimental results [63] show

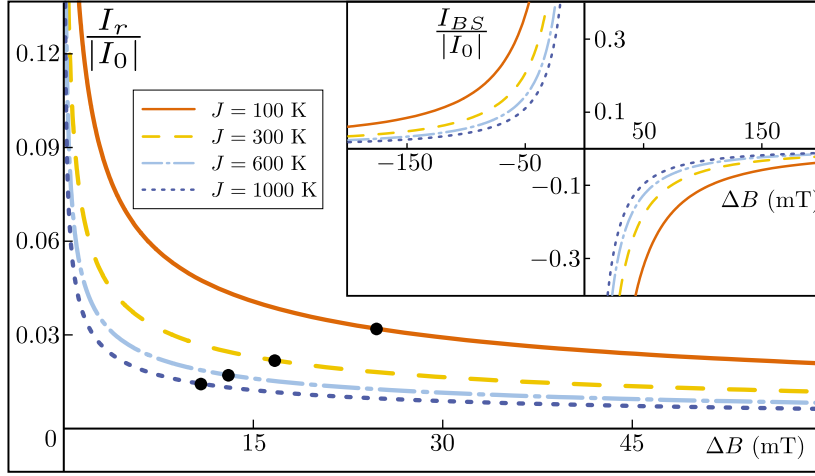


Figure 2.4: Normalized rectification current $I_r/|I_0|$ (main figure) and backscattering current $I_{BS}/|I_0|$ (inset) as a function of the applied magnetic field difference ΔB for different values of the exchange interaction J . Parameters are: $K = 0.63$, $B_0 = 750$ mT, and $\Delta' = 0.5$. The black dots in the main figure denote the values ΔB^* for which $\max[|I_{BS}(\Delta B^*)|, |I_{BS}(-\Delta B^*)|] = |I_0(\Delta B^*)|$. As explained in the text, our perturbative results are not valid for $|\Delta B| < |\Delta B^*|$.

that the exchange coupling in certain spin chains can be on the order of $J \approx 10^2 K$. The effect of a different exchange interaction is illustrated in Fig. 2.4. In the analysis of these results one must keep in mind that, since our perturbative calculation of $I_{BS}(\Delta B)$ diverges for $\Delta B \rightarrow 0$, it breaks down for field differences $|\Delta B| < |\Delta B^*|$, where ΔB^* is the field such that $\max[I_{BS}(\Delta B^*), I_{BS}(-\Delta B^*)] = I_0(\Delta B^*)$. Instead of showing the apparent divergent behavior the backscattering current must go to zero for $\Delta B < \Delta B^*$. With this in mind, Fig. 2.4 shows that a smaller exchange interaction J gives rise to a larger rectification current at equal ΔB . The maximum value of $I_r(\Delta B)$ will also be reached at a higher value of ΔB . In order to get the largest possible rectification current it is thus required to use a material with an exchange interaction as low as possible, with the constraint that it must be large enough to yield its maximum at reasonable values of ΔB .

In Fig. 2.5 we show the dependence of the backscattering and rectification current on the Luttinger Liquid parameter K . The behavior for smaller K is similar to the behavior shown for smaller J : the maximum rectification current is increased, but occurs at a higher value of ΔB . Indeed, we know that both $I_m(\Delta B)$ and $I_r(\Delta B)$ obey a powerlaw

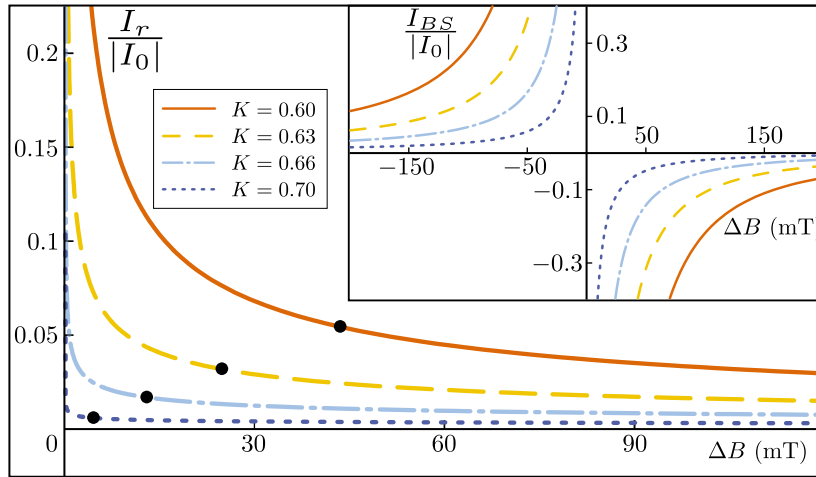


Figure 2.5: $I_{BS}/|I_0|$ as a function of the applied magnetic field difference ΔB for different values of K . Parameters are: $B_0 = 750$ mT, $J = 100$ K, and $\Delta' = 0.5$. See the caption of Fig. 2.4 for the explanation of the black dots.

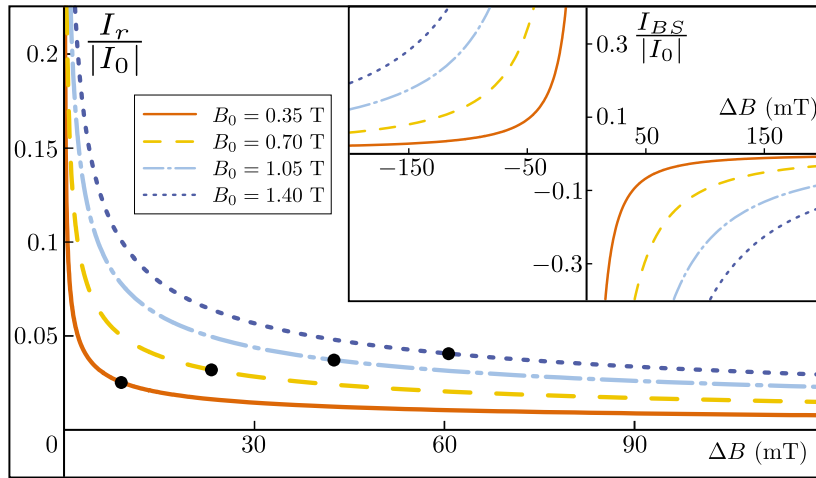


Figure 2.6: $I_{BS}/|I_0|$ as a function of the applied magnetic field difference ΔB for different values of B_0 . Parameters are: $K = 0.63$, $J = 100$ K, and $\Delta' = 0.5$. See the caption of Fig. 2.4 for the explanation of the black dots.

dependence of ΔB with negative exponent. Since the modulus of this exponent decreases for increasing K , the behavior is as expected.

Fig. 2.6 shows the dependence of the backscattering current on the applied magnetic field B_0 . A larger amount of doping clearly corresponds to larger possible rectification current, again at the price of a higher re-

quired magnetic field ΔB . This can be understood by realizing that B_0 determines to a large extent how much of the impurity the incoming excitations see at low energies $\Delta B \ll B_0$, as follows from the σ -dependence in the $\lambda_3^{a,b}$ -terms in the action Eq. (2.23).

In Ref. [30] it has been shown that N parallel uncoupled AF spin chains connected between two 3D AF spin reservoirs, each one carrying a magnetization current $I_m(\Delta B)$, give rise to an electric field

$$\mathbf{E}(\mathbf{r}) = N \frac{\mu_0}{2\pi} \frac{I_m(\Delta B)}{r^2} (0, \cos 2\phi, -\sin 2\phi) \quad (2.44)$$

Here the spin chains are assumed to extend in the x direction, and z is the quantization axis as before. Also, $r = \sqrt{y^2 + z^2}$, $\sin \phi = y/r$ and $\cos \phi = z/r$. We can use this electric field to measure the rectification current $I_r(\Delta B)$. To illustrate the method we assume $K = 0.6$, $B_0 = 750$ mT and $N = 10^4$. We apply the time-dependent field $\Delta B(t) = \Delta B \cos(\omega t)$ to the left reservoir. From Eq. (2.43) it follows that, if we trust our perturbative calculation of I_{BS} up to the value $\Delta B^* \approx -43$ mT, where $|I_0(\Delta B^*)| \approx |I_{BS}(\Delta B^*)|$, the difference in magnitude between $|I_m(\Delta B^*)|$ and $|I_m(-\Delta B^*)|$ is on the order of 10% of the unperturbed current $|I_0(\Delta B^*)|$. From Eq. (2.44), and assuming $r = 10^{-5}$, it then follows that the difference in voltage drop between two points $(0, r, 0)$ and $(0, 0, r)$ is $V_S \approx 10^{-13}$ V, which is within experimental reach. Here we note that as long as the driving frequency $\hbar\omega < g\mu_B\Delta B$, our calculation of the magnetization current in the DC-limit remains valid. A lower bound on the driving frequency is given by the inverse of the spin relaxation time τ_s . This time can be on the order of 10^{-7} s. [64] This allows us to use frequencies in the MHz-GHz range.

Another possibility to observe the rectification effect is by spin accumulation. By applying again an AC driving field to the left reservoir it is possible to measure an accumulation of spin in the right reservoir, since transport is asymmetric with respect to the sign of ΔB . We consider again 10^4 parallel spin chains with $K = 0.6$, consider $B_0 = 750$ mT, and an amplitude $\Delta B = 43$ mT for the driving field. For $\Delta B(t) < 0$ the magnetization current is always zero. For $\Delta B(t) > 0$ there is a nonzero magnetization current. Assuming that the magnetization current is 10% of the unperturbed magnetization current (the value at $\Delta B(t) = \Delta B$) over the entire range $(0, \Delta B)$, the rate of spin accumulation is about 10^{-11} JT $^{-1}$ s $^{-1} \approx 10^{12}$ magnons per second. We also note that, contrary to the electric case, where charge repulsion prevents a large charge accumulation, there is no strong mechanism that prevents spin accumulation in this scenario.

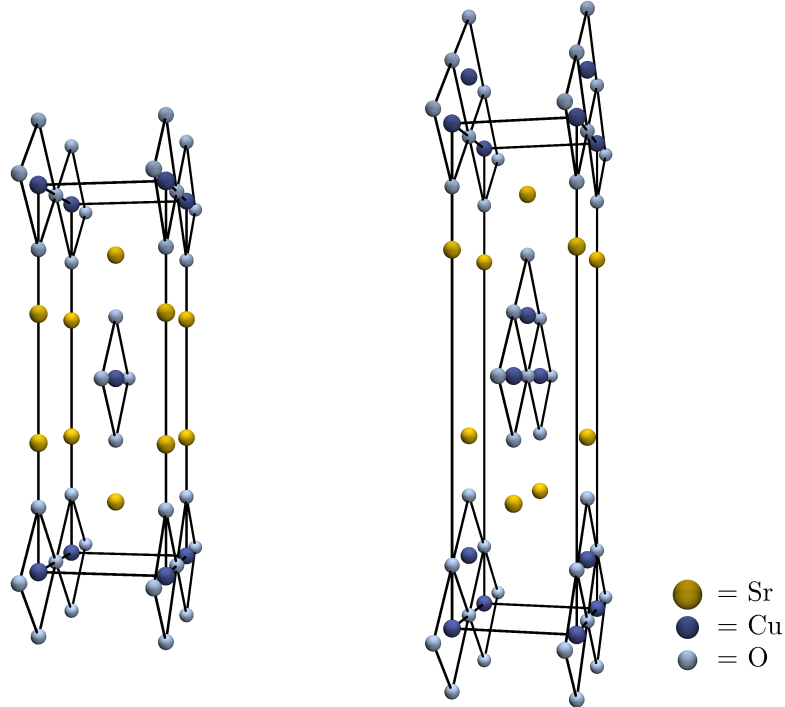


Figure 2.7: Unit cell of Sr_2CuO_3 (left) and SrCuO_2 (right). Lattice constants are respectively $a = 3.6 \text{ \AA}$, $b = 16.3 \text{ \AA}$, and $c = 3.9 \text{ \AA}$ for SrCuO_2 (see Ref. [65]), and $a = 3.5 \text{ \AA}$, $b = 3.9 \text{ \AA}$, and $c = 12.7 \text{ \AA}$ for Sr_2CuO_3 (see Ref. [66]). Both systems behave as collections of parallel 1D antiferromagnetic spin-1/2 chains in certain temperature ranges.

2.9 Experimental realizations

In this section, we will discuss several realizations of nonitinerant 1D systems. Bulk structures of cuprate compounds are exemplary systems which behave as a collection of 1D spin chains under certain conditions. The list of cuprates which show this behavior includes materials such as KCuF_3 , [67] Cs_2CoCl_4 , [68] Sr_2CuO_3 , and SrCuO_2 . [69, 70] To gain some more insight, we will consider the case of Sr_2CuO_3 , which is a cuprate with a relatively simple unit cell, see Fig 2.7 (left). Crystals of Sr_2CuO_3 contain 1D structures whose building blocks are CuO_4 quadrilateral structures which share the oxygen ions on adjacent corners. The neighboring magnetic Cu^{2+} ions are rather strongly exchange coupled with strength $J/k_B = 2200 \text{ K}$. [69] This coupling is due to the existence of

a superexchange path along the Cu-O-Cu bond. Furthermore, the inter-chain exchange interaction is expected to be as small as $J_{\perp}/J \sim 10^{-5}$. [71] In accordance with this, it has been observed that the system has 3D long range antiferromagnetic order only at very low temperatures up to around $T_N \sim 5$ K. [72] and undergoes a transition to a 1D ordered state around that temperature. Since there have been no signs of additional phase transitions (such as the commonly occurring spin-Peierls transition) in Sr_2CuO_3 over a temperature range between 5 and 800 K, [66] bulk structures of this cuprate are expected to behave as a collection of parallel spin chains which are described by the spin-1/2 isotropic Heisenberg antiferromagnets up to temperatures higher than 1000 K.

A similar cuprate, SrCuO_2 , has received a lot of attention recently; spin-charge separation was observed in this material using ARPES, [73] and in a recent experiment [74] it has been shown that the cuprate SrCuO_2 has a mean-free path for spinon excitations exceeding $1\mu\text{m}$. The latter shows that ballistic transport of magnetic excitations over relatively long distances in spin chains is indeed possible. As can be seen from Fig. 2.7 (right), SrCuO_2 has a slightly more complicated unit cell compared to Sr_2CuO_3 . SrCuO_2 contains zigzag Cu^{2+} chains due to CuO_4 quadrilateral structures which now share the oxygen ions on adjacent vertices. At low-temperatures, the zigzag chain is frustrated due to the competing antiferromagnetic straight Cu-O-Cu bonds (with strength $J \approx 2100$ K [69]) and the ferromagnetic diagonal Cu-O-Cu bonds (with strength $|J'| \approx (0.1 - 0.2)|J|$. [75]) This frustration, and presumably quantum fluctuations, [74] prevent the system from having long range 3D magnetic order at low temperatures up to $T_N \sim 1.5 - 2$ K. [76, 77] However, since $|J'| \ll |J|$, at higher temperature the diagonal bonds get randomized, and the zigzag chains can be described as two magnetically independent linear spin chains.

Both SrCuO_2 and Sr_2CuO_3 are described by the isotropic 1D $S = 1/2$ Heisenberg Hamiltonian. A material that is described by the anisotropic 1D spin-1/2 Heisenberg Hamiltonian is Cs_2CoCl_4 . Comparison of heat-capacity measurements [78] with numerical simulations, [79] as well as measurements of the in-plane magnetic susceptibility [80, 81] have shown that this system is well-described by the anisotropic Heisenberg Hamiltonian, Eq. (2.1), with antiferromagnetic exchange interaction $J/k_B \sim 3$ K and anisotropy $\Delta \approx 0.25$. The system undergoes a phase transition into the 1D ordered phase at $T_N \approx 0.22$ K. Because of the smaller magnitude of J , the antiferromagnetic order persists up to much lower temperatures than in SrCuO_2 and Sr_2CuO_3 .

2.10 Conclusions

In this chapter we have proposed various realizations of the rectification effect in spin chains, which consist of either ferromagnetically or antiferromagnetically coupled spins, adiabatically connected to two spin reservoirs. For both ferromagnetic and antiferromagnetic spin chains we find that the two crucial ingredients to achieve a nonzero rectification current are an anisotropy in the exchange interaction in combination with an offset magnetic field, both in the z direction. An enhanced anisotropy creates a gap in the excitation spectrum of the spin chain. Using the magnetic field to tune the chemical potential of the excitations to just below the lower edge of the gap then allows us to achieve a large rectification current for realistic values of the applied magnetic field. For antiferromagnetic coupling and suppressed exchange interaction in the z direction we find that a uniform anisotropy is not sufficient to achieve a sizable rectification effect. Instead we use a spatially varying anisotropy, which we attain in the form of a site impurity. Away from half-filling this impurity flows to strong coupling under renormalization, which allows us to achieve a sizable rectification effect for realistic values of the applied magnetic field. We have also proposed several ways to observe this rectification effect. Finally, we have given several examples of experimental realizations of spin chains.

CHAPTER 3

Finite-frequency response

Adapted from:
K. A. van Hoogdalem and D. Loss,
“Frequency-dependent transport through a spin chain”,
Phys. Rev. B **85**, 054413 (2012).

Motivated by potential applications in spintronics, we study frequency dependent transport of magnetization in nonitinerant 1D spin chains. We propose a system that behaves as a capacitor for the spin degree of freedom. It consists of a spin chain with two impurities a distance d apart. We find that at low energy (frequency) the impurities flow to strong coupling, thereby effectively cutting the chain into three parts, with the middle island containing a discrete number of spin excitations. At finite frequencies magnetization transport through the system increases. We find a strong dependence of the finite-frequency characteristics both on the anisotropy of the spin chain and the applied magnetic field. We propose a method to measure the finite-frequency conductance in this system.

3.1 Introduction

Inspired by possible applications in spintronics, we set out to design the spin analogues in insulating magnets of the different components that are used in modern electronics. In the previous chapter, we have shown that systems containing spin chains can be used as a spin diode (Ref. [82]

and Ch. 2). In this chapter, we propose a device based on spin chains that mimics the working of a capacitor, but for the spin degree of freedom. That is, a device which has a spin conductance that is zero for applied DC driving fields and increases with frequency for applied AC driving fields. Traditional capacitors have a wide range of applications in electronics, most notably in frequency selection, noise reduction, and temporary energy storage.

The device that we propose consists of a spin chain with anisotropy Δ_{ij} in the exchange interaction in the z direction, adiabatically connected to two 3D magnetic reservoirs. We introduce two impurities, that each model the replacement of a single atom, in the spin chain. A renormalization group argument shows that the impurities flow to strong coupling at low energies, or, equivalently, low frequencies. At low frequencies the chain is therefore in an insulating state, with an island containing a discrete number of spin excitations in the middle. We show that at higher frequency the spin conductance becomes nonzero; the system undergoes a transition to a conducting state. We show that the point at which this transition occurs can be tuned by an external magnetic field or the bulk anisotropy in the exchange interaction. Transport through double barrier systems has received attention recently, [83, 84, 85, 86, 87] but these studies were restricted to the itinerant electronic case. Here we focus on the nonitinerant magnetic case with an emphasis on applications.

In Section 3.2 we introduce our system and the techniques we use to analyze the system. Explicit expressions for the finite-frequency spin conductance of the system under consideration are derived in Section 3.3. This finite-frequency spin conductance contains all the required information to show that our system behaves as a spin capacitor. In Section 3.4 we present numerical results, conclusions are given in Section 3.5.

3.2 System and model

We have seen in the previous chapter that a spin chain of length L (see Fig. 3.1), which is adiabatically connected to two 3D spin reservoirs, can be described by the anisotropic Heisenberg Hamiltonian

$$H = \sum_{\langle ij \rangle} J_{ij} [S_i^x S_j^x + S_i^y S_j^y + \Delta_{ij} S_i^z S_j^z] + g\mu_B \sum_i B_i S_i^z, \quad (3.1)$$

where the summation is over nearest neighbors, and we avoid double counting of the bonds. Here S_i^α is the α -component of the spin operator at position \mathbf{r}_i . J_{ij} denotes the exchange interactions between the

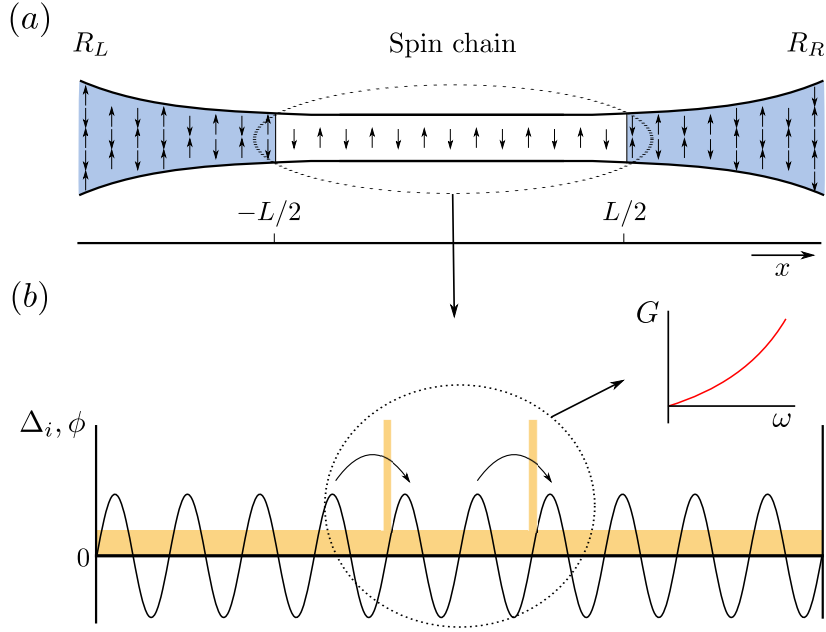


Figure 3.1: (a) Schematic view of the nonitinerant spin system. The 1D spin chain of finite length L is adiabatically connected (meaning that the length of the transition region $L_t \gg 4a$) to two spin reservoirs. (b) Illustration of the working principle behind the spin capacitor. Strong impurities pin the field $\phi(\mathbf{r})$, thereby blocking the system for magnetization transport.

two nearest neighbors at \mathbf{r}_i and \mathbf{r}_j . We assume an, in general spatially varying, anisotropy $\Delta_{ij} > 0$ in the exchange coupling. This anisotropy typically originates either from a Dzyaloshinskii-Moriya (DM) or dipole-dipole interaction between the different spins. [35] The last term in the Hamiltonian describes the Zeeman coupling between the external time-dependent magnetic field, $\mathbf{B}_i(t) = B_i(t)\mathbf{z}$, and the spin operator. \mathbf{z} denotes a unit vector, and the magnetic field is of the form $B_i(t) = B_0 - [1 - \theta(-L/2)] \Delta B \cos \omega t$. For our spin capacitor, we need to introduce two impurities in the spin chain. We propose to use an impurity of a specific type, a single instance of which, located at \mathbf{r}_{i_0} , is described by its anisotropy

$$\Delta_{ij} = \Delta \delta_{i,j-1} (\delta_{i,i_0} + \delta_{i,i_0+1}) \equiv \Delta_{i_0}. \quad (3.2)$$

Such an impurity describes the replacement of a single ion in the spin chain by another ion with a different anisotropy. We choose this form because it contains all the important physics for a general impurity. With two impurities, located at $\mathbf{r}_i = \pm d/2$, and allowing for a constant contri-

bution to the anisotropy, Δ' (which we assume to be smaller than 1), the anisotropy becomes

$$\Delta_{ij} = \Delta_{-d/2} + \Delta_{d/2} + \Delta'. \quad (3.3)$$

It is well known [48] that for the 1D spin chain we can map the Heisenberg Hamiltonian on a fermionic Hamiltonian by means of the Jordan-Wigner transformation. Assuming that $g\mu_B B \ll J$ and $\Delta_{ij} \ll 1$ we can take the continuum limit in the resulting fermionic Hamiltonian, which we can then linearize around the Fermi wave vector. In the process we need to introduce left- and right going fermions $\psi_{L/R}^\dagger(\mathbf{r})$. We can then perform a bosonization procedure [49, 50] using the density field $\phi(\mathbf{r})$ and its conjugate field $\theta(\mathbf{r})$, which satisfy $[\phi(x), \partial_{x'}\theta(x')] = i\pi\delta(x - x')$. Using the fermionic creation operator for $r = L/R$ -going particles

$$\psi_r^\dagger(x) = \frac{1}{\sqrt{2\pi a}} e^{-i\epsilon_r k_F x} e^{i[\epsilon_r \phi(x) - \theta(x)]}, \quad (3.4)$$

where a is the distance between two neighboring spins, and $\epsilon_r = \mp 1$, we arrive at the following real-time action describing the system

$$S[\phi] = S_0[\phi] + S_z[\phi] + S_B[\phi]. \quad (3.5)$$

Here $S_0[\phi]$ is the quadratic action which originates from the in plane terms and the forward scattering terms in the out-of-plane part of the Heisenberg Hamiltonian. It is given by

$$S_0[\phi] = \frac{\hbar}{2\pi K} \int d^2r \left[u (\partial_x \phi(\mathbf{r}))^2 - \frac{1}{u} (\partial_t \phi(\mathbf{r}))^2 \right]. \quad (3.6)$$

Here u is the propagation velocity of the bosonic excitations and K is the Luttinger Liquid interaction parameter which can be determined from the parameters J and Δ' of the spin chain from Bethe-Ansatz methods. [53] We denote $\mathbf{r} = (x, t)$. $S_B[\phi]$ describes the Zeeman coupling between magnetic field and the z component of the spin operator

$$S_B[\phi] = -\frac{g\mu_B}{\pi} \int d^2r \phi(\mathbf{r}) \partial_x B(\mathbf{r}). \quad (3.7)$$

Lastly, $S_z[\phi]$ contains the most relevant contributions coming from the two impurities. We have shown previously that, for an impurity of the form Eq. (3.2) centered at x_0 , the most relevant terms are given by (see Ref. [82] and Ch. 2)

$$S_{x_0}[\phi] = \frac{\sigma}{\pi^2} \int dt \left[\lambda_{x_0}^a \cos 2\phi(x_0, t) + \lambda_{x_0}^b \sin 2\phi(x_0, t) \right]. \quad (3.8)$$

Here, the couplings $\lambda_{x_0}^{a/b}$ are of order $J\Delta$. Also, $\sigma = Kg\mu_B B_0/(\hbar\omega_c)$ is the doping away from half-filling due to the magnetic field B_0 . The UV-cutoff of the theory, ω_c , is on the order of J/\hbar . For our system, $S_z[\phi] = S_{-d/2}[\phi] + S_{d/2}[\phi]$. Note that we must assume here that $2k_F d \neq \pi$, since otherwise the two impurities would cancel each other. To lowest order the backscattering terms flow under renormalization as $1 - K$. Since we work in the regime $1/2 \leq K < 1$ (which corresponds to $0 < \Delta' \leq 1$) the impurities flow to strong coupling for low energies. In this regime, the spin chain is effectively cut into three parts. The middle island ($-d/2 \leq x \leq d/2$) contains a discrete number of excitations, and tunneling through the island is only possible by co-tunneling processes, in which two excitations hop on and off the middle island simultaneously. These processes are strongly suppressed at low temperatures. For finite frequency, processes similar to photon-assisted tunneling become possible, so that we expect the magnetization current through the spin chain to increase as a function of frequency.

From Eq. (3.8) it is seen that the strength of the impurities is proportional to the filling σ . Hence, we can control the finite-frequency characteristics of the system by applying a constant magnetic field B_0 to our system. Most strikingly, this field allows us to control the frequency at which the system will become conducting in the spin sector. Since the Fermi wave vector depends on B_0 , this field also controls the number of spinons that are on the island for a given width d of the island. The number of spinons relative to half-filling can be estimated as $(d/a)\sigma$.

We can model the excitations in the two reservoirs by the quadratic Luttinger Liquid action as well. We will assume two reservoirs that are described by the the anisotropic Heisenberg Hamiltonian with $\Delta = 0$, so that the excitations in the reservoirs are free, and we have $K_r = 1$. For the following it is not strictly nessecary to use a free reservoir, indeed it is enough to have a mismatch in Luttinger Liquid interaction parameter between the spin chain and the two reservoirs.

3.3 Finite-frequency spin conductance

As long as we consider only magnetic fields that point along the quantization axis, the magnetization current $I_m(\mathbf{r})$ through the system can be determined from the conservation of spin, and is given by

$$I_m(\mathbf{r}) = -\frac{g\mu_B}{\pi} \partial_t \phi(\mathbf{r}). \quad (3.9)$$

The nonlocal differential finite-frequency conductivity $\sigma(x, x', \omega)$ is defined as the Fourier transform $\sigma(x, x', \omega) = \int dt e^{i\omega t} \sigma(x, x', t)$ of the real-time linear response of the magnetization current to an infinitesimal change in the time-dependent magnetic field gradient

$$\sigma(x, x', t - t') = \frac{\delta \langle I_m(\mathbf{r}) \rangle}{\delta [\partial_{x'} B(\mathbf{r}')]} \quad (3.10)$$

In circuit theory, the quantity which is of interest is the spin conductance $G(\omega)$, which we define for our system as

$$G(\omega) = \sigma(-L/2, L/2, \omega). \quad (3.11)$$

With this convention a positive magnetic field difference ΔB yields a positive magnetization current for the free system at zero frequency. To calculate the transport properties we use the Keldysh formalism. [61] We assume that at $t = -\infty$ the system is described by the quadratic action $S_0[\phi] + S_B[\phi]$ and that the perturbation $S_z[\phi]$ is turned on adiabatically. We calculate the conductivity to second order in $S_z[\phi]$. In this description the conductivity is given by

$$\sigma(x, x', t - t') = i \frac{g\mu_B}{\pi} \frac{\delta}{\delta [\partial_{x'} B(\mathbf{r}')]} \left(\frac{\delta Z[J]}{\delta J(\mathbf{r})} \right) \Big|_{J=0}. \quad (3.12)$$

Here, $Z[J]$ is the partition function of the system [see Eq. (B.2)], and $J(\mathbf{r})$ a generating functional. The evaluation of Eq. (3.12) can be done using the methods described in Appendix B. We will only summarize the important results here. We can show that the conductivity consists of two contributions

$$\sigma(x, x', \omega) = \sigma_0(x, x', \omega) + \sigma_{\text{BS}}(x, x', \omega). \quad (3.13)$$

The first contribution to the conductivity describes the system in the absence of impurities. It gives the exact magnetization current for the free system, since in the absence of impurities the current is linear in magnetic field gradient. The free conductivity is given by

$$\sigma_0(x, x', \omega) = - \left(\frac{g\mu_B}{\pi\sqrt{\hbar}} \right)^2 (i\omega) iG_0^R(x, x', \omega). \quad (3.14)$$

The retarded Green's function for x, x' in the chain or at the boundaries can be obtained from analytic continuation of the Matsubara Green's

function for the inhomogeneous Luttinger Liquid model. [57] If we assume infinitesimal dissipation in the leads, the retarded Green's function is given by

$$G_0^R(x, x', \omega) = \frac{\pi K}{2\omega} \left\{ 1 + \frac{1}{\gamma^{-1}e^{-i\tilde{\omega}} - \gamma e^{i\tilde{\omega}}} \times \sum_{r=\pm 1} \left[e^{ir\tilde{\omega}(\tilde{x}+\tilde{x}')} + \gamma^r \left(e^{-ir\tilde{\omega}|\tilde{x}-\tilde{x}'|} + r \right) e^{ir\tilde{\omega}} \right] \right\}. \quad (3.15)$$

Here $\gamma = (1 - \kappa)/(1 + \kappa)$ is the reflection coefficient for Andreev-like (in the sense that for some processes the transmission coefficient can be larger than 1) density wave scattering at the chain-reservoir interface, and $\kappa = K/K_r$. The dimensionless frequency $\tilde{\omega} = \omega/\omega_L$, where $\omega_L = u/L$ is the energy scale determined by the finite length of the spin chain. Also $\tilde{x} = x/L$. In the limit $\tilde{\omega} \rightarrow 0$ we have $G = K_r(g\mu_B)^2/h$ as expected.

The quantity $\sigma_{\text{BS}}(x, x', \omega)$ contains corrections to the conductivity coming from the impurities. For the situation with two impurities, it depends on the amplitude and both the absolute and relative position of the impurities, and is given by

$$\sigma_{\text{BS}}(x, x', \omega) = \left(\frac{\pi\sqrt{\hbar}}{g\mu_B} \right)^4 \sum_{\xi, \xi' = \pm d/2} \sigma_{\xi, \xi'}(x, x', \omega). \quad (3.16)$$

As it turns out, the terms with $\xi = \xi'$ reduce to the known result for a single impurity, [62, 88] the terms with $\xi \neq \xi'$ come from interference between the impurities located at $-d/2$ and $d/2$. Here, $\sigma_{\xi, \xi'}(x, x', \omega)$ is given by

$$\begin{aligned} \sigma_{\xi, \xi'}(x, x', \omega) &= -\frac{\sigma_0(x, \xi, \omega)}{\hbar\omega} \left[\sigma_0(\xi', x', \omega) iK(\xi, \xi', \omega) + \right. \\ &\quad \left. -\sigma_0(\xi, x', \omega) iK(\xi, \xi', 0) \right]. \end{aligned} \quad (3.17)$$

$K(\xi, \xi', \omega)$ denotes the retarded backscattering current-backscattering current correlator, which is defined as

$$iK(\xi, \xi', \omega) = \int_0^\infty d\tau e^{i\omega\tau} \langle [I_{\text{BS}}(\xi, \tau), I_{\text{BS}}(\xi', 0)] \rangle. \quad (3.18)$$

The backscattering current operator is defined as

$$\begin{aligned} I_{\text{BS}}(x_0, t) &= \frac{g\mu_B}{\pi\hbar} \frac{\delta S_{x_0}[\phi]}{\delta\phi(x_0, t)} \\ &= 2\frac{g\mu_B}{\pi\hbar} \left[\lambda_{x_0}^b \cos 2\phi(x_0, t) - \lambda_{x_0}^a \sin 2\phi(x_0, t) \right]. \end{aligned} \quad (3.19)$$

In taking the functional derivative, $\phi(x_0, t)$ is regarded as a function of t only. Some lengthy but straightforward algebra shows that we can rewrite Eq. (3.18) as

$$iK(\xi, \xi', \omega) = 2 \left(\frac{g\mu_B}{\pi\hbar} \right)^2 [\lambda_\xi^a \lambda_{\xi'}^a + \lambda_\xi^b \lambda_{\xi'}^b] \int_0^\infty d\tau e^{i\omega\tau} \times \left[e^{2C_0(\xi, \xi', \tau)} - e^{2C_0(\xi', \xi, -\tau)} \right], \quad (3.20)$$

where $C_0(x, x', \tau)$ is the regularized $\phi\phi$ -correlator at zero temperature for the free Luttinger Liquid action on a system of finite length L , given by

$$C_0(x, x', \tau) = \frac{K}{2} \left\{ \sum_{n \in \text{even}} \gamma^{|n|} \ln \left[\frac{n^2 + \alpha^2}{(n + \tilde{x} - \tilde{x}')^2 + \alpha^2(i\bar{\tau} + 1)^2} \right] + \frac{1}{2} \sum_{n \in \text{odd}} \gamma^{|n|} \ln \left[\frac{[(n + 2\tilde{x})^2 + \alpha^2][(n + 2\tilde{x}')^2 + \alpha^2]}{[(n + \tilde{x} + \tilde{x}')^2 + \alpha^2(i\bar{\tau} + 1)^2]^2} \right] \right\}. \quad (3.21)$$

Here $\bar{\tau} = \omega_c \tau$, $\alpha = \omega_L / \omega_c$, and ω_c is the UV-cutoff of the theory, which is on the order of J/\hbar . Finally, we have to replace the bare couplings λ in Eq. (3.20) by the renormalized couplings, given by $(\max[\omega_L, \omega] / \omega_c)^{-1+K} \lambda$. In the next section we will evaluate Eq. (3.16) numerically.

3.4 Results

We have shown in Sec. 3.3 that the spin conductance of our system, defined as $G(\omega) = \sigma(-L/2, L/2, \omega)$, consists of two parts: the free conductance $G_0(\omega)$ and the backscattering conductance $G_{\text{BS}}(\omega)$. These contributions are of opposite sign for low frequencies. Fig. 3.2 (top) shows a plot of $\log_{10} |G_{\text{BS}}(\omega)|$ ($G_{\text{BS}}(\omega)$ is here in units of $(g\mu_B)^2/h$) as a function of $\log_{10}(\omega/\omega_c)$ for different values of the Luttinger liquid parameter K . Different values of K correspond to different values of the constant anisotropy Δ' in the spin chain [see Eq. (3.3)]. It is seen that $G_{\text{BS}}(\omega)$ goes to zero at high frequencies. In the high-frequency regime the spin conductance is therefore determined by the free conductance $G_0(\omega)$ only, and hence the system is conducting. For lower frequencies the backscattering conductance $G_{\text{BS}}(\omega)$ grows, so that the total spin conductance decreases. Since our calculation of $G_{\text{BS}}(\omega)$ is perturbative in the strength of the impurities, we cannot trust our calculations at frequencies $\omega \lesssim \omega^*$, where ω^* is the frequency such that $|G_{\text{BS}}(\omega^*)| = |G_0(\omega^*)|$. Indeed, instead of the

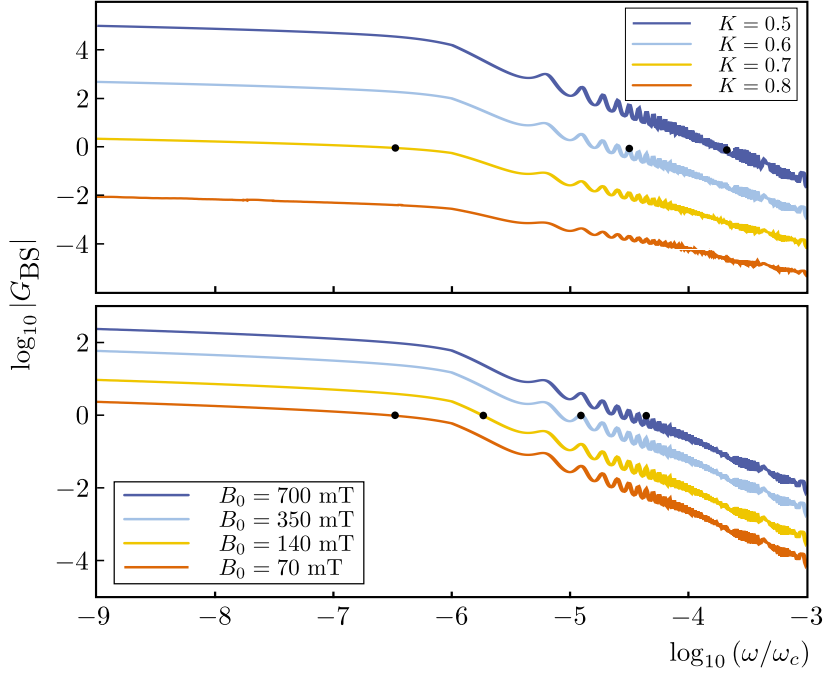


Figure 3.2: (top) Plot of $\log_{10} |G_{\text{BS}}(\omega)|$ (in units of $(g\mu_B)^2/h$) as a function of $\log_{10}(\omega/\omega_c)$ for different values of the Luttinger liquid interaction parameter K (increasing from top to bottom). Used parameters are $B_0 = 70$ mT, $J = 10^2$ K, $L = 10^6 a$, $d = 10^4 a$, $K_r = 1$, and $\Delta = 0.3$. The black dots denote the frequencies ω^* where $|G_0(\omega^*)| = |G_{\text{BS}}(\omega^*)|$. Our perturbative results cannot be used for $\omega < \omega^*$. (bottom) Idem for different values of B_0 (decreasing from top to bottom). Used parameters are $K = 0.7$, $J = 10^2$ K, $L = 10^6 a$, $d = 10^4 a$, $K_r = 1$, and $\Delta = 0.3$. The oscillatory behavior is explained in the caption of Fig. 3.3 and the associated part in the text.

behavior shown in Fig. 3.2 the total spin conductance $G(\omega)$ is approximately zero at frequencies below ω^* . Therefore, ω^* is approximately the frequency at which the system undergoes the transition from insulating to conducting behavior.

Interestingly, we see that the backscattering conductance is strongly dependent on the Luttinger liquid parameter K . If we focus again on the conductance at the frequency ω^* , we see that an increase from $K = 0.6$ to $K = 0.7$ leads to a decrease of the frequency at which the system switches between conducting and insulating behavior of approximately 2 orders of magnitude. We note that we have $\omega_c \approx J/\hbar$, which for $J = 10^2$ K is approximately $\omega_c \approx 2.1 \cdot 10^{12}$ rad s $^{-1}$. The previously discussed increase

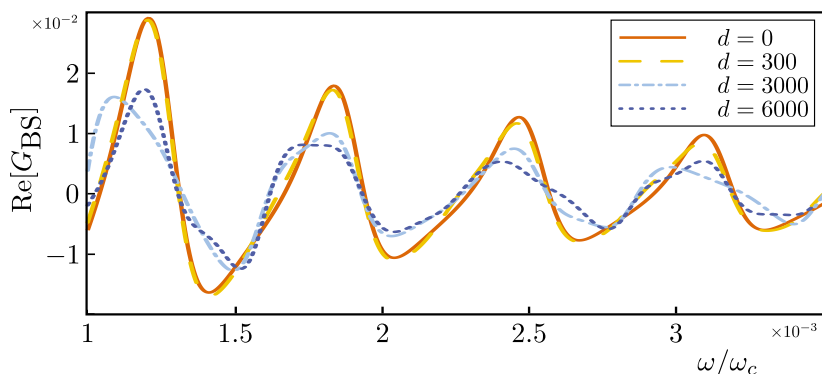


Figure 3.3: Real part of the backscattering conductance $G_{\text{BS}}(\omega)$ as a function of ω/ω_c for different values of the impurity separation d (in units of a). Used values are $B_0 = 1.4$ T, $J = 10^2$ K, $L = 10^4 a$, $K = 0.7$, $K_r = 1$, and $\Delta = 0.2$. It is seen that, independent of d , the conductance oscillates with period $2\pi\omega_L$ (we estimate $(\omega_L/\omega_c) \approx a/L$ here, the values for the free system). The values of d only influences the shape of the oscillations, not the period.

in ω^* is therefore approximately from $7.4 \cdot 10^5$ rad s $^{-1}$ to $6.7 \cdot 10^7$ rad s $^{-1}$.

We see from Fig. 3.2 (bottom) that the frequency ω^* strongly depends on the applied magnetic field B_0 as well. This is caused by the fact that the strength of the impurity is proportional to B_0 , see Eq. (3.8). This strong dependence is convenient for possible applications, since it allows us to create an externally tunable capacitor. For the parameters in Fig. 3.2 we see that by increasing B_0 from $B_0 = 70$ mT to $B_0 = 700$ mT, we can increase ω^* from $7.4 \cdot 10^5$ rad s $^{-1}$ to $9.5 \cdot 10^7$ rad s $^{-1}$.

In Fig. 3.3 we show the dependence of $G_{\text{BS}}(\omega)$ on the distance d between the two impurities. Regardless of d , it is seen that the conductance oscillates with frequency $2\pi\omega_L$ (see caption). These oscillations are caused by interference of the bosonic excitations due to Andreev-like reflections at the boundaries between reservoir and spin chain. It has been shown that, in the presence of a double barrier structure in the chain, additional oscillations with frequency determined by the parameters d/L and $(L-d)/(2L)$ are visible in the current at finite driving field. [87] These oscillations do not show up in the conductance at zero ΔB ; however, they are expected show up in the conductance at finite ΔB . Here, d changes the shape of the oscillations, but not the frequency. All the calculations here were done at $T = 0$. Generally, the effect of finite temperature is to wash out the fluctuations.

The finite-frequency spin conductance could be measured by mea-

asuring the spin accumulation in a system consisting of a spin diode of the form proposed in Ref. [82] in series with the spin capacitor proposed here, between two spin reservoirs. We can apply the driving field $\Delta B(t)$ to the left reservoir, and measure the spin accumulation in the right reservoir. In this setup, the spin accumulation is zero when the spin capacitor is in the insulating state. As was shown in Ref. [82], if we consider 10^4 parallel spin chains with $K = 0.6$ in a magnetic field $B_0 = 750$ mT, and amplitude of the driving field $\Delta B = 43$ mT, we have a spin accumulation of approximately 10^{12} magnons per seconds if the capacitor is in the conducting state.

3.5 Conclusions

In this chapter we have proposed a spin capacitor in a system consisting of a 1D nonitinerant spin chain adiabatically connected to two spin reservoirs. The spin chain is required to have an anisotropy in the exchange interaction. We have shown that the replacement of a single atom in the spin chain leads to a local backscattering term in the Hamiltonian that flows to strong coupling at low energies. By including two such impurities in the spin chain we got a device which is insulating at zero frequency driving field ΔB , and has a spin conductance that grows in magnitude under an increase in frequency of the driving field. We have studied the influence of the anisotropy in the exchange interaction Δ and the external magnetic field B_0 , and have found that both have a strong influence on the finite frequency characteristics of the system. We have proposed a way to measure the effects.

CHAPTER 4

Transistor behavior

Adapted from:
K. A. van Hoogdalem and D. Loss,
“Ultrafast magnon transistor at room temperature”,
Phys. Rev. B **88**, 024420 (2013).

We study sequential tunneling of magnetic excitations in nonitinerant systems through triangular molecular magnets. It is known that the quantum state of these molecular magnets can be controlled by application of an electric- or a magnetic field. Here, we use this fact to control the flow of a pure magnetization current through the molecular magnet by electric- or magnetic means. This allows us to design a system that behaves as a magnon-transistor. We show how to combine three magnon-transistors to form a NAND-gate, and give several possible realizations of the latter, one of which could function at room temperature using transistors with a 11 ns switching time.

4.1 Introduction

In spintronic devices in insulating magnets, information about the logic state can be encoded in collective magnetic excitations, typically either spinons or magnons. [2] Due to the nature of these carriers, power dissipation in such nonitinerant devices is anticipated to be much lower [14, 15] than in their electronic counterparts, as well as in spintronics devices in semiconductors. [89] As excess heating is a limiting factor in modern

electronics, spintronics in insulating magnets is considered a contender to become the next computing paradigm. [22, 24, 26, 30, 82, 90, 91, 92]

Since any classical algorithm can be implemented using a combination of transistors only, the design of this element in insulating magnets is a pivotal issue. Here, we theoretically show that it is possible to make a transistor in which the logic state is encoded in purely magnetic excitations, and whose operation can be controlled by either a magnetic- or electric field. In our transistor, triangular molecular magnets [93, 94, 95, 96, 97] take the role of gate, and we model the source and drain by spin reservoirs. We show that our transistor, which could operate at high clock speed at room temperature, can be used to implement the NAND-gate, one of the two existing universal gates for classical computation.

One of the earliest proposals for a spin-based logic device is the spin-field-effect transistor due to Datta and Das. [8, 98] Other proposals include spin-field-effect transistors in non-ballistic systems [99] and rings, [100] a spin Hall effect transistor, [101] an adiabatic spin transistor, [102] and a bipolar magnetic junction transistor. [103, 104, 105] However, all these proposals have in common the fact that they concern spintronics in semiconductors. In contrast, for the reasons explained above, we focus on spintronics in magnet insulators.

In our system, transport of magnetization occurs primarily by sequential tunneling of magnons (for ferromagnetic reservoirs) or spinons (for antiferromagnetic reservoirs) through a molecular magnet. We will show how it is possible to suppress or increase this sequential tunneling (and thereby switch between the insulating and conducting state of the transistor) by changing the internal state of the molecule through external fields, either electric or magnetic. Molecular magnets are especially suitable due to their chemical variety and controllability, as well as their relatively large size, which makes control of the state easier. For similar reasons, they have been proposed as good building blocks for novel spin-polarized-, [106] as well as quantum computing devices. [107, 108, 109]

This chapter is organized as follows. In Sec. 4.2 we introduce in more detail the previously mentioned system in which we will create our transistor. In Sec. 4.3 we calculate the tunneling rates of magnons/spinons through a triangular molecular magnet, and calculate the spin current through the molecular magnet from these rates. In Sec. 4.4 we show how controlling the state of a molecular magnet by electric- or magnetic fields allows us to design a transistor for either magnons or spinons. In Sec. 4.5 we focus on possible implementations of our transistor. Finally, we discuss certain constraints on our results in Sec. 4.6.

4.2 System

The system we employ consists of a triangular molecular magnet such as $\{\text{Cu}_3\}$ (see Ref. [110]), weakly exchange-coupled to two identical spin reservoirs. Initially, we will assume that a single spin in each reservoir is coupled to a single spin located on a vertex of the triangular molecule, see Fig. 4.1(a)-(b). We will consider both one-dimensional (1D) and two-dimensional (2D) ferromagnetic (FM) spin reservoirs as well as 1D anti-ferromagnetic (AF) spin reservoirs.

Both spin reservoirs, the molecular magnet, and the weak coupling between the subsystems are described by the isotropic Heisenberg Hamiltonian with Dzyaloshinskii-Moriya (DM) interaction

$$H = \sum_{\langle ij \rangle} J_{ij} \mathbf{s}_i \cdot \mathbf{s}_j + \mathbf{D}_{ij} \cdot (\mathbf{s}_i \times \mathbf{s}_j). \quad (4.1)$$

The exchange interaction J_{ij} and DM vector $\mathbf{D}_{ij} = D_{ij} \mathbf{z}$ are assumed to be constant for each subsystem. Here, \mathbf{z} denotes a unit vector. We assume that for the reservoirs $J_{ij} = J$ and $D_{ij} = D$, for the molecule $J_{ij} = J_M$ and $D_{ij} = D_M/\sqrt{3}$, and the coupling between the molecule and the left (right) reservoir is described by Eq. (4.1) with $J_{ij} = J'_{1(2)}$ and $D_{ij} = 0$ [see Fig. 4.1(b)]. We will assume that the J'_i 's set the smallest energy scale in the system, so that we can analyze tunneling processes using perturbation theory. In our model, a finite spin current is induced by application of a magnetic field ΔB to the left spin reservoir, which creates a non-equilibrium distribution of magnetic excitations. In reality, due to the finite lifetime of the magnetic excitations, a steady state spin current has to be generated using e.g. an AC magnet field difference, a static temperature difference, [22] or spin pumping. [21, 24]

When $D_M \ll J_M$, the low-energy subspace of the triangular magnetic molecule consists of a quadruplet with total spin 1/2, and the eigenstates of the Hamiltonian can be labeled as $|m_S, m_C\rangle$ (see Refs. [111, 112]). These states are eigenstates of the z projections of two mutually commuting effective spin-1/2 degrees of freedom: the total-spin operator $\mathbf{S} = \mathbf{s}_1 + \mathbf{s}_2 + \mathbf{s}_3$ (with eigenvalues $m_S = \pm 1/2$) and the chirality operator \mathbf{C} (with eigenvalues $m_C = \pm 1$). The chirality operator can be defined by its z component: $C^z = (4/\sqrt{3}) \mathbf{s}_1 \cdot (\mathbf{s}_2 \times \mathbf{s}_3)$. An in-plane electric field $\mathbf{E} = E^x \mathbf{x} + E^y \mathbf{y}$ couples to the chirality through the spin-electric effect; [111, 112, 113] the coupling of a magnetic field $\mathbf{B} = B \mathbf{z}$ to the total spin is described by the Zeeman interaction. Here, \mathbf{x} , \mathbf{y} , and \mathbf{z} denote unit vectors. The Hamiltonian for the low-energy subspace is [111, 112]

$$H_M = g_M \mu_B B S^z + d \mathbf{E}' \cdot \mathbf{C}^{\parallel} + D_M S^z C^z. \quad (4.2)$$

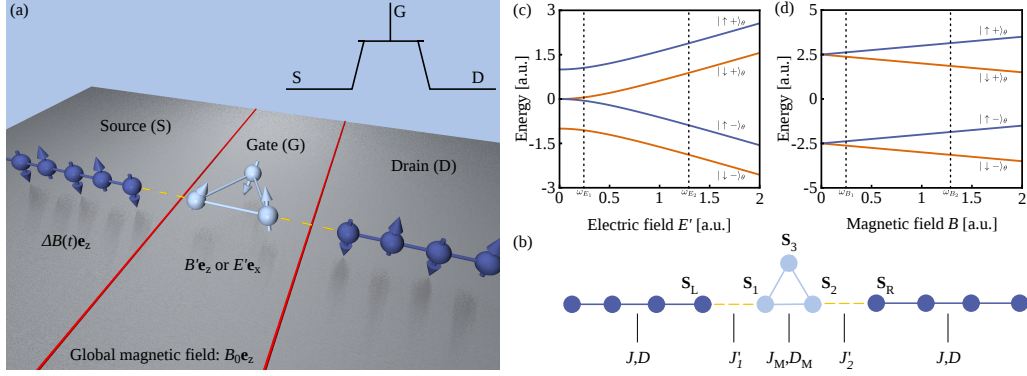


Figure 4.1: (a)-(b) Pictorial representation of a single purely magnetic spin transistor, including Heisenberg parameters of the subsystems and the different magnetic- and electric fields. The field B_0 is applied to both spin reservoirs (here shown as 1D AF spin chains) and the molecular magnet, the magnetic field $\Delta B(t)$ is applied only to the left reservoir, and the fields E' and B' are applied only to the molecular magnet. The left reservoir acts as source-terminal of the transistor, the molecular magnet as gate, and the right reservoir as drain (see inset). (c)-(d) Excitation spectrum corresponding to the Hamiltonian in Eq. (4.2). In (c) we choose $g_M \mu_B B = D_M = 1$, in (d) we put $D_M = 5$ and $E' = 0$.

We split the magnetic field $\mathbf{B} = B\mathbf{z}$ that is applied to the molecular magnet into two contributions, $B = B' + B_0$, where B' is the magnitude of a local magnetic field that is applied only to the molecular magnet, and B_0 is the magnitude of a global magnetic field that is applied to the entire system [see Fig. 4.1(a)]. Furthermore, d is the effective dipole moment of the molecule, E' is the rotated electric field, [111, 112] and $\mathbf{C}^\parallel = C^x \mathbf{x} + C^y \mathbf{y}$. The g -factor of the molecular magnet is denoted g_M .

Assuming that $\mathbf{E}' = E' \mathbf{x}$, we can rewrite Eq. (4.2) in diagonal form as

$$H_M = g_M \mu_B B S_\theta^z + 2\sqrt{(D_M/2)^2 + (dE')^2} S_\theta^z C_\theta^z. \quad (4.3)$$

Here, \mathbf{S}_θ (\mathbf{C}_θ) denotes the total-spin (chirality) operator with respect to the basis given by $|\uparrow, +\rangle_\theta = \sin \theta |\uparrow, +\rangle + \cos \theta |\uparrow, -\rangle$, $|\uparrow, -\rangle_\theta = -\cos \theta |\uparrow, +\rangle + \sin \theta |\uparrow, -\rangle$, and $|\downarrow, +\rangle_\theta$, $|\downarrow, -\rangle_\theta$ the same but with the total spin flipped and $\theta \rightarrow -\theta$. We defined $\tan \theta = [\sqrt{(D_M/2)^2 + (dE')^2} + D_M/2]/dE'$. The spectrum of the triangular molecular magnet is depicted in Fig. 4.1(c)-(d).

In the setup depicted in Fig. 4.1(a), tunneling of magnetic excitations between the left (right) spin reservoir and the molecular magnet is described by the isotropic Heisenberg exchange interaction between $\mathbf{s}_{L(R)}$

and $\mathbf{s}_{1(2)}$ [see Fig. 4.1(b)]. The corresponding Hamiltonian is given by $H_{L(R)} = J'_{1(2)} \mathbf{s}_{L(R)} \cdot \mathbf{s}_{1(2)}$. Later, we will also consider the scenario in which a spin \mathbf{s}_M in a reservoir is coupled to the third vertex of the triangular molecular magnet, \mathbf{s}_3 . The Hamiltonian that describes this coupling is given by $H_M = J'_3 \mathbf{s}_M \cdot \mathbf{s}_3$.

We want to find the effective Hamiltonian that describes the coupling $J'_i \mathbf{s}_j \cdot \mathbf{s}_i$ between a spin \mathbf{s}_i on the molecular magnet and a spin \mathbf{s}_j in a reservoir (hence $\{i, j\} = \{1, L\}, \{2, R\}, \{3, M\}$) within the low-energy subspace of the molecular magnet spanned by the basis $|m_S, m_C\rangle$ defined above. In doing so, we neglect transitions to the higher-lying $\mathbf{S} = 3/2$ subspace of the molecule. This is allowed as long as we restrict ourselves to energies much smaller than J_M . By evaluating all relevant matrix elements $\langle m_S, m_C | J'_i \mathbf{s}_j \cdot \mathbf{s}_i | m'_S, m'_C \rangle$, we find the effective Hamiltonian

$$H_j = \mathbf{s}_j \cdot \bar{\bar{J}}_i(\mathbf{C}_\theta) \cdot \mathbf{S}_\theta + K_i s_j^z C_\theta^z. \quad (4.4)$$

Here, $\bar{\bar{J}}_i(\mathbf{C}_\theta)$ is an antisymmetric 3×3 -matrix. We interpret the first term in Eq. (4.4) as effectively describing tunneling of spin excitations from the spin reservoir onto the total spin of the molecular magnet and vice versa, with a tunneling strength that depends on the chirality state of the molecule. This term leads therefore to magnetization transport and is the one of interest to us. The second term does not induce hopping of magnetic excitations. We will show at the end of this section that its main effect for FM reservoirs is that of a static perturbation on the chirality state of the molecule, due to the static equilibrium magnetization Sz of a FM reservoir. In Sec. 4.3 we will show that s_j^z is not the most relevant operator (in the renormalization-group sense) for AF reservoirs, so that we can ignore the second term for AF reservoirs.

The matrix $\bar{\bar{J}}_i(\mathbf{C}_\theta)$ can be written generally as

$$\bar{\bar{J}}_i(\mathbf{C}_\theta) = \frac{J'_i}{3} \begin{pmatrix} A_i & B_i & 0 \\ -B_i & A_i & 0 \\ 0 & 0 & C_i \end{pmatrix}. \quad (4.5)$$

We find that $A_1 = -\cos(2\theta) - 2C_\theta^x$, $B_1 = -\sin(2\theta)C_\theta^y$, and $C_1 = 1 + 2\cos(2\theta)C_\theta^x$. Furthermore, $A_2 = -\cos(2\theta) + C_\theta^x - \sqrt{3}\cos(2\theta)C_\theta^y$, $B_2 = -\sqrt{3}\sin(2\theta) - \sin(2\theta)C_\theta^y$, and $C_2 = 1 + \sqrt{3}C_\theta^y - \cos(2\theta)C_\theta^x$. Lastly, we find $A_3 = -\cos(2\theta) + C_\theta^x + \sqrt{3}\cos(2\theta)C_\theta^y$, $B_3 = \sqrt{3}\sin(2\theta) - \sin(2\theta)C_\theta^y$, and $C_3 = 1 - \sqrt{3}C_\theta^y - \cos(2\theta)C_\theta^x$. The different functions K_i are given by $K_1 = -\sin(2\theta)$ and $K_2 = K_3 = \sin(2\theta)/2$.

We note that in the scenario where a single reservoir-spin $\mathbf{s}_{L(R)}$ is exchange-coupled to all three spins \mathbf{s}_i of the molecular magnet with equal strength

J' , and we also put $E' = 0$, the effective Hamiltonian is simply $J' \mathbf{s}_{L(R)} \cdot \mathbf{S}_\theta$. In this case, the tunneling of magnetic excitations no longer depends on the chirality of the molecule.

The first thing we see from Eq. (4.4) is that a static equilibrium magnetization Sz of a reservoir acts as a constant perturbation on the state of the molecular magnet through the relevant exchange interaction between reservoir and molecule. We will show that it is possible to make this perturbation trivial, or even beneficial to our purposes, in all cases under consideration. Additional dynamics of the systems is due to the behavior of magnetic excitations which exist on top of the equilibrium magnetization. We will study this dynamics next.

4.3 Transition rates and spin current

To determine the spin current through the molecular magnet for the setup in Fig. 4.1(a), we use a master-equation approach. We assume that energy is conserved in all tunneling processes, and ignore higher-order effects. The transition rates from initial state $|i\rangle$ to final state $|f\rangle$ due to tunneling processes between the left (right) reservoir and the molecule are denoted by $R_{if}^{L(R)}$. Using Fermi's golden rule, we can calculate $R_{if}^{L(R)}$ to second order in $J'_{1(2)}$. We find

$$R_{if}^L = \frac{1}{\hbar^2} \int_{-\infty}^{\infty} d\tau \langle i | H'_L(\tau) | f \rangle \langle f | H'_L(0) | i \rangle. \quad (4.6)$$

The rates R_{if}^R are given by Eq. (4.6) with H'_L replaced by H'_R . The apostrophe denotes an operator in the interaction representation with respect to the Hamiltonian of the uncoupled subsystems. The nontrivial part of the problem reduces then to finding correlation functions such as $\langle s_L^+(\tau) s_L^-(0) \rangle$ in the spin reservoirs, where $s_L^{+(-)}(\tau)$ denotes the spin raising (lowering) operator. In the next two sections we will find the relevant expressions for both FM and AF spin reservoirs.

Calculation of the spin current requires both the transition rates as well as the probabilities P_i that the molecule is in the state $|i\rangle$. We define the vector $\mathbf{P} = (P_{\uparrow+}, P_{\uparrow-}, P_{\downarrow+}, P_{\downarrow-})$. The time evolution of the occupation probability vector \mathbf{P} is then given by $d\mathbf{P}/dt = \hat{R}\mathbf{P}$, where \hat{R} is the 4x4 matrix that contains the appropriate transition rates. The steady state probabilities are contained in the kernel of \hat{R} , normalized such that $\sum_i P_i = 1$. Hence, \mathbf{P} is uniquely determined by the transition rates. The spin current I_S is then defined as the net rate with which excitations leave the left

reservoir

$$I_S = (R_{\downarrow+\uparrow+}^L + R_{\downarrow+\uparrow-}^L) P_{\downarrow+} + (R_{\downarrow-\uparrow+}^L + R_{\downarrow-\uparrow-}^L) P_{\downarrow-} - (R_{\uparrow+\downarrow+}^L + R_{\uparrow+\downarrow-}^L) P_{\uparrow+} - (R_{\uparrow-\downarrow+}^L + R_{\uparrow-\downarrow-}^L) P_{\uparrow-}. \quad (4.7)$$

Next, we will calculate the relevant transition rates for the different types of reservoirs.

FM reservoirs

We first consider the simplest case of tunneling of magnons between a triangular molecular magnet and 1D FM reservoirs. We assume for simplicity that the FM reservoirs are described by the isotropic Heisenberg Hamiltonian, *i.e.* $D = 0$. Using the Holstein-Primakoff transformation,[2] we can map a 1D FM system with spins $S \gg 1/2$ on a system of non-interacting bosonic particles (magnons). In the presence of a magnetic field $B_0 \mathbf{z}$, these magnons have a dispersion $\hbar\omega_q = 4|J|S \sin^2(qa/2) + g_R \mu_B B_0$. Here, q is the wave vector of the magnons, a is the lattice spacing of the reservoir, and g_R is the g -factor of the reservoir. The Holstein-Primakoff transformation allows us to obtain the correlation functions that are required to find the transition rates by rewriting $\langle s_L^+(\tau) s_L^-(0) \rangle$ etc. in terms of the bosonic operators a_q^\dagger, a_q . We find the rates

$$R_{\uparrow+\downarrow+}^L = \left(\frac{J_1^L \xi_+^L}{3\hbar} \right)^2 \frac{S}{2\pi} K_{\text{FM}}(\omega_B + \omega_E - \omega_{\Delta B}),$$

$$R_{\uparrow+\downarrow-}^L = \left(\frac{J_1^L \eta_+^L}{3\hbar} \right)^2 \frac{S}{2\pi} K_{\text{FM}}(\omega_B - \omega_{\Delta B}). \quad (4.8)$$

The energy scales are given by $\hbar\omega_B = g_M \mu_B B$, $\hbar\omega_{\Delta B} = g_R \mu_B \Delta B$, and $\hbar\omega_E = 2\sqrt{(D_M/2)^2 + (dE')^2}$. Also, $\xi_+^L = \cos(2\theta)$ and $\eta_+^L = 2 - \sin(2\theta)$. Furthermore, $K_{\text{FM}}(\omega) = \rho_{\text{1D}}(\omega_q) [1 + n_B(\omega_q)]|_{\omega_q=\omega}$, where $\rho_{\text{1D}}(\omega_q) = a |\partial\omega_q/\partial q|^{-1}$ is proportional to the density of states (DOS) in the reservoir, and $n_B(\omega_q)$ is the Bose-Einstein distribution of the magnons.

To get the other rates, we note that the only effect of inverting the total spin while keeping chirality unchanged (in the initial and final state simultaneously) is to replace $1 + n_B(\omega_q) \rightarrow n_B(\omega_q)$ as well as $\xi_+^L \rightarrow \xi_-^L = \xi_+^L$ and $\eta_+^L \rightarrow \eta_-^L = 2 + \sin(2\theta)$ in Eqs. (4.8); inverting both the chiralities while keeping the total spin constant changes $\omega_E \rightarrow -\omega_E$, $\xi_+^L \rightarrow \xi_-^L$, and $\eta_+^L \rightarrow \eta_-^L$; finally, flipping both total spins and chiralities simultaneously requires us to replace $1 + n_B(\omega_q) \rightarrow n_B(\omega_q)$ and $\omega_E \rightarrow -\omega_E$.

To obtain the rates for tunneling between the molecule and the right reservoir, we put $\omega_{\Delta B} = 0$ in Eqs. (4.8) and the derived rates. Furthermore, we replace $\xi_{\pm}^L \rightarrow \xi_{\pm}^R = |\cos(2\theta) + i\sqrt{3}\sin(2\theta)|$, $\eta_{\pm}^L \rightarrow \eta_{\pm}^R = 2|1 \pm \sin(2\theta) + i\sqrt{3}\cos(2\theta)|$, and $J'_1 \rightarrow J'_2$.

The transition rates due to a coupling H_M can be calculated analogously, and we refrain from repeating those steps here. For the chosen setup, the resulting rates due to a coupling H_M are the same as those due to a coupling H_R , except for the replacement $J'_2 \rightarrow J'_3$. We also mention here that in the remainder of this work we will always choose our parameters (specifically J'_1, J'_2 , and possibly J'_3) in such a way that processes that only flip the chirality but not the total spin [such processes would be described for instance by a term $s_j^z C_{\theta}^x$ in Eq. (4.4)] cannot occur. Hence, we can put these rates to zero.

To obtain the rates for a system with 2D FM reservoirs, we simply replace $\rho_{1D}(\omega_q)$ in Eqs. (4.8) by the 2D DOS, which for small $|\mathbf{q}|$ is given by $\rho_{2D}(\omega_q) = \hbar/(4S|J|)$.

AF reservoirs

Next, we will derive the rates for tunneling of spinons between semi-infinite AF spin-1/2 chains and a triangular molecular magnet. In order to do so, we start by giving a description of the spin chains in terms of Luttinger liquid theory, which turns out to be a convenient framework for our purpose. For concreteness, we focus on the description of the left spin chain. Eq. (4.1) can then be mapped on the anisotropic Heisenberg Hamiltonian with anisotropy $\Delta = J/\sqrt{J^2 + D^2}$ by performing a position-dependent rotation in spin space. After performing a Jordan-Wigner transformation, taking the continuum limit of the resulting fermionic Hamiltonian, and subsequent bosonization, the resulting Hamiltonian describing the left spin chain [for which $x \in (-\infty, 0)$] becomes [48]

$$H_L = \frac{\hbar}{2\pi} \int_{-\infty}^0 dx \left[uK (\partial_x \vartheta(x))^2 + \frac{u}{K} (\partial_x \varphi(x))^2 \right]. \quad (4.9)$$

The bosonic density field $\varphi(x)$ and its conjugate momentum field $\vartheta(x)$ satisfy $[\varphi(x), \partial_{x'} \vartheta(x')] = i\pi\delta(x - x')$. The sound velocity u of the bosonic excitations as well as the interaction parameter K can be determined from the parameters J and D of the spin chain using Bethe Ansatz results. [53] At the isotropic point $K = 1/2$, and $K = 1$ describes the free model. To analyze the hopping between spin chain and molecular magnet, we will need the continuum form of the spin operators in the spin

chain. These are given by [51]

$$\begin{aligned} s^-(x) &= \frac{e^{i\vartheta(x)}}{\sqrt{2\pi a}} (-1)^x [\cos(2\varphi(x) - 2k_F x) + 1], \\ s^z(x) &= -\frac{1}{\pi} \partial_x \varphi(x) + \frac{1}{\pi a} \cos[2\varphi(x) - 2k_F x]. \end{aligned} \quad (4.10)$$

Here, a is the lattice spacing of the spin chain, and $k_F = \pi/2a + g_R \mu_B B_0 / u \hbar$ is the Fermi wave vector. For simplicity, we will ignore the small contribution proportional to B_0 in the expression for the Fermi wave vector. Since the spin chain is semi-infinite (with its last spin at $x = -a$), we require that the wave function vanishes at the origin. This constrains the density field to a constant value at the origin, such that $\cos \varphi(0) = 0$. To analyze the behavior of the spin fields at the origin, we introduce chiral fields $\varphi_{L/R}(x) = K\vartheta(x) \pm \varphi(x)$, which are related on the entire space by the constraint on the density field at the origin. [51] This allows us to map Eq. (4.9) on a quadratic Hamiltonian that only depends on $\varphi_L(x)$. Performing a renormalization group (RG) analysis on the spin operators near the boundary then yields that $s^z(0)$ is a marginal operator, and $s^\pm(0)$ scales as $1 - 1/(2K)$, so that it is relevant for systems with finite DM interaction. Since $s^z(0)$ is less relevant than $s^\pm(0)$, we will ignore the former in our perturbative analysis (assuming low enough energies). This allows us to ignore perturbations due to the interaction between the molecular magnet and the $s^z(0)$ terms in Eq. (4.4) for AF reservoirs. Since the RG flow is stopped either by temperature or by the relevant energy scale E_M of the molecular magnet, this gives the constraint on the tunneling $J'_i [\max(k_B T, E_M)/J]^{-1+1/(2K)} \ll J$ for our sequential tunneling approach to be valid.

In order to calculate the required transition rates, we need to calculate spin-spin correlation functions at the boundary of the spin chain. Since the density field is constant at the boundary, the sole relevant correlation function is that of the momentum field $\vartheta(t) \equiv \vartheta(0, t)$. At finite temperature T , it is given by

$$\langle [\vartheta(t) - \vartheta(0)]^2 \rangle = \frac{2}{K} \ln \left[\left(\frac{i\hbar\omega_C}{\pi\theta_0} \right) \sinh \left(\frac{\pi\theta_0 [t - i\delta]}{\hbar} \right) \right]. \quad (4.11)$$

Here, $\theta_0 = k_B T$, and ω_C is the UV-cutoff of the theory. For this model it is approximated as $\omega_C \approx J/\hbar$. δ is a positive infinitesimal. The analysis of the right spin chains goes along the same lines, and we will refrain from repeating the steps here.

To calculate the transition rates for AF reservoirs we substitute Eqs. (4.10) in Eq. (4.6). Using the correlation function Eq. (4.11) and the fact that $\varphi(x)$ is constant at the boundary then gives the rates

$$\begin{aligned} R_{\uparrow+\downarrow+}^L &= \left(\frac{J'_1 \zeta_+^L}{3\hbar\omega_C} \right)^2 K_{\text{AF}}(\omega_B + \omega_E - \omega_{\Delta B}), \\ R_{\uparrow+\downarrow-}^L &= \left(\frac{J'_1 \nu_+^L}{3\hbar\omega_C} \right)^2 K_{\text{AF}}(\omega_B - \omega_{\Delta B}). \end{aligned} \quad (4.12)$$

Here, $\zeta_+^L = d_L \cos(2\theta)/2$, $\nu_+^L = d_L[1 - \sin(2\theta)/2]$, and $d_L = \sqrt{2/\pi}$. We have ignored a small k_F -dependent contribution to d_L here. The function $K_{\text{AF}}(\omega)$ describes the influence of the spin chain on the transition rate and is given by

$$\begin{aligned} K_{\text{AF}}(\omega) &= \omega_C^2 \int_{-\infty}^{\infty} d\tau e^{i\omega\tau} e^{-\frac{1}{2}([\vartheta(\tau) - \vartheta(0)]^2)} \\ &= \omega_T \left(\frac{\omega_T}{\omega_C} \right)^{-2 + \frac{1}{K}} e^{\pi\omega/\omega_T} \frac{|\Gamma(1/(2K) + i\omega/\omega_T)|^2}{\Gamma(1/K)}. \end{aligned} \quad (4.13)$$

Here, $\omega_T = 2\pi\theta_0/\hbar$.

To get the other rates, we note that the only effect of inverting the total spin while keeping chirality unchanged (in the initial and final state simultaneously) is to change the sign of ω_B , $\omega_{\Delta B}$, and ω_E , as well as to $\zeta_+^L \rightarrow \zeta_-^L = \zeta_+^L$ and $\nu_+^L \rightarrow \nu_-^L = d_L[1 + \sin(2\theta)/2]$; inverting both the chiralities while keeping the total spin constant changes $\omega_E \rightarrow -\omega_E$, $\zeta_+^L \rightarrow \zeta_-^L$, and $\nu_+^L \rightarrow \nu_-^L$; finally, flipping both total spins and chiralities simultaneously requires us to change the sign of ω_B and $\omega_{\Delta B}$ only.

To obtain the rates with the respect to the right spin chain, we put $\omega_{\Delta B} = 0$ in Eqs. (4.12) and the derived rates. Furthermore, we replace $\zeta_{\pm}^L \rightarrow \zeta_{\pm}^R = d_R |\cos(2\theta) + i\sqrt{3}\sin(2\theta)|/2$, $\nu_{\pm}^L \rightarrow \nu_{\pm}^R = d_R |1 \pm \sin(2\theta) + i\sqrt{3}\cos(2\theta)|/2$, and $J'_1 \rightarrow J'_2$. The constant $d_R = d_L$.

The transition rates due to a coupling H_M can be calculated analogously, and we refrain from repeating those steps here. As in the FM case, the resulting rates are the same as those due to a coupling H_R for the chosen setup, except for the replacement $J'_2 \rightarrow J'_3$.

We note that processes that flip chirality but not the total spin are proportional to s_j^z . Since we have shown that this operator is less relevant than s_j^{\pm} , we can ignore such processes and put these rates to zero.

At this point, we have derived the transition rates for both AF and FM reservoirs. As we have seen, the main difference in the resulting

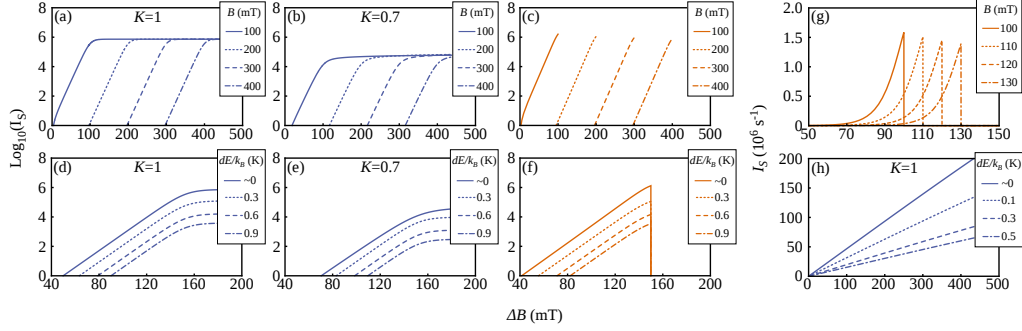


Figure 4.2: (a)-(b) $\log_{10}(I_S)$ versus ΔB for different values of the magnetic field B , for 1D AF reservoirs with different Luttinger liquid parameters K . Due to the gapless nature of the spinons, we can always set $B = B_0$ and $B' = 0$ when considering AF reservoirs. (c) $\log_{10}(I_S)$ versus ΔB for different values of the magnetic field B , for 1D FM reservoirs. Here, $B_0 = 1 \mu\text{T}$ and $B' \approx B$. (d)-(e) $\log_{10}(I_S)$ versus ΔB for different values of dE' , for AF reservoirs with different Luttinger liquid parameters K . We assumed $D_M/k_B = 0.6 \text{ K}$ and $B_0 = 150 \text{ mT}$. (f) $\log_{10}(I_S)$ versus ΔB for different values of dE' , for the FM system. Here, $B_0 = 1 \mu\text{T}$ and $B' = 150 \text{ mT}$. We assumed $D_M/k_B = 0.6 \text{ K}$. (g) Illustration of the alternative switching mechanism for FM reservoirs. When the level splitting of the molecular magnet is smaller than the minimum energy of a magnon in the lead, the system is in the insulating phase. Again, $B_0 = 1 \mu\text{T}$. The plots (a)-(g) are for parameters $J/k_B = 100 \text{ K}$, $T = 10 \text{ mK}$, and $J'_1/k_B = J'_2/k_B = 0.05 \text{ K}$ (see text). For the FM plots, $S = 1$. In (d)-(f) we have assumed that the left (right) reservoir is coupled to spin 2(3) in the molecular magnet with strength $J'_{1(2)}$. This setup is beneficial, since in this way both reservoirs decouple from the molecular magnet for $dE' \gg D_M$. (h) I_S versus ΔB for different values of dE' for the AF system, at an experimentally accessible temperature. Parameters are $J/k_B = 100 \text{ K}$, $J'/k_B = 2 \text{ K}$, $D_M/k_B = 0.3 \text{ K}$, $B = 75 \text{ mT}$, and $T = 1 \text{ K}$.

rates is the replacement of the bosonic DOS and distribution function by correlation functions typical for Luttinger liquid models. We note here that, at low energies, the bosonic character of the magnons in the FM system yields larger spin currents than the fermionic spinons, which is extremely beneficial for the application we have in mind here.

4.4 Transistor behavior

Next, we discuss two different ways in which our setup can be used as a logic switch whose working is controlled by an external magnetic field. This is one of two functionalities of a transistor, the other being that of amplification of a signal. We will briefly get back to this second functionality later in this section. For the description of the first mechanism by which our setup can be used as a logic switch, we assume that $k_B T \ll \hbar\omega_{\Delta B}, \hbar\omega_B \ll D_M$, so that we only need to take the states $|\uparrow, -\rangle_\theta$ and $|\downarrow, +\rangle_\theta$ into account. We will assume $B_0 = 0$ in our explanation for simplicity. Referring back to Fig. 4.1(d), we see that spin transport through the molecule will be strongly suppressed for magnetic field differences such that $\omega_{\Delta B} \ll \omega_B$, since in this regime the vast majority of the excitations in the reservoirs lack the required energy to induce a spin-flip on the molecule; For $\omega_{\Delta B} \lesssim \omega_B$, transport increases rapidly with $\omega_{\Delta B}$. Hence, for magnetic field gradients $\omega_{\Delta B} \approx \omega_{B_1}$, our setup can be switched between the insulating- (for $\omega_B \approx \omega_{B_2}$) and conducting (for $\omega_B \approx \omega_{B_1}$) state. This is shown in Fig. 4.2(a)-(c).

The system with FM reservoirs offer an additional possibility to switch between the insulating and conducting state: When $\omega_{\Delta B} > \omega_B$, the minimum energy of the magnons in the reservoir exceeds the level splitting of the molecular magnet. In this case, the system is also insulating (neglecting higher order processes). This behavior has been indicated in Fig. 4.2(g). The use of this mechanism to switch between insulating and conducting states requires smaller magnetic fields compared to the previously discussed mechanism. Furthermore, this method does not require the assumptions on temperature put forward in the previous paragraph.

The second scheme may allow us to achieve amplification of an input signal in systems with FM reservoirs under certain conditions. We consider the magnetic field B applied to the molecular magnet to be the input signal, and the magnetization of the drain to be the output signal. ΔB is assumed to be constant. It is important to remember that the bosonic distribution of magnons is peaked at low energies, *i.e.* $n_B(\omega_q) \gg 1$ at small ω_q and low temperatures. This translate into sizable currents at given (small) values of ΔB when the system is in the conducting phase. By switching ω_B between just below $\omega_{\Delta B}$ and just above $\omega_{\Delta B}$, we can then control this relatively large spin current by a small change in B . This can be viewed as a type of amplification.

Lastly, we will discuss how the switching behavior can be controlled by an electric field. The mechanism is different from that for magnetic control, since an electric field does not influence the splitting between

the two lowest states with opposite total spin. However, we note that when $k_B T, \hbar\omega_{\Delta B}, \hbar\omega_B \ll \hbar\omega_E$, transport occurs through transitions between states in the subspace spanned by $|\uparrow, -\rangle_\theta$ and $|\downarrow, +\rangle_\theta$; transitions to the states $|\uparrow, +\rangle_\theta$ and $|\downarrow, -\rangle_\theta$ are forbidden under these conditions since they cannot conserve energy. To illustrate the mechanism through which we can control the switching behavior by an electric field, we note that it follows from the expressions for the transition rates $R_{\uparrow\downarrow}^R$ and $R_{\downarrow\uparrow}^R$ in the previous sections that when $\theta \rightarrow \pi/4$, i.e. when $dE' \gg D_M$, the molecular magnet and the right spin reservoir are effectively decoupled in the low-energy subspace in the setup described there. This can be seen from the fact that the prefactors $\eta_{\pm}^R, \nu_{\pm}^R \rightarrow 0$ for $\theta \rightarrow \pi/4$.

Fig. 4.2(d)-(f) shows this switching behavior as a function of applied electric field. To determine the required strength of the electric field, we note that if we assume that the effective dipole moment lies between $d = (10^{-4} - 1)eR$ (see Ref. [113]), where $R \approx 1$ nm is the bond length of the molecular magnet, then $dE'/k_B = 0.1$ K corresponds to an electric field $E' \sim (10^8 - 10^4) \text{ V m}^{-1}$.

In Fig. 4.2 we assumed in plane Heisenberg exchange interaction between reservoirs and vertices for all AF reservoirs. This is motivated by the fact that the $s^z(0)$ -operator in the AF reservoirs is irrelevant compared to the $s^\pm(0)$ operators. For FM reservoirs we assumed isotropic coupling J'_1 and J'_2 . Additionally, we assumed that the third vertex of each molecular magnet is coupled to a separate reservoir by an Ising-like interaction with strength $J'_3 = J'$. The reason behind this assumption is that in this way the sole effect of the equilibrium magnetization of the reservoirs on the Hamiltonian of the molecular magnets is to act as an effective magnetic field $J'Sz$. This effective field for the parameters in Fig. 4.2 (a)-(g) is on the order of 75 mT, and can take the role of B' . This reduces (or could even completely take over the role of) the required external magnetic field B' . We emphasize that the assumption of coupling to an additional third reservoir will not be needed for the experimental realizations of the magnon-transistor in the next section.

4.5 Experimental realizations

A single magnetic dipole moving with constant velocity \mathbf{v} gives rise to a magnetic field $\mathbf{B}_{\text{dip}}(\mathbf{r}) = \frac{\mu_0}{4\pi} \frac{g\mu_B}{r^3} [3(\mathbf{z} \cdot \hat{\mathbf{e}}_r) \hat{\mathbf{e}}_r - \mathbf{z}]$ in its rest frame, as well as an electric field $\mathbf{E}_{\text{dip}}(\mathbf{r}) = \mathbf{v} \times \mathbf{B}_{\text{dip}}(\mathbf{r})$ in the laboratory frame. Conceivably, it is therefore possible to use the setup depicted in Fig. 4.3(a) to measure the switching behavior of a collection of spinon-transistors due

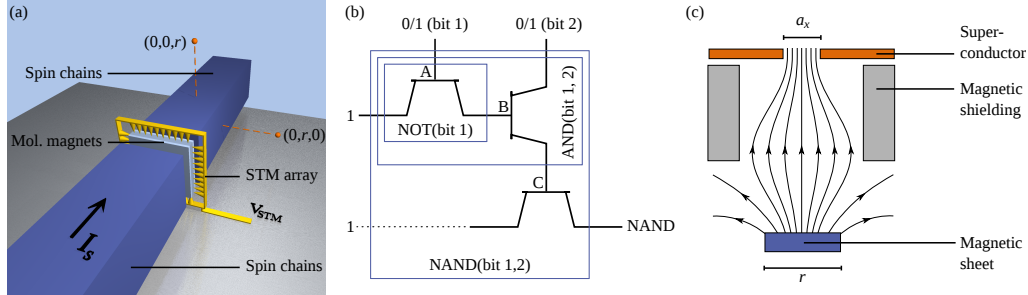


Figure 4.3: (a) Proposed setup to measure the switching effect due to the spin-electric effect. The setup consists of a single-layer crystal of triangular magnets, of dimension $0.2 \times 0.2 \mu\text{m}$. The crystal contains $\sim 4 \cdot 10^4$ molecules, given a lattice constant of 1 nm. The crystal is weakly exchange-coupled to a bulk collection of AF 1D spin chains, such as is realized in SrCuO_2 (Ref. [74]) or Cs_2CoCl_4 (Ref. [68]). Assuming the lattice constant is commensurate with that of the crystal, the setup contains $\sim 4 \cdot 10^4$ parallel transistors. The $\sim 10^3$ molecules at the edge can be accessed electrically by an array of STM tips. Using our previous estimate for d and the values from the text, fields between $10^8 - 10^4 \text{ V m}^{-1}$ are required to switch between insulating and conducting state. (b) Combining three transistors into a single NAND-gate. (c) Proposed setup to enhance the magnetic field due to the accumulated magnons. The role of the perforated superconductor is to increase the density of magnetic-field lines due to the magnetic field \mathbf{B}_{mag} and thereby increase the magnetic field acting on the molecular magnet. The crystal of molecular magnets is placed directly above the hole in the superconductor. We denote by f the portion of the total flux directly on the surface of the magnet that can be enhanced into the area of the molecular magnets. a_x and a_y (not shown) are the dimensions of the hole of the superconductor, which should equal those of the crystal of molecular magnets.

to the spin-electric coupling at temperatures of $\sim 1 \text{ K}$. This can be done by measuring the difference in voltage drop between points $(0, 0, r)$ and $(0, r, 0)$ in the insulating- [at $dE' \approx 2D_M$] and conducting (at $dE' \approx 0$) state. For the parameters in Fig. 4.2(h), and for $\Delta B \approx 200 \text{ mT}$, the difference in spinon current between the two states is $\sim 3 \cdot 10^{10} \text{ spinons s}^{-1}$. For $r = 1 \mu\text{m}$, this leads to a difference in voltage drop of $\sim 10^{-13} \text{ V}$, which is within experimental reach. [114] The strength of the required switching field E' can be achieved near a STM-tip for molecules with reasonable d , see the caption of Fig. 4.3(a). This experiment would be interesting in its

own right, since to our knowledge there have been no measurements of the spin-electric effect yet.

By combining three transistors as shown in Fig. 4.3(b), we can create a purely magnetic NAND-gate. The NAND-gate is a two-bit gate that gives a logical 0 as outcome if and only if both the input bits are 1, and yields a logical 1 otherwise. We will show how it may be possible to implement a NAND-gate consisting of magnon-transistors using readily available materials at ~ 10 K, and we will indicate the requirements for a working NAND-gate at room temperature.

Within a single transistor, the two FM spin reservoirs act respectively as source and drain. In our proposal, a finite non-equilibrium magnetization of the source (drain) encodes the logical state 1 of the source (drain); the logical state 0 has only the equilibrium magnetization present. A finite non-equilibrium magnetization of a reservoir is caused by having an excess number of magnons in that reservoir. The logic state at the gate is encoded in the strength of the local magnetic field, such that the transistor is insulating (conducting) if the logical state of the gate is 1 (0). Here, we propose to use the magnetic dipole field $\mathbf{B}_{\text{mag}} = B_{\text{mag}}\mathbf{z}$ due to the excess N accumulated magnons in the 1-state of the relevant terminal as gate-field at the points A-C in Fig. 4.3(b).

We use the setup in which the left (right) reservoir in a given transistor is exchange-coupled to all three vertices of the triangular magnet of that transistor with equal strength $J'_{1(2)}$ (see Sec. 4.2), and put $E' = 0$. We assume that $J'_1 > 0$, so that the coupling between the left reservoir and the molecular magnet is antiferromagnetic; we set $J'_2 < 0$, so that the coupling between the right reservoir and the molecular magnet is ferromagnetic. It is important to remember that both reservoirs are assumed to be ferromagnetic, but they are not necessarily identical. Therefore, they could be engineered in such a way that J'_1 and J'_2 have the properties stated above. In an experiment, J'_1 and J'_2 should be chosen such that the effects of the equilibrium magnetization of the reservoirs on the state of the molecular magnet (see end of Sec. 4.2) approximately cancel each other, up to the required value of B' in the conducting state of the transistor. This solves the issue of having to create relatively large local magnetic fields B' in our proposal.

If the ordering of the energy levels of the molecule is such as depicted in Fig. 4.1(d), we only need to consider transitions between the states $|\downarrow, +\rangle_\theta$ and $|\uparrow, +\rangle_\theta$. To switch between the insulating- and conducting state of a single transistor, we use the fact that the system is insulating for $\omega_E + \omega_{B_{\text{mag}}} > \omega_{\Delta B}$, and conducting for $\omega_E + \omega_{B_{\text{mag}}} < \omega_{\Delta B}$. Due to thermal fluctuations, the magnetic field \mathbf{B}_{mag} is not constant. These fluctuations

limit the fidelity of our NAND-gate. We characterize the fluctuations by the standard deviation $\sigma = \langle [\hat{n} - \langle \hat{n} \rangle]^2 \rangle^{1/2}$ of the number of magnons n on the gate, and calculate σ using the equilibrium distribution of the magnons using the grand canonical ensemble.

For the implementation at temperatures $T \sim 10$ K, we consider quasi-2D FM reservoirs of thickness d with spin $S = 10$, $|J|/k_B = 5$ K, and lattice spacing $a = 1$ nm. These are the approximate values for yttrium iron garnet (YIG), a material that is often considered appropriate for applications in spintronics. For the source and drain, we consider a quasi-2D sample of dimensions $300 \text{ nm} \times 300 \text{ nm}$. For simplicity, we assume a single layer sample with $d = 1$ nm, and we put $J'_1/k_B = -J'_2/k_B = 1$ K in our calculation. As our gate, we use a single layer crystal of molecular magnets with $D_M/k_B = 0.26$ K (this corresponds to 200 mT), and $J_M/k_B \gg 10$ K. Lower J_M 's can be used when the experiment is performed at a lower temperature, making the use of materials such as $\{\text{Cu}_3\}$ (see Ref. [110]) feasible. Assuming matching lattice constants, this setup contains 300 parallel single-molecule transistors. We estimate the field at the position of the molecular magnet [see Fig. 4.3(c)] due to the N magnons as $|\mathbf{B}_{\text{mag}}| \approx \frac{1}{2}\mu_0 N g \mu_B f / (d a_x a_y)$ (see caption of Fig. 4.3(c) for the definitions). Additionally, we use parameters $g_M = g_R = 2$, $f = 0.15$, $B_0 = 200$ mT, $B' = -160$ mT in the insulating phase and $B' = -140$ mT in the conducting phase, and $\Delta B = 50$ mT. In the conducting state, we find a magnon current exceeding $1.5 \cdot 10^{10} \text{ s}^{-1}$, which amounts to a switching time of a transistor of ~ 300 ns. In our model, the fidelity of a single-NAND-gate then exceeds 99.9%.

By using materials with an increased g -factor, we can create a NAND-gate that functions at room temperature, consisting of transistors with a ~ 11 ns switching time. We use the same setup as in the previous paragraph, but with parameters $S = 3$, $|J|/k_B = 500$ K, $a = 1$ nm for the 2D FM reservoir; $D_M/k_B = 2.6$ K (this corresponds to 200 mT for the g -factor under consideration), and $J_M/k_B \gg 300$ K for the molecular magnet; and $J'_1/k_B = -J'_2/k_B = 100$ K, $g_M = g_R = 20$, $f = 0.015$, $B_0 = 1$ T (easily achievable near the surface of a FM), $B' = -160$ mT in the insulating phase and $B' = -140$ mT in the conducting phase, and $\Delta B = 50$ mT. Evidently, the development of molecular magnets with an exchange interaction $J_M/k_B \gg 300$ K, needed in order to have stable molecular magnets at room temperature, will require a certain amount of experimental progress: typical values of currently existing molecular magnets are in the range of 1-10 K. However, there is nothing fundamental that forbids the existence of molecular magnets with larger exchange interaction. We find a magnon current exceeding $3.7 \cdot 10^{11} \text{ s}^{-1}$ in the conducting

state, which corresponds to a 11 ns switching time. Reducing the magnon fluctuations on the gate can further reduce the switching time. As before, the fidelity of a single NAND-gate exceeds 99.9%.

4.6 Discussions

In this section, we will discuss several different requirements that have to be fulfilled for our perturbative calculations of the tunneling current through the molecular magnet to be valid. The first constraint on our calculations concerns the validity of our spin wave analysis of the FM spin chains; the number of magnons per site has to satisfy $\langle a_i^\dagger a_i \rangle \ll 2S$. In our calculations, the average number of magnons per site is typically 0.05-0.13, so that non-interaction spin wave theory is valid. The AF theory is valid for energies much smaller than the exchange interaction J .

We checked the validity of our sequential tunneling approach in a self-consistent manner. For the AF reservoirs, the criterion is simply that the tunneling current is much smaller than the current in the ballistic system, that is $I_S(\Delta B) \ll g\mu_B\Delta B/h$. For the FM reservoirs, we require that the broadening of the energy levels of the molecule is smaller than the unperturbed level splitting. In other words, all transition rates $R_{if}^{L/R}$ of the FM system satisfy

$$R_{if}^{L/R}/n_B(\omega_i - \omega_f) \ll |\epsilon_i^0 - \epsilon_f^0|/\hbar, \quad (4.14)$$

where $\epsilon_i^0, \epsilon_f^0$ are the unperturbed energies of the states $|i\rangle, |f\rangle$.

Another constraint is given by the fact that, near Breit-Wigner resonances, the current through the molecular magnet can be strongly increased due to coherent tunneling processes. This only holds at low temperatures, at higher temperatures the broadening of the thermal distribution destroys coherent tunneling, and the sequential tunneling approach is valid again. The minimal temperature T for FM reservoirs is given by

$$R_{if}^{L/R}/n_B(\omega_i - \omega_f) \ll k_B T/\hbar. \quad (4.15)$$

All our calculations are at high enough temperature for the sequential tunneling approach to be valid for the FM system.

We note that relaxation of the state of the molecular magnet can be neglected as long as the coupling strength between the reservoirs and the molecular magnet exceeds the coupling between the molecular magnet and hyperfine- and phonon baths.

4.7 Conclusions

Using a sequential tunneling approach, we have studied transport of magnons and spinons through a triangular molecular magnet which is weakly coupled to two spin reservoirs. We have shown that, by changing the state of the molecular magnet through application of an electric- or magnetic field, we can control the magnitude of the spin current through the molecular magnet. We used this fact to propose a magnon-transistor, whose operation can be controlled by an electric- or magnetic field. We have shown for which parameters our transistor could operate at room temperature with a 11 ns switching time. We have shown how several magnon-transistors can be combined to create a NAND-gate.

Part II

Thermal transport in textured ferromagnets

CHAPTER 5

Thermal Hall effects

Adapted from:

K. A. van Hoogdalem, Y. Tserkovnyak, and D. Loss,
“Magnetic texture-induced thermal Hall effects”,
Phys. Rev. B **87**, 024402 (2013).

Magnetic excitations in ferromagnetic systems with a noncollinear ground state magnetization experience a fictitious magnetic field due to the equilibrium magnetic texture. Here, we investigate how such fictitious fields lead to thermal Hall effects in two-dimensional insulating magnets in which the magnetic texture is caused by spin-orbit interaction. Besides the well-known geometric texture contribution to the fictitious magnetic field in such systems, there exists also an equally important contribution due to the original spin-orbit term in the free energy. We consider the different possible ground states in the phase diagram of a two-dimensional ferromagnet with spin-orbit interaction: the spiral state and the skyrmion lattice, and find that thermal Hall effects can occur in certain domain walls as well as the skyrmion lattice.

5.1 Introduction

Hall effects for magnon currents are of interest both from a fundamental point of view as well as from the point of view of applications. Even though the physical magnetic field does not directly couple to the orbital motion of neutral magnons, certain kinds of spin-orbit interactions can

lead to Hall phenomena similar to those of a charged particle in a magnetic field. Mechanisms that have been shown to give rise to nonzero Hall conductances in certain insulating magnets include coupling of spin chirality to a magnetic field [115] and Dzyaloshinskii-Moriya (DM) interaction. [116] Of interest for applications is the fact that Hall effects in insulating magnets allow one to control the magnon spin current.

Recently, Katsura *et al.* predicted [115] a nonzero thermal Hall conductivity for the Heisenberg model on the Kagomé lattice. The finite conductivity originates from the fact that the coupling of spin chirality to an applied magnetic field leads to a fictitious magnetic flux for the magnons in the specific case of the Kagomé lattice. Later, Onose *et al.* measured [116] the thermal Hall effect in the pyrochlore ferromagnet $\text{Lu}_2\text{V}_2\text{O}_7$. In this experiment, the combination of DM interaction and the pyrochlore structure leads to the finite thermal Hall conductivity.

In those previous studies, the thermal Hall effect was considered using a quantum mechanical lattice model as starting point. The symmetry of the underlying lattice played a crucial role. We take a different approach and consider insulating ferromagnets with a noncollinear ground state magnetic texture, which we model using a phenomenological description. It is well known that the effect of the presence of a noncollinear ground state on the elementary excitations in a ferromagnet can be captured by introducing a fictitious electromagnetic potential in the equation of motion for the magnons. [28, 29] Spin-orbit interactions generally also contribute non-Abelian gauge fields into the magnetic Hamiltonian. [117] Furthermore, non-linearized gauge fields for Dzyaloshinskii-Moriya interaction were derived in Ref. [118] using the CP^1 representation. There are correspondingly two contributions to the fictitious electromagnetic potential. The first one only depends on the equilibrium magnetic texture, the second depends on the form of the free energy that gives rise to the noncollinear ground state in the first place, *i.e.* the contribution to the free energy due to spin-orbit interaction. Since both contributions are determined by the spin-orbit interaction, they will generally be of similar magnitude.

It has been shown that the fictitious electromagnetic potential couples the motion of magnetic texture and that of heat currents. [119] This coupling reveals itself through local cooling by magnetic texture dynamics [119] and thermally induced motion of magnetic textures such as domain walls. [120, 121]

This chapter is organized as follows. In Section 5.2 we introduce our system and derive the fictitious electromagnetic vector potential that acts on the magnons, which turns out to include an often-overlooked contri-

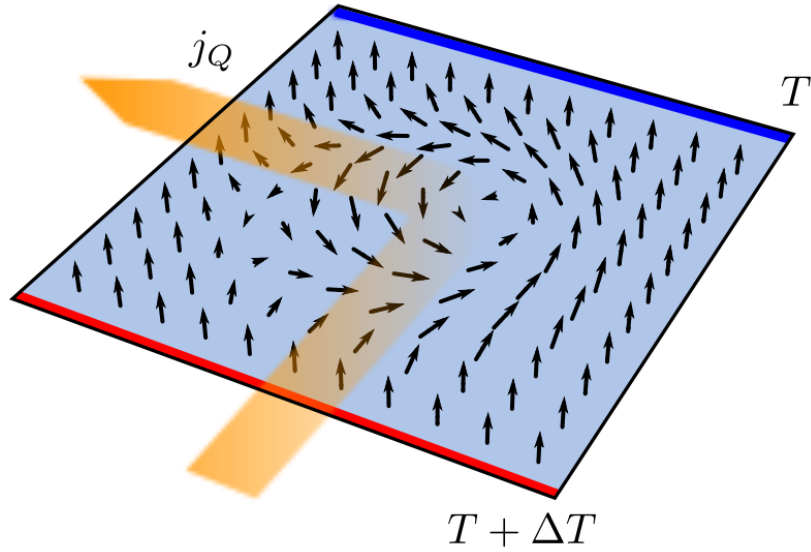


Figure 5.1: Pictorial representation of the thermal spin Hall effect. A temperature difference ΔT applied to a sample leads to a finite heat current. Since the heat current is carried by the magnons in the system, the fictitious magnetic field that magnons experience due to a non-trivial magnetic ground state will lead to a finite thermal Hall conductivity.

bution. In Sec. 5.3 we derive the relevant ground state properties of the different ground states in the phase diagram of the insulating ferromagnet with nonzero Dzyaloshinskii-Moriya interaction. In Sec. 5.4 we calculate the band structure of one of the ground states, the triangular skyrmion lattice, and calculate its thermal Hall conductivity.

5.2 Magnons in the presence of magnetic texture

We consider a two-dimensional non-itinerant ferromagnet in the x - y plane with spatially varying and time-dependent spin density $s\mathbf{m}(\mathbf{r}, t)$. The spin density is related to the magnetization $\mathbf{M}(\mathbf{r}, t)$ as $s\mathbf{m}(\mathbf{r}, t) = \mathbf{M}(\mathbf{r}, t)/\gamma$, where γ is the gyromagnetic ratio ($\gamma < 0$ for electrons). The magnitude s of the spin density is assumed to be constant, and $\mathbf{m}(\mathbf{r}, t)$ is a unit vector. The system is described by the Lagrangian [28, 29]

$$\mathcal{L} = \int d^2\mathbf{r} [\mathbf{D}(\mathbf{m}) \cdot \dot{\mathbf{m}} - F(\mathbf{m}, \partial_j \mathbf{m})]. \quad (5.1)$$

Here $\mathbf{D} = s\hbar(\mathbf{n}_D \times \mathbf{m}) / (1 + \mathbf{m} \cdot \mathbf{n}_D)$ is the vector potential corresponding to the Wess-Zumino action with an arbitrary \mathbf{n}_D pointing along the Dirac string. $F(\mathbf{m}, \partial_j \mathbf{m})$ is the magnetic free energy density of the system, which we assume to be of the form (here $j = x, y$; double indices are summed over)

$$F(\mathbf{m}, \partial_j \mathbf{m}) = \frac{Js}{2} (\partial_j \mathbf{m})^2 - M_s \mathbf{m} \cdot \mathbf{H} + sF_\Gamma(\mathbf{m}, \partial_j \mathbf{m}). \quad (5.2)$$

Here J is the strength of the exchange interaction, $M_s = \gamma s$ is the saturation magnetization, \mathbf{H} the external magnetic field (which we will always assume to be in the z direction), and $F_\Gamma(\mathbf{m}, \partial_j \mathbf{m})$ describes terms due to broken symmetries. For isotropic ferromagnets in the exchange approximation, the leading order terms in the free energy are quadratic in the texture [first term in Eq. (5.1)]. Breaking inversion symmetry by spin-orbit interactions, while still retaining isotropy in the x - y plane, allows us to construct terms that are first order in texture. These terms are given by

$$F_\Gamma(\mathbf{m}, \partial_j \mathbf{m}) = \Gamma_R m_z \nabla \cdot \mathbf{m} + \Gamma_{DM} \mathbf{m} \cdot (\nabla \times \mathbf{m}). \quad (5.3)$$

We defined $\nabla = \partial_x \mathbf{x} + \partial_y \mathbf{y}$, where \mathbf{x}, \mathbf{y} are unit vectors. The first term is due to structural inversion symmetry breaking and hence is anisotropic in the z direction. Such terms occur in systems with finite Rashba spin-orbit interaction [122] or on the surface of a topological insulator. [123] The second term describes DM interaction, [36, 37] which originates from the breaking of bulk inversion symmetry and is therefore isotropic. We note that the two terms in Eq. (5.3) are equivalent (up to an irrelevant boundary term) under a simple rotation around the z axis in spin space. Since such a rotation does not have any additional effect on the equation of motion for the magnetization, Eq. (5.4), we can always absorb the term proportional to Γ_R in the term proportional to Γ_{DM} . We will therefore put Γ_R to zero in the remainder of this work. For simplicity, we have ignored a term $-\kappa m_z^2$ that would describe easy axis anisotropy, and a term $-M_s \mathbf{m} \cdot \mathbf{H}_m / 2$, where \mathbf{H}_m describes the magnetic stray field, in Eq. (5.2).

Substitution of Eq. (5.1) in the Euler-Lagrange equation leads to the Landau-Lifshitz equation

$$s\hbar \dot{\mathbf{m}} - \mathbf{m} \times \delta_{\mathbf{m}} \mathcal{F}(\mathbf{m}, \partial_j \mathbf{m}) = 0, \quad (5.4)$$

where $\mathcal{F}(\mathbf{m}, \partial_j \mathbf{m})$ is the total magnetic free energy of the system. We split the magnetization \mathbf{m} in a static equilibrium magnetization \mathbf{m}_0 and

small fast oscillations $\delta\mathbf{m}$ (spin waves) around the equilibrium magnetization. To lowest order in $\delta\mathbf{m}$ the two are orthogonal. In a textured magnet $\mathbf{m}_0 = \mathbf{m}_0(\mathbf{r})$, which makes finding the elementary excitations a nontrivial task. To circumvent this issue we introduce a coordinate transformation $\mathbf{m}'(\mathbf{r}) = \hat{R}(\mathbf{r})\mathbf{m}(\mathbf{r})$, where $\hat{R}(\mathbf{r})$ is such that the new equilibrium magnetization \mathbf{m}'_0 is constant and parallel to the z axis. In this coordinate frame the spin waves are in the x - y plane.

The 3×3 matrix \hat{R} describes a local rotation over an angle π around the axis defined by the unit vector $\mathbf{n} = [\mathbf{z} + \mathbf{m}_0] / [2 \cos(\theta/2)]$. Here, θ is the polar angle of \mathbf{m}_0 , and \mathbf{z} is a unit vector. Using Rodrigues' rotation formula, we find $\hat{R} = 2\mathbf{nn}^T - \hat{1}$. The effect of the transformation to the new coordinate system is that we have to use the covariant form of the differential operators, $\partial_\mu \rightarrow (\partial_\mu + \hat{A}_\mu)$, with $\hat{A}_\mu = \hat{R}^{-1}(\partial_\mu \hat{R})$, in the Landau-Lifshitz equation. The subscript μ describes both time ($\mu = 0$) and space ($\mu = 1, 2$) coordinates.

In the new coordinate system, the Landau-Lifshitz equation for the free energy Eq. (5.2) becomes

$$i\hbar\dot{m}_+ = [J(\nabla/i + \mathbf{A})^2 + \varphi] m_+. \quad (5.5)$$

Here, $m_\pm = (\delta m'_x \pm i\delta m'_y)/\sqrt{2}$ describe circular spin waves in the rotated frame of reference. Furthermore, $\varphi = \mathbf{m}_0 \cdot \mathbf{H}/s + \hbar[\hat{R}^{-1}(\partial_t \hat{R})]_{12}$, and the components of the vector potential \mathbf{A} are given by $A_j = \hat{A}_j|_{12}$. The skew-symmetric matrices \hat{A}_j are here defined as $\hat{A}_j = \hat{R}(\partial_j - \zeta \hat{I}_j)\hat{R}$. In the latter equation we defined $\zeta = \Gamma_{\text{DM}}/J$, and the matrices

$$\hat{I}_x = \begin{pmatrix} 0 & 0 & 0 \\ 0 & 0 & -1 \\ 0 & 1 & 0 \end{pmatrix} \text{ and } \hat{I}_y = \begin{pmatrix} 0 & 0 & 1 \\ 0 & 0 & 0 \\ -1 & 0 & 0 \end{pmatrix}. \quad (5.6)$$

We see that the components A_j of the fictitious magnetic vector potential consist of two contributions. The first comes from the exchange interaction in the presence of magnetic texture; the second (texture-independent) part originates from the DM interaction term in the free energy. While it may be tempting to neglect the latter contribution, we will show here that it has important consequences. Indeed, typically both contributions will be of the same order of magnitude. This is because the magnetic texture itself is caused by the DM interaction, and will therefore manifest itself on lengthscales J/Γ_{DM} .

We can quantize Eq. (5.5) by introducing the bosonic creation operator $b^\dagger \propto m_+$. This quantization works since m'_+ and m'_- satisfy approximate bosonic commutation relations in the limit of small deviations from

equilibrium. After quantization, Eq. (5.5) can be interpreted as the von Neumann equation belonging to the Hamiltonian

$$\mathcal{H} = \int d^2\mathbf{r} b^\dagger [J(\nabla/i + \mathbf{A})^2 + \varphi] b. \quad (5.7)$$

Therefore, the elementary excitations of the system behave as noninteracting bosonic quasiparticles. The effect of the smoothly-varying equilibrium magnetization is captured by the inclusion of a fictitious magnetic vector potential \mathbf{A} and electric potential φ .

In the derivation of Eq. (5.5) we have assumed that the length of a typical wave packet is much smaller than the spatial extension over which the magnetic texture varies. We will refer to this as the adiabatic approximation. [124] Using this assumption, we have neglected terms in Eq. (5.5) that are higher order in texture. Such terms, which become important at lower wave vectors, lead to two distinct effects. [124] Firstly, a term $-J[(\hat{\mathcal{A}}_x|_{13})^2 + (\hat{\mathcal{A}}_x|_{23})^2 + (\hat{\mathcal{A}}_y|_{13})^2 + (\hat{\mathcal{A}}_y|_{23})^2]/2$, which is quadratic in magnetic texture, has to be added to the fictitious electric potential φ in Eq (5.5) at low wave vectors. Secondly, at low wave vectors one needs to add to the right-hand side of Eq. (5.5) a term $J[(\hat{\mathcal{A}}_x|_{13} + i\hat{\mathcal{A}}_x|_{23})^2 + (\hat{\mathcal{A}}_y|_{13} + i\hat{\mathcal{A}}_y|_{23})^2]m_-$, which introduces a finite ellipticity of the magnons.

5.3 Textured ground states

In this section we will present the different possible ground states for systems with free energy given by Eq. (5.2) (with $\Gamma_R = 0$), as a function of the external magnetic field $\mathbf{H} = H\mathbf{z}$. We will also present the fictitious magnetic vector potentials that find their origin in these textured ground states. It has been shown [125, 118] that as the magnetic field H increases from zero, the ground state of a two-dimensional ferromagnet with spin-orbit interaction changes from a spiral state for $H < H_{c1}$, to a skyrmion lattice state for magnetic fields $H_{c1} < H < H_{c2}$, and finally to the ferromagnetic ground state for $H > H_{c2}$. Both critical fields H_{c1} and H_{c2} are typically of the order Γ_{DM}^2/J (see Refs. [118, 126]). This last observation, in combination with the adiabatic assumption and the fact that the equilibrium magnetization is time independent, allows us to neglect the fictitious electric potential φ in Eq. (5.7). Since the ferromagnetic ground state has no magnetic texture, it is of no interest for our purposes. In this section we will therefore derive the properties of the spiral- and skyrmion lattice ground state.

Spiral state

Following Ref. [125] we will derive the properties of the spiral ground state $\mathbf{m}_0(\mathbf{r})$ of a two-dimensional ferromagnet with DM interaction. We write $\mathbf{m}_0(\mathbf{r})$ in the following form

$$\mathbf{m}_0(\mathbf{r}) = \cos \xi \sin \theta \mathbf{x} + \sin \xi \sin \theta \mathbf{y} + \cos \theta \mathbf{z}. \quad (5.8)$$

For the spiral state, $\theta = \theta(y)$ and ξ is a constant. With these constraints, the free energy becomes a functional that depends only on $\theta(y)$ and $\partial_y \theta(y)$. Minimizing this functional with respect to $\theta(y)$ gives the following differential equation

$$\partial_y^2 \theta + \alpha \sin \theta = 0, \quad (5.9)$$

where we defined $\alpha = -\gamma H/J$. Eq. (5.9) is the equation of motion for the mathematical pendulum. The general solution is given in implicit form by the expression

$$\int_0^{\theta(y)} \frac{d\theta}{2} \frac{1}{\sqrt{1 - m^2 \sin^2 \theta/2}} = \frac{1}{2} \beta y, \quad (5.10)$$

where $m = 4\alpha/(2\alpha + C)$ and $\beta = \sqrt{2\alpha + C}$. Alternatively, we can write $\theta(y) = 2\phi(\beta y/2, m)$, where $\phi(u, m)$ is the amplitude of the Jacobi elliptic function. The constant C is the first constant of integration. To determine it, we use the fact that $\theta(y)$ is a periodic function with period y_0 . By integrating the inverse of the first integral $\partial_y \theta$ of Eq. (5.9) over one period we can determine y_0 as

$$y_0 = \int_0^{2\pi} d\theta \frac{1}{\sqrt{2\alpha \cos \theta + C}}. \quad (5.11)$$

To fix C , we minimize the average free energy $(1/y_0) \int_0^{y_0} F(\theta, \partial_y \theta)$, which leads to the following implicit expression for C

$$\int_0^{2\pi} d\theta \sqrt{2\alpha \cos \theta + C} = 2\pi \zeta. \quad (5.12)$$

The minimization of the average free energy also fixes $\cos \xi = 1$. From this we see that the ground state is a spiral state whose structure locally resembles a Bloch domain wall, as is expected for the DM interaction. [125] We also note that in the case of zero magnetic field ($\alpha = 0$) the spiral state is described by a simple sinusoid with period $y_0 = 2\pi/\zeta$, whereas for finite magnetic field the mirror symmetry with respect to the

$x - y$ plane is broken. Eq. (5.12) also puts a constraint on the maximum value of H for which the spiral state is stable.

Some general observations can be made with regard to the fictitious magnetic vector potential due to the spiral ground state. For the ground state Eq. (5.8) with $\theta = \theta(y)$ and ξ constant, the fictitious vector potential is $\mathbf{A}(y) = \zeta \sin \theta(y) \mathbf{x}$. This potential is caused solely by the DM contribution to \mathbf{A} , the geometric texture contribution is zero everywhere. The z component of the fictitious magnetic field that the magnons experience is given by $B_z(y) = \nabla \times \mathbf{A}|_z = -\zeta \partial_y \theta(y) \cos \theta(y)$. It is easily seen that the total fictitious magnetic flux over one period of the spiral $\langle B_z \rangle = \int_0^{y_0} dy B_z(y) = 0$. The fictitious magnetic field $B_z(y)$ has been plotted in Fig. 5.2 for different magnitudes of the applied magnetic field $\mathbf{H} = H\mathbf{z}$. Transport in the presence of a magnetic field that is spatially varying in one direction and has zero average has been studied extensively (see Ref. [127] for a recent review). It is well known that these systems do not display a finite Hall conductivity. However, such magnetic fields have been predicted to influence the longitudinal conductance, due to the presence of localized snake orbits at energies that are low compared to the cyclotron frequency associated with the amplitude of the magnetic field. [128, 129] From our analysis it is also seen that one-dimensional textures can give rise to a nonzero average fictitious magnetic flux for certain domain walls, since these consist of only half a period of the spiral. Hence, such domain walls will display the thermal Hall effect.

Lastly, we note that a proper statistical mechanical description of the spiral phase in three dimensions (or less) requires the inclusion of leading-order non-linearities in the free energy. [130] The role of those non-linearities in the thermal Hall physics is yet to be understood.

Skyrmion lattice

For magnetic fields $H_{c1} < H < H_{c2}$ the ground state of the two-dimensional ferromagnet with DM interaction is a skyrmion lattice. [126] This triangular lattice has basis vectors $\mathbf{a}_1 = a\mathbf{x}$ and $\mathbf{a}_2 = (a/2)\mathbf{x} + (a\sqrt{3}/2)\mathbf{y}$, and contains skyrmions with radius R . The size of a single unit cell is $(\sqrt{3}/2)a^2$, where $a = 2R$. The magnetization $\mathbf{m}_0(\mathbf{r})$ of a single skyrmion of radius R centered at the origin is parametrized in polar coordinates (ρ, ϕ) by Eq. (5.8) with $\theta = \theta(\rho)$ and boundary conditions

$$\theta(0) = \pi \text{ and } \theta(R) = 0. \quad (5.13)$$

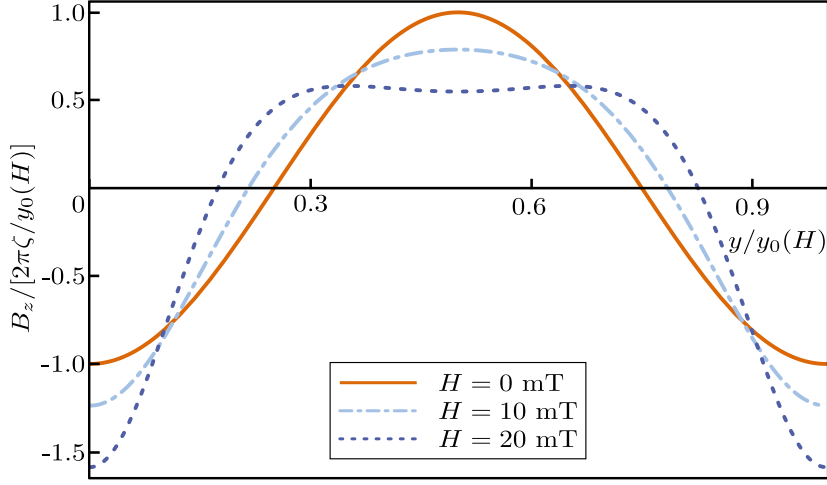


Figure 5.2: Fictitious magnetic field due to the spiral ground state. Parameters are $\zeta = 70 \mu\text{m}^{-1}$, $J/(k_B\epsilon^2) = 63 \text{ K}$, and the interatomic spacing is taken to be $\epsilon = 4.5 \text{ \AA}$. (See Ref. [126]) To make the connection to electromagnetism, we note that a fictitious field $B_z = 2\pi\zeta/y_0(0) \approx 5 \cdot 10^{15} \text{ m}^{-2}$ acting on a spin wave gives rise to the same magnetic length as a $\frac{\hbar}{e}\zeta^2 \approx 3 \text{ T}$ magnetic field acting on a free electron.

Furthermore, $\xi = N\phi - \pi/2$, where N is the charge of the skyrmion. We will assume $N = 1$ throughout. The magnetization profile can in principle be determined numerically by minimizing the free energy with the aforementioned boundary conditions. However, for simplicity we will assume a linear dependence $\theta(\rho) = \pi(1 - \rho/R)$ for our analysis of the texture-induced thermal Hall effect.

In polar coordinates the fictitious magnetic vector potential $\mathbf{A}(\mathbf{r})$ due to a single skyrmion centered at the origin is given by (here $0 \leq \rho \leq R$ and ϕ is a unit vector)

$$\mathbf{A}(\mathbf{r}) = \left[\frac{\cos\theta(\rho) - 1}{\rho} - \zeta \cos\theta(\rho) \right] \phi. \quad (5.14)$$

The z component of the fictitious magnetic field for this vector potential is given by $B_z(\rho) = \rho^{-1}\partial_\rho(\rho A_\phi)$. It follows that the total flux through a unit cell is $\langle B_z \rangle = 2\pi \int_0^R d\rho \rho B_z = 4\pi$. This means that each unit cell contains two magnetic flux quanta. The nonzero average flux is caused by the texture contribution to $\mathbf{A}(\mathbf{r})$, the DM-interaction contribution averages to zero. From the fact that the average magnetic flux is nonzero, it follows that the skyrmion lattice has a nonzero Hall conductivity. One

might then be inclined to take the average value of the fictitious magnetic field and ignore the spatial dependence when calculating the thermal Hall conductivity of the skyrmion lattice. However, we will show shortly that the spatial variation of the fictitious magnetic field is substantial, so that we should take both contributions into account in our analysis.

To illustrate this point, let us consider the situation in which $R = \pi/\zeta$. In that case $B_z(\rho) = \zeta^2 \cos \theta(\rho)$. The spatial variation is therefore large enough that the fictitious field switches from a negative minimum at $\rho = 0$ to a positive maximum at $\rho = R$. Such large variations have been shown to have a significant influence on the band structure of magnetic lattices. [131]

For what follows, it will be convenient to formally split the fictitious magnetic vector potential in two parts, $\mathbf{A}(\mathbf{r}) = \mathbf{A}_0(\mathbf{r}) + \mathbf{A}'(\mathbf{r})$, where $\mathbf{A}_0(\mathbf{r})$ describes the contribution from the homogeneous nonzero average fictitious magnetic flux, and $\mathbf{A}'(\mathbf{r})$ the periodic contribution with zero average (we work in the Landau gauge)

$$\begin{aligned}\mathbf{A}_0(\mathbf{r}) &= -B_0 y \mathbf{x}, \\ \mathbf{A}'(\mathbf{r}) &= \sum_{\tau, \eta} [A_x(\tau, \eta) \mathbf{x} + A_y(\tau, \eta) \mathbf{y}] e^{i(\tau \mathbf{k}_1 + \eta \mathbf{k}_2) \cdot \mathbf{r}}.\end{aligned}\quad (5.15)$$

Here, $B_0 = 8\pi/(\sqrt{3}a^2)$ is the average fictitious magnetic field, and $\mathbf{k}_1 = (2\pi/a)(\mathbf{x} - \mathbf{y}/\sqrt{3})$ and $\mathbf{k}_2 = (2\pi/a)(2/\sqrt{3})\mathbf{y}$ are the basis vectors of the reciprocal lattice, such that the periodic part of the fictitious vector potential satisfies $\mathbf{A}'(\mathbf{r} + \mathbf{a}_1) = \mathbf{A}'(\mathbf{r} + \mathbf{a}_2) = \mathbf{A}'(\mathbf{r})$. Such spatially varying magnetic fields are known to give rise to a finite Hall conductivity, even in the absence of a nonzero average. [132]

5.4 Thermal Hall conductivity of the skyrmion lattice

Since the magnetic excitations of the skyrmion lattice can be described by a free bosonic Hamiltonian with a spatially varying fictitious magnetic field with on average two magnetic flux quanta per unit cell and the same symmetry as the skyrmion lattice, the eigenstates of the skyrmion lattice are magnetic Bloch states. In Sec. 5.4 we will determine the excitation spectrum and explicit form of these states. In Sec. 5.4 we will show how the thermal Hall conductivity of the skyrmion lattice is determined by the Berry curvature of these magnetic Bloch states.

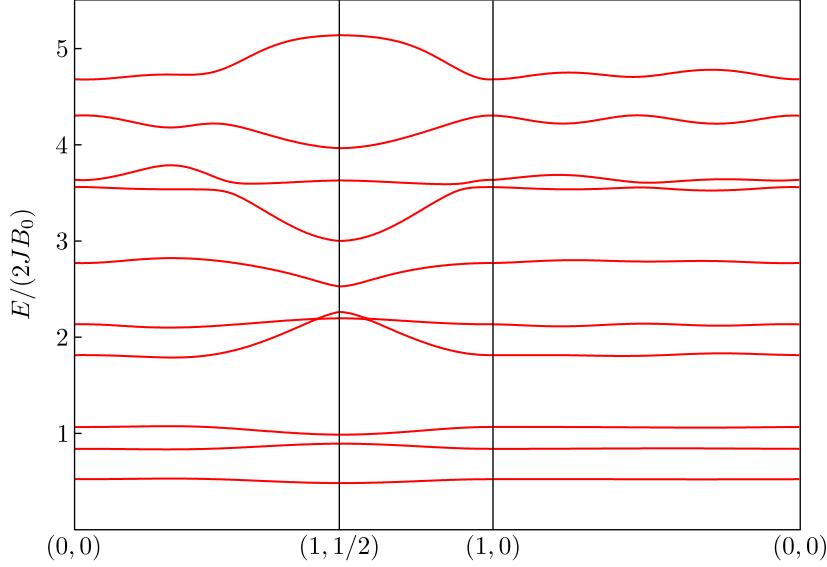


Figure 5.3: Band structure of the skyrmion lattice with parameters $R = 45$ nm, $\zeta = 70 \mu\text{m}^{-1}$, and $2JB_0/k_B \approx 50$ mK. The labels on the horizontal axis denote (k_1, k_2) , with the wave vectors normalized to $2\pi/a$.

Diagonalization

To find the elementary excitations of the skyrmion lattice, we need to diagonalize the Hamiltonian \mathcal{H} in Eq. (5.7) with the fictitious magnetic vector potential given in Eq. (5.14). We do this by numerically diagonalizing the matrix that results from rewriting \mathcal{H} in the basis of the Landau levels that describe excitations with the appropriate symmetry in the presence of the fictitious magnetic vector potential $\mathbf{A}_0(\mathbf{r})$ only. Our derivation follows that of Ref. [131], with the difference that we consider the case with two flux quanta instead of one flux quantum per unit cell.

The eigenstates of a free system of dimensions $L \times L$ with only a homogeneous magnetic field $B_0\mathbf{z}$ and without any underlying symmetries are given by

$$\psi_{nk_x}(\mathbf{r}) = \frac{N_n}{\sqrt{L}} e^{-ik_x x} \varphi_n(B_0^{\frac{1}{2}} y + B_0^{-\frac{1}{2}} k_x), \quad (5.16)$$

where $N_n = \frac{1}{\sqrt{2^n n!}} \left(\frac{B_0}{\pi}\right)^{\frac{1}{4}}$ and $\varphi_n(x) = e^{-x^2/2} H_n(x)$, with $H_n(x)$ the n -th Hermite polynomial. The corresponding energies are $E_n = 2JB_0(n + 1/2)$. To account for the presence of the triangular lattice, and the fact that every unit cell contains two flux quanta, we need to find the most

general linear combination of eigenstates that satisfies

$$\begin{aligned}\hat{M}_{\mathbf{a}_1}\psi_{nm\mathbf{k}}(\mathbf{r}) &= e^{ik_1a}\psi_{nm\mathbf{k}}(\mathbf{r}), \\ \hat{M}_{\mathbf{a}_2}\psi_{nm\mathbf{k}}(\mathbf{r}) &= e^{ik_2a}\psi_{nm\mathbf{k}}(\mathbf{r}).\end{aligned}\quad (5.17)$$

Here, k_1 and k_2 are defined such that $(2\pi/a)\mathbf{k} = k_1\mathbf{k}_1 + k_2\mathbf{k}_2$. Furthermore, \mathbf{k} is restricted to lie within the first Brillouin zone. We will discuss the origin of the quantum number m later. We have to work with magnetic translation operators $\hat{M}_{\mathbf{a}_{1,2}}$ since the canonical momentum is no longer a good quantum number in the presence of the vector potential $\mathbf{A}_0(\mathbf{r})$. These magnetic translation operators are defined as $\hat{M}_{\mathbf{a}_1} = \hat{T}_{\mathbf{a}_1}$ and $\hat{M}_{\mathbf{a}_2} = \exp[-i(4\pi/a)x]\hat{T}_{\mathbf{a}_2}$, where $\hat{T}_{\mathbf{a}_{1,2}}$ are the usual translation operators. The appropriate eigenstates are then given by

$$\begin{aligned}\psi_{nm\mathbf{k}}(\mathbf{r}) &= \sum_{l=-\infty}^{\infty} (-1)^{(l+\frac{m}{2})(l+\frac{m}{2}-1)} e^{-i(l+\frac{m}{2})(\frac{k_1}{2}-k_2)a} \\ &\quad \times \psi_{n,-k_1-(l+\frac{m}{2})\frac{4\pi}{a}}.\end{aligned}\quad (5.18)$$

The quantum number m , which in our case can take values 0 or 1, accounts for the fact that in the presence of a natural number p of flux quanta per unit cell each magnetic band will split up in p subbands. These subbands are degenerate for a constant magnetic field, but will in general split for a spatially varying magnetic field, as we will see later. The set of wave functions defined in Eq. (5.18) constitutes a complete orthonormal basis with triangular symmetry. The eigenfunctions are chosen in such a way that perturbations in the fictitious magnetic vector potential that are periodic in the triangular lattice are diagonal in the momenta k_1 and k_2 .

We are now in a position to calculate the matrix elements of \mathcal{H} with respect to the basis defined by the eigenstates in Eq. (5.18). We rewrite $\mathcal{H} = \mathcal{H}_0 + \mathcal{H}_1 + \mathcal{H}_2$, where the subscript denotes the order in which $\mathbf{A}'(\mathbf{r})$ occurs in the respective term. The matrix elements of \mathcal{H}_0 are then trivially given by (we have suppressed the \mathbf{k} -dependence of the eigenstates in our notation)

$$\langle n', m' | \mathcal{H}_0 | n, m \rangle = 2JB_0 (n + 1/2) \delta_{n,n'} \delta_{m,m'}. \quad (5.19)$$

The matrix elements of \mathcal{H}_1 are given by

$$\begin{aligned} \langle n', m' | \mathcal{H}_1 | n, m \rangle_{n' \geq n} &= J \sum_{\tau, \eta} \delta_{m'-m, \tau}^{(\text{mod } 2)} B(\tau, \eta) \\ &\times \left[L_n^{n'-n}(z_{\tau\eta}) - \left(\frac{n+n'}{z_{\tau\eta}} L_n^{n'-n}(z_{\tau\eta}) - \frac{2n'}{z_{\tau\eta}} L_{n-1}^{n'-n}(z_{\tau\eta}) \right) \right] \\ &\times (-1)^{m\eta} G_{n'n}(\tau, \eta), \end{aligned} \quad (5.20)$$

and the matrix elements of \mathcal{H}_2 by

$$\begin{aligned} \langle n', m' | \mathcal{H}_2 | n, m \rangle_{n' \geq n} &= J \sum_{\tau', \eta', \tau, \eta} \delta_{m'-m, \tau'+\tau}^{(\text{mod } 2)} \\ &\times [A_x(\tau', \eta') A_x(\tau, \eta) + A_y(\tau', \eta') A_y(\tau, \eta)] \\ &\times (-1)^{m(\eta'+\eta)} G_{n'n}(\tau' + \tau, \eta' + \eta). \end{aligned} \quad (5.21)$$

We defined the function

$$\begin{aligned} G_{n'n}(\tau, \eta) &= \left(\frac{n!}{n'} \right)^{1/2} (\sqrt{2/B_0} \pi)^{n'-n} \left[i \frac{2\eta - \tau}{\sqrt{3}a} - \frac{\tau}{a} \right]^{n'-n} \\ &\times e^{-z_{\tau\eta}/2} e^{\pi i \tau \eta / 2} e^{i \eta k_1 a / 2} e^{i \tau (k_2 a + \pi) / 2}. \end{aligned} \quad (5.22)$$

Furthermore, we defined $z_{\tau\eta} = (2\pi/\sqrt{3})(\tau^2 - \tau\eta + \eta^2)$. The function $L_n^\alpha(x)$ is the associated Laguerre polynomial. The function $\delta_{i,j}^{(\text{mod } 2)}$ is defined as $\delta_{i,j}^{(\text{mod } 2)} = 1$ when $i = j \pmod{2}$, and $\delta_{i,j}^{(\text{mod } 2)} = 0$ otherwise. The first 10 subbands of the band structure of the skyrmion lattice with parameters $2JB_0/k_B \approx 50$ mK, $R = 45$ nm, and $\zeta = 70 \mu\text{m}^{-1}$ (similar values to those found in Ref. [126]) are given in Fig. 5.3. In our numerical calculation we used the fact that the coupling between two band decays super-exponentially [to be precise, it decays as $\sqrt{(n!/n')}$], so that only a limited number of bands have to be taken into account. It is seen that the inclusion of the spatially varying fictitious magnetic field has a pronounced effect, leading both to different splittings of the different subbands, as well as substantial broadening of the subbands. From Fig. ?? it is seen that the typical level splitting between magnetic subbands is 50 mK, which sets the temperature scale on which the system is in the quantum Hall regime. Systems with larger ratio Γ_{DM}^2/J will display quantum Hall behavior at higher temperatures. We note that finite Gilbert damping α will broaden the different magnetic subbands by an amount $(\Delta\omega/\omega) = 2\alpha$. Eventually this will destroy the visibility of individual subbands. However, since the Gilbert damping is around $\alpha \sim 10^{-3}$ in a range of different materials, this only becomes problematic at high magnetic subbands.

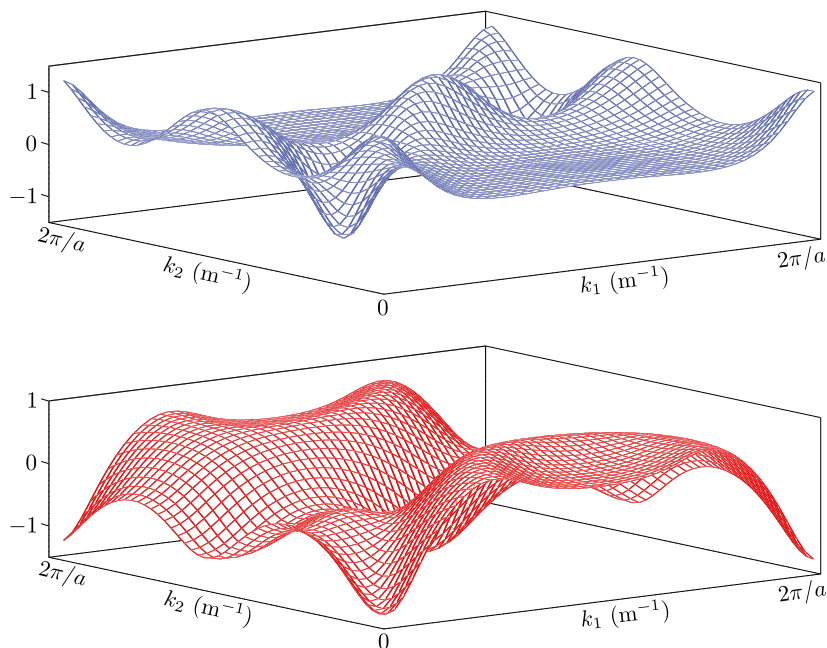


Figure 5.4: Berry curvature of the two highest magnetic subbands in Fig. 5.3 in a single Brillouin zone. The subband corresponding to the top figure does not carry a net curvature, the bottom figure carries 2π .

We note that within our model we do not find the expected Goldstone modes associated with the skyrmion lattice. [133] We argue that this is due to our adiabatic assumption, which breaks down for the smallest wave vectors. Assuming a quadratic dispersion for the magnons, we can estimate the magnitude $|\mathbf{k}_m|$ of the characteristic wave vector of the magnons that make up the lowest magnetic subband as $J|\mathbf{k}_m|^2 = JB_0$, which leads to a typical magnon wave length $\lambda_m \sim a$. The wave vector $|\mathbf{k}_m|$ increases for higher subbands. Since the accuracy of our model increases with increasing wave vector, our description improves for higher magnetic subbands.

In the next section we will investigate the effect of the finite bandwidth of the magnetic subbands on the thermal Hall conductivity of the skyrmion lattice.

Thermal Hall conductivity

It is well known [134] that the semi-classical dynamics of a wave packet in the basis of the magnetic Bloch states $u_{n\mathbf{k}}(\mathbf{r}) = e^{-i\mathbf{k}\cdot\mathbf{r}}\psi_{n\mathbf{k}}(\mathbf{r})$ is described

by

$$\dot{\mathbf{r}} = \partial_{\mathbf{k}} E_n(\mathbf{k}) - \dot{\mathbf{k}} \times \boldsymbol{\Omega}_n(\mathbf{k}) \text{ and } \hbar \dot{\mathbf{k}} = 0. \quad (5.23)$$

We have assumed here that there are no electric fields present and that the states $u_{n\mathbf{k}}(\mathbf{r})$ are the eigenstates of the Hamiltonian \mathcal{H} including the fictitious magnetic vector potential $\mathbf{A}(\mathbf{r})$. $\boldsymbol{\Omega}_n(\mathbf{k})$ is the Berry curvature of the n 'th magnetic Bloch band. Since we consider a two-dimensional system, only its z component is relevant. It is given by

$$\Omega_n(\mathbf{k}) = 2\text{Im} \left[\left\langle \frac{u_{n\mathbf{k}}(\mathbf{r})}{\partial k_x} \left| \frac{u_{n\mathbf{k}}(\mathbf{r})}{\partial k_y} \right. \right\rangle \right]. \quad (5.24)$$

For the skyrmion lattice, the magnetic Bloch states are given by

$$u_{n\mathbf{k}}(\mathbf{r}) = e^{-i\mathbf{k}\cdot\mathbf{r}} \sum_{n',m'} c_{n'm'\mathbf{k}}^n \psi_{n'm'\mathbf{k}}(\mathbf{r}). \quad (5.25)$$

The weights $c_{n'm'\mathbf{k}}^n$ follow from the diagonalization performed in Sec. 5.4. It should be noted that every completely filled subband carries a total Berry curvature that is a multiple of 2π , in accordance with the quantization of the TKNN invariant. [135]

Matsumotu *et al.* have shown [136] that the thermal Hall conductivity for a system described by Eq. (5.23) is given by

$$\kappa_{xy} = \frac{k_B^2 T}{\hbar V} \sum_{n,\mathbf{k}} c_2(\rho_{n\mathbf{k}}) \Omega_n(\mathbf{k}). \quad (5.26)$$

Here $c_2(\rho) = (1 + \rho) \left(\log \frac{1+\rho}{\rho} \right)^2 - (\log \rho)^2 - 2\text{Li}_2(-\rho)$ describes the effect of the thermal distribution of the magnons, and $\rho(\epsilon) = (\exp^{\beta(\epsilon-\mu)} - 1)^{-1}$ is the Bose-Einstein distribution function.

Fig. 5.4 shows the Berry curvature for the two highest magnetic subbands in Fig. 5.3. Together with the band structure given in Fig. ?? the Berry curvature completely determines the thermal Hall conductivity, as can be seen from Eq. (5.26). The position and width of the magnetic subbands determine at which energies states become available for thermal transport, the Berry curvature determines the extend to which these states contribute to the thermal Hall conductivity.

We have shown then that the spatially varying fictitious magnetic field gives rise to a nontrivial structure of the Berry curvature as well as a broadening of the magnetic subbands. As follows from Eq. (5.26), the

combination of these two effects may be studied experimentally by measuring κ_{xy} as a function of temperature. As the temperature increases, the thermal distribution of the bosonic magnons broadens, which enables the higher bands to contribute to thermal transport.

Alternatively, one can probe the chiral subgap edge states (above the bands whose total TKNN number is odd) directly by microwave means. The first magnetic subband corresponds to several GHz, which falls within the scope of standard microwave techniques. Excitation of some of the low-energy modes of the skyrmion lattice by microwave radiation has been performed [137] and analyzed. [138] The magnonic reflectionless wave guide modes are analogous to those found in photonic crystals [139] and can provide intriguing spintronics applications. Magnonic edge states have recently been proposed to exist in YIG without any equilibrium spin texture but with an array with an array of Fe-filled pillars, in which ellipticity of magnons due to dipolar interactions can give rise to magnonic bands with a nonzero TKNN invariant. [140]

5.5 Conclusions

We have studied how fictitious magnetic fields, which are caused by a textured equilibrium magnetization, lead to thermal Hall effects in two-dimensional insulating magnets in which the nontrivial equilibrium magnetization is caused by spin-orbit interaction. We have given a general expression for the fictitious magnetic vector potential, and found that it consists of two contributions: a geometric texture contribution and a contribution due to the original spin-orbit term in the free energy. We have shown that both contributions are generally of the same order of magnitude.

We have derived the relevant properties of the two ground states of interest to us (the spiral state and the skyrmion lattice state) in the phase diagram of a two-dimensional non-itinerant ferromagnet with nonzero Dzyaloshinskii-Moriya interaction. We have found that a system which has the spiral state as magnetic ground state does not have a finite thermal Hall conductivity. However, we predicted that certain domain wall structures do display thermal Hall effects.

We have numerically diagonalized the Hamiltonian describing the triangular skyrmion lattice. We found that due to the spatially varying fictitious magnetic vector potential, the excitation spectrum consists of broadened magnetic subbands. We have calculated the Berry curvature of the magnetic subbands, and showed that the Berry curvature in com-

bination with the excitation spectrum completely determines the thermal Hall conductivity of the skyrmion lattice. At present, we are only able to capture the contribution to the thermal Hall conductivity from higher magnetic subbands, as well as thermal- or microwave transport through the associated edge states. In order to properly describe the lowest subbands, our model has to be amended to capture non-adiabatic magnon-transport effects, in the way described at the end of Sec. 5.2.

Appendix

Determining Luttinger Liquid parameters from the non-linear sigma model.

In this section we calculate the magnetic susceptibility of a 3D antiferromagnet, denoted by $\chi_{\alpha\beta}^{3D}(q)$. In the continuum limit, the magnetic susceptibility is defined as

$$\chi_{\alpha\beta}^{3D}(q) = \left(\frac{g\mu_B}{a^3}\right)^2 \frac{1}{\hbar} \int d^4s e^{iq \cdot s} \langle T_\tau S_\alpha(s) S_\beta(0) \rangle, \quad (\text{A.1})$$

where $s = (\tau, \mathbf{r})^T$, $q = (\omega_n, \mathbf{k})^T$, and $q \cdot s = \omega_n \tau - \mathbf{k} \cdot \mathbf{r}$.

We start from the isotropic Heisenberg model in three dimensions, described by Eq. (2.1) with $\Delta_{ij} = 1$ and $B_i = 0$. We introduce the unit vector field $\mathbf{n}_i^s = \mathbf{S}_i/S$. This vector field can be written as a staggered Néel vector part \mathbf{n}_i plus a fluctuating part \mathbf{l}_i , both of which are slowly varying on the scale a

$$\mathbf{n}_i^s = (-1)^i \mathbf{n}_i \sqrt{1 - a^2 \mathbf{l}_i^2} + a \mathbf{l}_i \approx (-1)^i \mathbf{n}_i + a \mathbf{l}_i. \quad (\text{A.2})$$

In the continuum limit it can be shown [141] that the imaginary time action describing this system can be approximated as $S[\mathbf{n}, \mathbf{l}] = S_0[\mathbf{n}, \mathbf{l}] + S_l[\mathbf{n}, \mathbf{l}]$, where

$$S_0[\mathbf{n}, \mathbf{l}] = \frac{\hbar}{2\gamma} \int d^4s \left[\frac{1}{c} (\partial_\tau \mathbf{n})^2 + \sum_{i=1}^3 c (\partial_{r_i} \mathbf{n})^2 \right], \quad (\text{A.3})$$

$$S_l[\mathbf{n}, \mathbf{l}] = 12\hbar\alpha \int d^4s \left[\mathbf{1} + i \frac{1}{48a^2\alpha} (\mathbf{n} \times \partial_\tau \mathbf{n}) \right]^2. \quad (\text{A.4})$$

APPENDIX A. DETERMINING LUTTINGER LIQUID PARAMETERS
92 FROM THE NON-LINEAR SIGMA MODEL.

Here, $\alpha = J/(8a\hbar)$, $c = \sqrt{3}Ja/\hbar$, and $\gamma = 4\sqrt{3}a^2$. From a substitution of Eq. (A.2) in Eq. (A.1) it is clear that we can write

$$\chi_{\alpha\beta}^{3D}(q) = \left(\frac{g\mu_B}{2a^2}\right)^2 \frac{1}{\hbar} \int d^4s e^{iq \cdot s} \langle T_\tau l_\alpha(s) l_\beta(0) \rangle_S, \quad (\text{A.5})$$

where the Green's function is calculated with respect to the action $S[\mathbf{n}, \mathbf{l}]$. The Green's function can then be determined from the partition function $Z = \int D\mathbf{n} D\mathbf{l} \delta(\mathbf{n}^2 - 1) \exp(-\hbar^{-1}S[\mathbf{n}, \mathbf{l}])$. We can perform the functional integration over \mathbf{l} in Eq. (A.5) to arrive at

$$\chi_{\alpha\beta}^{3D}(q) = \left(\frac{g\mu_B}{\gamma}\right)^2 \frac{1}{\hbar c} \left[\gamma \delta_{\alpha\beta} - \int d^4s e^{-q \cdot s} \times \left\langle (\mathbf{n} \times \partial_\tau \mathbf{n})_\alpha(s) (\mathbf{n} \times \partial_\tau \mathbf{n})_\beta(0) \right\rangle_{S_0} \right], \quad (\text{A.6})$$

where we replaced $\tau \rightarrow c\tau$. Here, the average is with respect to $S_0[\mathbf{n}, \mathbf{l}]$. Assuming the magnetization is ordered along the z axis, we write $\mathbf{n} = (\sigma_1, \sigma_2, \Pi)^T$. The σ_i 's describe thermal fluctuations perpendicular to the direction of order, [142] and $\Pi = \sqrt{1 - \sigma^2}$. Also, $\sigma = (\sigma_1, \sigma_2)^T$. For low temperatures, we can then rewrite the action of Eq. (A.3) as

$$S_0[\sigma] = -\frac{\hbar}{2\gamma} \int d^4s \sigma \cdot \left[\partial_\tau^2 + \sum_{i=1}^3 \partial_{x_i}^2 \right] \sigma. \quad (\text{A.7})$$

From this and Eq. (A.6) it then follows that the magnetic susceptibility in the gapless direction is given by

$$\chi^{3D}(q) = \frac{(g\mu_B)^2 c}{\hbar} \frac{\mathbf{q}^2}{\gamma \omega_n^2 + (c\mathbf{q})^2}. \quad (\text{A.8})$$

To compare this relation to the magnetic susceptibility in one dimension, we use $\chi^{1D}(q) = a^2 \chi^{3D}(q)$. Since we know [48] that in the Luttinger Liquid model

$$\chi_{zz}^{\text{LL}}(q) = \frac{(g\mu_B)^2 uK}{\hbar} \frac{\mathbf{q}^2}{\pi (u\mathbf{q})^2 + \omega_n^2}, \quad (\text{A.9})$$

we have

$$u_r = \sqrt{3}Ja/\hbar \quad K_r = \pi/(4\sqrt{3}) \quad (\text{A.10})$$

as effective Luttinger Liquid parameters of the 3D reservoirs.

Calculation of the magnetization current in the Keldysh formalism

In this appendix we will show how to calculate the magnetization current $I_m(\Delta B)$ in a system described by the action $S[\phi] = S_0[\phi] + S_I[\phi] + S_B[\phi]$. According to Eq. (2.35), the magnetization current is given by

$$I_m = -\frac{g\mu_B}{\pi} \partial_t \frac{1}{2} \sum_{\eta=\pm} \langle \phi^\eta(\mathbf{r}) \rangle_S = \frac{g\mu_B i}{\pi} \partial_t \left(\frac{\delta Z[J(\mathbf{r})]}{\delta J(\mathbf{r})} \right). \quad (\text{B.1})$$

The partition function can be written in vectorized form as

$$\begin{aligned} Z[J(\mathbf{r})] = & \int D\phi \exp \left[-\frac{1}{2} \int d^2r d^2r' \times \right. \\ & \left. [\phi(\mathbf{r}) \cdot G_0(\mathbf{r}, \mathbf{r}') \phi(\mathbf{r}') - 2i\delta(\mathbf{r} - \mathbf{r}') \phi(\mathbf{r}) \cdot Q\mathbf{J}(\mathbf{r}')] \right] \times \\ & \exp \left[-\frac{i\sigma\lambda_3^a}{\pi^2\hbar} \int_{-\infty}^{\infty} dt \sum_{\eta=\pm} \eta \cos [2\phi^\eta(0, t)] \right], \end{aligned} \quad (\text{B.2})$$

where we have defined

$$\begin{aligned}
 \phi(\mathbf{r}) &= \begin{pmatrix} \phi^+(\mathbf{r}) \\ \phi^-(\mathbf{r}) \end{pmatrix}, \\
 \mathbf{J}(\mathbf{r}) &= \sqrt{2} \begin{pmatrix} -\frac{g\mu_B}{\pi\hbar} \partial_x B(\mathbf{r}) \\ J(\mathbf{r})/2 \end{pmatrix}, \\
 Q &= \frac{1}{\sqrt{2}} \begin{pmatrix} 1 & -1 \\ 1 & 1 \end{pmatrix}, \\
 G_0(\mathbf{r}, \mathbf{r}') &= \begin{pmatrix} G_0^{++}(\mathbf{r}, \mathbf{r}') & G_0^{+-}(\mathbf{r}, \mathbf{r}') \\ G_0^{-+}(\mathbf{r}, \mathbf{r}') & G_0^{--}(\mathbf{r}, \mathbf{r}') \end{pmatrix}.
 \end{aligned} \tag{B.3}$$

Here $G_0^{\eta,\eta'}(\mathbf{r}, \mathbf{r}')$ is the contour-ordered Green's function

$$G_0^{\eta,\eta'}(\mathbf{r}, \mathbf{r}') = \left\langle T_c \phi^\eta(\mathbf{r}) \phi^{\eta'}(\mathbf{r}') \right\rangle_{S_0}. \tag{B.4}$$

We will also need the retarded, advanced, and Keldysh Green's functions $G_0^{R/A/K}(\mathbf{r}, \mathbf{r}')$, which are related to the contour-ordered Green's functions in the usual way. Performing the linear transformation $\phi'(\mathbf{r}) = \phi(\mathbf{r}) - i \int d\mathbf{r}' G_0(\mathbf{r}, \mathbf{r}') Q^T \mathbf{J}(\mathbf{r}')$ shows that the partition function can be factorized into two parts, the first one containing the quadratic part of the action, the second containing the backscattering term. The magnetization current is therefore made up of two contributions. The first, I_0 , comes from the quadratic action, and describes the magnetization current in the absence of any backscattering. The second, I_{3a} , originates from the backscattering term. Using the explicit form for the magnetic field Eq. (2.12) it turns out that the expression for the unperturbed magnetization current is given by

$$I_0 = i \frac{(g\mu_B)^2}{\pi^2 \hbar} \Delta B \partial_t \int_{-\infty}^{\infty} dt' G_0^R(\mathbf{r}; -L/2, t'). \tag{B.5}$$

Since this is exactly the expression for the magnetization current in the linear response regime, [30] which yields $I_0 = K_r \frac{(g\mu_B)^2}{h} \Delta B$, we can infer that

$$\int_{-\infty}^{\infty} dt' i G_0^R(\mathbf{r}; -L/2, t') = \frac{\pi K_r t}{2}. \tag{B.6}$$

To calculate the contribution from the backscattering term we perform the functional derivative of the partition function with respect to $J(\mathbf{r})$. The resulting expression is

$$\begin{aligned}
 I_{3a} &= -\frac{2g\mu_B \sigma \lambda_3^a}{\pi^3 \hbar} \partial_t \int_{-\infty}^{\infty} dt' i G_0^R(\mathbf{r}; 0, t') \times \\
 &\quad \left\langle \sin [2\phi^+(0, t') - 2\gamma t'] \right\rangle_S,
 \end{aligned} \tag{B.7}$$

where $\gamma = K_r \frac{g\mu_B \Delta B}{\hbar}$. Expanding this term in λ_3^a gives

$$I_{3a} = i \frac{2g\mu_B \sigma^2 (\lambda_3^a)^2}{\pi^5 \hbar^2} \partial_t \int_{-\infty}^{\infty} dt' i G_0^R(\mathbf{r}; 0, t') dt'' \times \sum_{\eta=\pm} \eta \langle \sin [2\phi'^+(0, t') - 2\gamma t'] \cos [2\phi'^\eta(0, t'') - 2\gamma t''] \rangle_{S_0}.$$

Since contour-ordering reduces to time-ordering for two fields on the same branch of the Keldysh contour, and because the system in equilibrium is time-reversal invariant, the term with the fields at times t' and t'' on the same branch averages to zero. Switching the variable of integration to $\tau = t' - t''$ and using Eq. (B.6) it is seen that the contribution from the backscattering term is given by

$$I_{3a} = \frac{g\mu_B \sigma^2 (\lambda_{3,R}^a)^2}{\pi^4} \frac{1}{a_s} K_r A_0(\Delta B). \quad (\text{B.8})$$

Here $a_s = a/u$ can be interpreted as the cutoff in the time domain. As before, we identify the cutoff in time with the cutoff in frequency: $a_s = \omega_c^{-1}$, so that we can write the expression for the backscattering current in terms of the dimensionless parameters $\lambda_{3,R}^a = \lambda_3^a / (\hbar\omega_c)$, $\gamma_R = K_r g\mu_B \Delta B / (\hbar\omega_c)$ and $\bar{\tau} = \tau/a_s$. Here

$$A_0(\Delta B) = \frac{i}{2} \int_{-\infty}^{\infty} d\bar{\tau} \sin [2\gamma_R \bar{\tau}] e^{-2\langle T_c [\phi^+(0, \tau) - \phi^-(0, 0)]^2 \rangle_{S_0}}. \quad (\text{B.9})$$

The contour-ordered correlation function can be determined from the inhomogeneous Luttinger Liquid model [57] and the fluctuation-dissipation theorem, and can be written in terms of $\bar{\tau}$ as

$$\langle T_c [\phi^+(0, \tau) - \phi^-(0, 0)]^2 \rangle_{S_0} = K \log [-i\bar{\tau} + 1]. \quad (\text{B.10})$$

With this expression we can rewrite Eq. (B.9) as a function of γ_R and K only

$$A_0(\Delta B) = -\frac{K 4^K \pi}{\Gamma(1 + 2K)} \gamma_R |\gamma_R|^{-2+2K} e^{-2|\gamma_R|}. \quad (\text{B.11})$$

Next we discuss the contribution of the $\frac{a\lambda_4^a}{\pi^2} \partial_x \phi(0, t) \cos 2\phi(0, t)$ term from Eq. (3.8). We again perform the linear transformation $\phi(\mathbf{r}) \rightarrow \phi'(\mathbf{r})$, which yields

$$I_{4a} = -\frac{2g\mu_B \lambda_4^a a}{\pi^3 \hbar} \partial_t \int_{-\infty}^{\infty} dt' i G_0^R(\mathbf{r}; 0, t') \times \langle \partial_{x'} \phi'^+(0, t') \sin [2\phi'^+(0, t') - 2\gamma t'] \rangle_S. \quad (\text{B.12})$$

There is also an additional term in the expression for the magnetization current introduced by the linear transformation, which is proportional to the expression $\partial_x \int dt G_0^R(0, t; \mathbf{r}'')$. Eq. (B.6) however shows that this term is zero. We can expand Eq. (B.12) in λ_4^a

$$I_{4a} = i \frac{2g\mu_B (\lambda_4^a)^2 a^2}{\pi^5 \hbar^2} \partial_t \int_{-\infty}^{\infty} dt' i G_0^R(\mathbf{r}; 0, t') dt'' \times \sum_{\eta=\pm} \eta \langle \partial_{x'} \phi'^{\eta}(0, t') \sin [2\phi'^{\eta}(0, t') - 2\gamma t'] \times \partial_{x''} \phi''^{\eta}(0, t'') \cos [2\phi''^{\eta}(0, t'') - 2\gamma t''] \rangle_{S_0}. \quad (\text{B.13})$$

We now use the results from Appendix C to evaluate the correlation function

$$\partial_x \partial_{x'} \langle T_c \phi^+(0, t) \phi^-(0, t') \rangle_{S_0} = \frac{2}{(ua_s)^2} \left(\frac{1 + i\bar{\tau}}{1 + \bar{\tau}^2} \right)^2. \quad (\text{B.14})$$

We also use that $\partial_x \langle T_c \phi^+(0, t) \phi^-(0, t') \rangle_{S_0} = 0$, so that the magnetization current is given by

$$I_{BS} = \frac{g\mu_B (\lambda_{4,R}^a)^2}{\pi^4} \frac{1}{a_s} K_r A_1(\Delta B). \quad (\text{B.15})$$

Where the dependence on the parameters of the spin chain and the applied magnetic field difference is contained in the function $A_1(\Delta B)$

$$A_1(\Delta B) = i \frac{(ua_s)^2}{2} \int_{-\infty}^{\infty} d\bar{\tau} e^{-2\langle T_c [\phi^+(0, \tau) - \phi^-(0, 0)]^2 \rangle_{S_0}} \times \langle \partial_x \phi'(0, \tau) \partial_x \phi'(0, 0) \rangle_{S_0} \sin [2\gamma_R \bar{\tau}], \quad (\text{B.16})$$

where we again used that terms containing correlators with both fields on the same branch of the contour vanish. Straightforward manipulations show that $A_1(\Delta B)$ is given by

$$A_1(\Delta B) = -\frac{4^K \pi}{\Gamma(2 + 2K)} \gamma_R |\gamma_R|^{2K} e^{-2|\gamma_R|}. \quad (\text{B.17})$$

Correlators

In this appendix we show how to calculate a correlation function of the form

$$\langle T_c \Pi_i \partial_{x_i} \phi(x_i, t_i) e^{i \sum_j A_j \phi(x_j, t_j)} \rangle_{S_0}. \quad (\text{C.1})$$

First of all, we can pull the derivatives outside of the expectation value. therefore, we can calculate $\langle T_c \Pi_i \phi(x_i, t_i) e^{i \sum_j A_j \phi(x_j, t_j)} \rangle_{S_0}$ instead and take the derivatives afterwards. For a lighter notation we prove the required results in discrete space, making the connection: $\phi_i = \phi(\mathbf{r}_i)$. We use the main result of Gaussian integration [143]

$$\int d\phi e^{-\frac{1}{2} \phi^T \cdot \bar{G} \phi + \mathbf{j}^T \cdot \phi} \propto e^{\mathbf{j}^T \cdot \bar{G}^{-1} \mathbf{j}}. \quad (\text{C.2})$$

Given the partition function

$$Z = \int d\phi e^{-\frac{1}{2} \phi^T \cdot \bar{G} \phi}, \quad (\text{C.3})$$

we can then calculate for instance $\langle \phi_i \phi_j \rangle_{S_0}$ by letting $\partial_{j_n j_m}^2 \big|_{j=0}$ work on both sides of Eq. (C.2). To calculate the required correlator, Eq. (C.1), we replace $\mathbf{j} \rightarrow \mathbf{j} + \mathbf{b}$ in Eq. (C.2), where \mathbf{b} consists of the components: $b_i = \sum_j A_j \delta_{ij}$. By letting $\partial_{j_n} \big|_{j=0}$ work on both sides of this equation we arrive at

$$\langle \phi_n e^{\mathbf{b}^T \cdot \phi} \rangle = \bar{G}_{nl} b_l e^{\frac{1}{2} \mathbf{b}^T \cdot \bar{G}^{-1} \mathbf{b}}. \quad (\text{C.4})$$

Here we sum over double indices. We also used the fact that \bar{G}^{-1} is a symmetric matrix, e.g. $G_{nm}^{-1} = G_{mn}^{-1}$, which is true since it contains contour ordered correlation functions. By letting $\partial_{j_n j_m}^2 \big|_{j=0}$ work on Eq. (C.2)

we get

$$\langle \phi_n \phi_m e^{\mathbf{b}^T \cdot \phi} \rangle = [\bar{G}_{mn}^{-1} + \bar{G}_{ml}^{-1} b_l \bar{G}_{nl}^{-1} b_l] e^{\frac{1}{2} \mathbf{b}^T \cdot \bar{G}^{-1} \mathbf{b}}. \quad (\text{C.5})$$

Both two equations above are valid when $\sum_j A_j = 0$, otherwise the correlators vanish.

Bibliography

- [1] 'Electromagnetism', Encyclopaedia Britannica Online Academic Edition, Encyclopaedia Britannica Inc., retrieved 17 Aug. 2012.
- [2] D.C. Mattis, *The Theory of Magnetism I* (Springer-Verlag, Berlin, 1981).
- [3] W. Gilbert (translated by P. Fleury Mottelay), *De Magnete* (Dover Publications, New York, 1991).
- [4] J. D. Jackson, *Classical Electrodynamics* (John Wiley & Sons, 1999)
- [5] I. Žutić, J. Fabian, and S. Das Sarma, *Rev. Mod. Phys.* **76**, 323 (2004).
- [6] M.N. Baibich, J.M. Broto, A. Fert, F. Nguyen van Dau, F. Petroff, P. Eitenne, G. Creuzet, A. Friederich, and J. Chazelas, *Phys. Rev. Lett.* **61**, 2472 (1988).
- [7] G. Binasch, P. Grünberg, F. Saurenbach, and W. Zinn, *Phys. Rev.* **39**, 4828 (1989).
- [8] S. Datta and B. Das, *Appl. Phys. Lett.* **56**, 665 (1990).
- [9] *Semiconductor Spintronics and Quantum Computation*, edited by D.D. Awschalom, D. Loss, and N. Samarth (Springer-Verlag, Berlin, 2002).
- [10] D.D. Awschalom and M.E. Flatté, *Nature Phys.* **3**, 153 (2007).
- [11] J.-M. Tang, J. Levy, and M. E. Flatté, *Phys. Rev. Lett.* **97**, 106803 (2006).

- [12] H. Ohno, D. Chiba, F. Matsukura, T. Omiya, E. Abe, T. Dietl, Y. Ohno, and K. Ohtani, *Nature* **408**, 944 (2000).
- [13] D. Chiba, M. Yamanouchi, F. Matsukura, and H. Ohno, *Science* **301**, 943945 (2003).
- [14] B. Trauzettel, P. Simon, and D. Loss, *Phys. Rev. Lett.* **101**, 017202 (2008).
- [15] K.C. Hall and M.E. Flatté, *Appl. Phys. Lett.* **88**, 162503 (2006).
- [16] I.V. Ovchinnikov and K.L. Wang, *Appl. Phys. Lett.* **92**, 093503 (2008).
- [17] A. Chen, A.P. Jacob, C.Y. Sung, K.L. Wang, A. Khitun, W. Porod, 2009 Symposium on VLSI Technology, pp.132-133, 16-18 June 2009.
- [18] M.Z. Hasan and C.L. Kane, *Rev. Mod. Phys.* **82**, 3045-3067 (2010).
- [19] S. Murakami, N. Nagaosa, and S.-C. Zhang, *Phys. Rev. Lett.* **93**, 156804 (2004).
- [20] E.B. Sonin, *Adv. in Phys.* **59**, 181 (2010).
- [21] A. Brataas, Y. Tserkovnyak, G.E.W. Bauer, and B.I. Halperin, *Phys. Rev. B* **66**, 060404(R) (2002) have proposed this mechanism to generate of a spin current in the absence of a net charge current, K. Nakata and G. Tatara, arXiv:1101.2137v1 [cond-mat.mes-hall] have proposed spin pumping as a mechanism to generate a pure spin current.
- [22] K. Uchida, J. Xiao, H. Adachi, J. Ohe, S. Takahashi, J. Ieda, T. Ota, Y. Kajiwara, H. Umezawa, H. Kawai, G. E.W. Bauer, S. Maekawa, and E. Saitoh, *Nature Materials* **9**, 894 (2010).
- [23] M. Weiler, M. Althammer, F. D. Czeschka, H. Huebl, M. S. Wagner, M. Opel, I.-M. Imort, G. Reiss, A. Thomas, R. Gross, and S. T. B. Goennenwein, *Phys. Rev. Lett.* **108**, 106602 (2012).
- [24] Y. Kajiwara, K. Harii, S. Takahashi, J. Ohe, K. Uchida, M. Mizuguchi, H. Umezawa, H. Kawai, K. Ando, K. Takanashi, S. Maekawa, and E. Saitoh, *Nature* **464**, 262 (2010).

- [25] C. W. Sandweg, Y. Kajiwara, A. V. Chumak, A. A. Serga, V. I. Vasyuchka, M. B. Jungfleisch, E. Saitoh, and B. Hillebrands, *Phys. Rev. Lett.* **106**, 216601 (2011).
- [26] M. P. Kostylev, A. A. Serga, T. Schneider, B. Leven, and B. Hillebrands, *Appl. Phys. Lett.* **87**, 153501 (2005).
- [27] T. Schneider, A. A. Serga, B. Leven, B. Hillebrands, R. L. Stamps, and M. P. Kostylev, *Appl. Phys. Lett.* **92**, 022505 (2008).
- [28] D. D. Sheka, I. A. Yastremsky, B. A. Ivanov, G. M. Wysin, and F. G. Mertens, *Phys. Rev. B* **69**, 054429 (2004).
- [29] V. K. Dugaev, P. Bruno, B. Canals, and C. Lacroix, *Phys. Rev. B* **72**, 024456 (2005).
- [30] F. Meier and D. Loss, *Phys. Rev. Lett.* **90**, 167204 (2003).
- [31] D. L. Mills and I. E. Dzyaloshinskii, *Phys. Rev. B* **78**, 184422 (2008).
- [32] P. Rovillain, R. de Sousa, Y. Gallais, A. Sacuto, M. A. Masson, D. Colson, A. Forget, M. Bibes, A. Barthélémy, and M. Cazayous, *Nature Materials* **9**, 975979 (2010).
- [33] T. Liu and G. Vignale, *Phys. Rev. Lett.* **106**, 247203 (2011).
- [34] P. W. Anderson, *Phys. Rev.* **115**, 2 (1959).
- [35] W. Nolting and A. Ramakanth, *Quantum Theory of Magnetism*, (Springer-Verlag, Berlin Heidelberg, Germany, 2009).
- [36] I. Dzyaloshinskii, *J. Phys. Chem. Solids* **4**, 241 (1958).
- [37] T. Moriya, *Phys. Rev.* **120**, 91 (1960).
- [38] E. M. Lifshitz and L. P. Pitaevskii, *Statistical Physics, Part 2*, Vol. 9 of *Course on Theoretical Physics* (Butterworth-Heinenann Ltd., Oxford, 1995).
- [39] T. Christen and M. Büttiker, *Europhys. Lett.* **35**, 523 (1996).
- [40] D.E. Feldman, S. Scheidl, and V.M. Vinokur, *Phys. Rev. Lett.* **94**, 186809 (2005).

- [41] A. De Martino, R. Egger, and A.M. Tsvelik, Phys. Rev. Lett. **97**, 076402 (2006).
- [42] B. Braunecker, D.E. Feldman, and F. Li, Phys. Rev. B **76**, 085119 (2007).
- [43] D. Sánchez and M. Büttiker, Phys. Rev. Lett. **93**, 106802 (2004).
- [44] B. Spivak and A. Zyuzin, Phys. Rev. Lett. **93**, 226801 (2004).
- [45] A.V. Andreev and L.I. Glazman, Phys. Rev. Lett. **97**, 266806 (2006).
- [46] H. Bethe, Z. Physik **71**, 205 (1931).
- [47] S. Datta, *Electronic Transport in Mesoscopic Systems* (Cambridge University Press, Cambridge, England, 1995).
- [48] T. Giamarchi, *Quantum Physics in One Dimension* (Clarendon Press, Oxford, 2003).
- [49] J. von Delft and H. Schoeller, Ann. Phys. (Leipzig) **7**, 225 (1998).
- [50] D. Sénéchal, arXiv:cond-mat/9908262v1.
- [51] S. Eggert and I. Affleck, Phys. Rev. B **46**, 10866 (1992).
- [52] E. Orignac and T. Giamarchi, Phys. Rev. B **57**, 5812 (1998).
- [53] F.D.M. Haldane, Phys. Rev. Lett. **45**, 1358 (1980).
- [54] J. Des Cloizeaux and M. Gaudin, J. Math. Phys. **7**, 1384 (1966).
- [55] A. Luther and V. J. Emery, Phys. Rev. Lett. **33**, 589 (1974).
- [56] H.J. Schulz, Phys. Rev. B **22**, 5274 (1980).
- [57] D. L. Maslov and M. Stone, Phys. Rev. B **52**, R5539 (1995).
- [58] O.A. Starykh and D.L. Maslov, Phys. Rev. Lett. **80**, 1694 (1998).
- [59] V.V. Ponomarenko and N. Nagaosa, Phys. Rev. Lett. **81**, 2304 (1998).

- [60] M. Garst, D.S. Novikov, A. Stern, and L.I. Glazman, *Phys. Rev. B* **77**, 035128 (2008).
- [61] L. V. Keldysh, *Sov. Phys. JETP* **20**, 1018 (1965); J. Rammer and H. Smith, *Rev. Mod. Phys.* **58**, 323 (1986).
- [62] F. Dolcini, B. Trauzettel, I. Safi, and H. Grabert, *Phys. Rev. B* **71**, 165309 (2005).
- [63] E.g. in KCuF_3 , see Ref. [67]. For different materials the exchange interaction can be significantly different, see e.g. Ref. [69], which reports that $J \approx 2 \cdot 10^3$ K for Sr_2CuO_3 and SrCuO_2 .
- [64] Z. Zhang, P. C. Hammel, M. Midzor, M. L. Roukes, and J. R. Childress, *Appl. Phys. Lett.* **73**, 2036 (1998).
- [65] L. Teske and H. Mller-Buschbaum, *Z. Anorg. Allg. Chem.* **379**, 234 (1971).
- [66] T. Ami, M. K. Crawford, R. L. Harlow, Z. R. Wang, D. C. Johnston, Q. Huang, R. W. Erwin, *Phys. Rev. B* **51**, 5994 (1995).
- [67] D.A. Tennant, R.A. Cowley, S.E. Nagler, and A.M. Tsvelik, *Phys. Rev. B* **52**, 13368 (1995).
- [68] M. Kenzelmann, R. Coldea, D. A. Tennant, D. Visser, M. Hofmann, P. Smeibidl, and Z. Tylczynski, *Phys. Rev. B* **65**, 144432 (2002).
- [69] N. Motoyama, H. Eisaki, and S. Uchida, *Phys. Rev. Lett.* **76**, 3212 (1996).
- [70] A.V. Sologubenko, K. Giannò, H.R. Ott, A. Vietkine, and A. Revcolevschi, *Phys. Rev. B* **64**, 054412 (2001).
- [71] T. Oguchi, *Phys. Rev.* **133**, A1098 (1964).
- [72] A. Keren, L. P. Le, G. M. Luke, B. J. Sternlieb, W. D. Wu, Y. J. Uemura, S. Tajima, and S. Uchida, *Phys. Rev. B* **48**, 12926 (1993).
- [73] B. J. Kim, H. Koh, E. Rotenberg, S.-J. Oh, H. Eisaki, N. Motoyama, S. Uchida, T. Tohyama, S. Maekawa, Z.-X. Shen, and C. Kim, *Nat. Physics* **2**, 397 (2006).

- [74] N. Hlubek, P. Ribeiro, R. Saint-Martin, A. Revcolevschi, G. Roth, G. Behr, B. Büchner, and C. Hess, *Phys. Rev. B* **81**, 020405(R) (2010).
- [75] T. M. Rice, S. Gopalan, and M. Sigrist, *Europhys. Lett.* **23**, 445 (1993).
- [76] M. Matsuda, K. Katsumata, T. Osafune, N. Motoyama, H. Eisaki, S. Uchida, T. Yokoo, S. M. Shapiro, G. Shirane, and J. L. Zarestky, *Phys. Rev. B* **56**, 14499 (1997).
- [77] I. A. Zaliznyak, C. Broholm, M. Kibune, M. Nohara, and H. Takagi, *Phys. Rev. Lett.* **83**, 5370 (1999).
- [78] H. A. Algra, L. J. de Jongh, H. W. J. Blote, W. J. Huiskamp, and R. L. Carlin, *Physica B & C* **82B**, 239 (1976).
- [79] S. Katsura, *Phys. Rev.* **127**, 1508 (1962).
- [80] J. N. McElearney, S. Merchant, G. E. Shankle, and R. L. Carlin, *J. Chem. Phys.* **66**, 450 (1977).
- [81] P. M. Duxbury, J. Oitmaa, M. N. Barber, A. van der Bilt, K. O. Joung, and R. L. Carlin, *Phys. Rev. B* **24**, 5149 (1981).
- [82] K. A. van Hoogdalem and D. Loss, *Phys Rev. B* **84**, 024402 (2011).
- [83] A. Furusaki, and N. Nagaosa, *Phys. Rev. B* **47**, 3827 (1993).
- [84] M. Sasseti, F. Napoli, and U. Weiss, *Phys. Rev. B* **52**, 11213 (1995).
- [85] C. S. Peça, L. Balents, and K. J. Wiese, *Phys. Rev. B* **68**, 205423 (2003).
- [86] P. Recher, N. Y. Kim, and Y. Yamamoto, *Phys. Rev. B* **74**, 235438 (2006).
- [87] S. Wang, L. Zhou and Z. Y. Zeng, *Phys. Rev. B* **81**, 155438 (2010).
- [88] I. Safi, C. Bena, and A. Crépieux, *Phys. Rev. B* **78**, 205422 (2008).

- [89] S. A. Wolf, D. D. Awschalom, R. A. Buhrman, J. M. Daughton, S. von Molnár, M. L. Roukes, A. Y. Chtchelkanova, D. M. Treger, *Science* **294**, 1488-1495 (2001).
- [90] A. J. Heinrich, J. A. Gupta, C. P. Lutz, and D. M. Eigler, *Science* **306**, 466 (2004).
- [91] A. Imre, G. Csaba, L. Ji, A. Orlov, G. H. Bernstein, and W. Porod, *Science* **311**, 205-208 (2006).
- [92] A. A. Khajetoorians, J. Wiebe, B. Chilian, and R. Wiesendanger, *Science* **27**, 1062-1064 (2011).
- [93] S. Gatteschi, R. Sessoli, and J. Villain, *Molecular Nanomagnets*, (Oxford University Press, New York, 2007).
- [94] R. Sessoli, D. Gatteschi, A. Caneschi, and M. A. Novak, *Nature* **365**, 141-143 (1993).
- [95] L. Thomas, F. Lioni, R. Ballou, D. Gatteschi, R. Sessoli, and B. Barbara, *Nature* **383**, 145-147 (1996).
- [96] J. R. Friedman, M. P. Sarachik, J. Tejada, R. Ziolo, *Phys. Rev. Lett.* **76**, 3830 (1996).
- [97] A. Ardavan, O. Rival, J. J. L. Morton, S. J. Blundell, A. M. Tyryshkin, G. A. Timco, and R. E. P. Winpenny, *Phys. Rev. Lett.* **98**, 057201 (2007).
- [98] H. C. Koo, J. H. Kwon, J. Eom, J. Chang, S. H. Han, and M. Johnson, *Science* **325**, 1515 (2009).
- [99] J. Schliemann, J. C. Egues, and D. Loss, *Phys. Rev. Lett.* **90**, 146801 (2003).
- [100] A. Aharony, Y. Tokura, G. Z. Cohen, O. Entin-Wohlman and S. Katsumoto, *Phys. Rev. B* **84**, 035323 (2011).
- [101] J. Wunderlich, B.-G. Park, A. C. Irvine, L. P. Zârbo, E. Rozkottová, P. Nemeč, V. Novák, J. Sinova, and T. Jungwirth, *Science* **330**, 1801 (2010).
- [102] C. Betthausen, T. Dollinger, H. Saarikoski, V. Kolkovsky, G. Karczewski, T. Wojtowicz, K. Richter, and D. Weiss, *Science* **337**, 324 (2012).

- [103] J. Fabian, I. Žutić, and S. Das Sarma, *Appl. Phys. Lett.* **84**, 85 (2003).
- [104] J. Fabian and I. Žutić, *Phys. Rev. B* **69**, 115314 (2004).
- [105] N. Rangaraju, J. A. Peters, and B. W. Wessels, *Phys. Rev. Lett.* **105**, 117202 (2010).
- [106] L. Bogani and W. Wernsdorfer, *Nat. Materials* **7**, 179-186 (2008).
- [107] M. N. Leuenberger and D. Loss, *Nature* **410**, 789-793 (2001).
- [108] J. Lehmann, A. Gaita-Ariño, E. Coronado, and D. Loss, *Nat. Nanotechnology* **2**, 312-317 (2007).
- [109] F. Troiani, A. Ghirri, M. Affronte, S. Carretta, P. Santini, G. Amoretti, S. Piligkos, G. Timco, and R. E. P. Winpenny, *Phys. Rev. Lett.* **94**, 207208 (2005).
- [110] K.-Y. Choi, Y. H. Matsuda, H. Nojiri, U. Kortz, F. Hussain, A. C. Stowe, C. Ramsey, and N. S. Dalal, *Phys. Rev. Lett.* **96**, 107202 (2006).
- [111] M. Trif, F. Troiani, D. Stepanenko, and D. Loss, *Phys. Rev. Lett.* **101**, 217201 (2008).
- [112] M. Trif, F. Troiani, D. Stepanenko, and D. Loss, *Phys. Rev. B* **82**, 045429 (2010).
- [113] M. F. Islam, J. F. Noss, C. M. Canali, and M. Pederson, *Phys. Rev. B* **82**, 155446 (2010).
- [114] A. H. Miklich, D. Koelle, F. Ludwig, D. T. Nemeth, E. Dantsker, J. Clarke, *Appl. Phys. Lett.* **66**, 230-232 (1995).
- [115] H. Katsura, N. Nagaosa, and P. A. Lee, *Phys. Rev. Lett.* **104**, 066403 (2010).
- [116] Y. Onose, T. Ideue, H. Katsura, Y. Shiomi, N. Nagaosa, and Y. Tokura, *Science* **329**, 297 (2010).
- [117] Y.-Q. Li, Y.-H. Liu, and Y. Zhou, *Phys. Rev. B* **84**, 205123 (2011).

- [118] J. H. Han, J. Zang, Z. Yang, J.-H. Park, and N. Nagaosa, *Phys. Rev. B* **82**, 094429 (2010).
- [119] A. A. Kovalev and Y. Tserkovnyak, *Phys. Rev. B* **80**, 100408(R) (2009).
- [120] M. Hatami, G. E. W. Bauer, Q. Zhang, and P. J. Kelly, *Phys. Rev. Lett.* **99** 066603 (2007) and *ibid.*, *Phys. Rev. B* **79**, 174426 (2009).
- [121] L. Berger, *J. Appl. Phys.* **58**, 450 (1985), S. U. Jen and L. Berger, *J. Appl. Phys.* **59**, 1278 (1986), and *ibid*, 1285 (1986).
- [122] Yu. A. Bychkov and E. I. Rashba, *J. Phys. C: Solid State Phys.* **17**, 6039 (1984).
- [123] Y. Tserkovnyak and D. Loss, *Phys. Rev. Lett.* **108**, 187201 (2012).
- [124] A. A. Kovalev and Y. Tserkovnyak, *Europhys. Lett.* **97**, 67002 (2012).
- [125] A. Bogdanov and A. Hubert, *J. of Mag. and Mag. Mat.* **138**, 255 (1994).
- [126] X. Z. Yu, Y. Onose, N. Kanazawa, J. H. Park, J. H. Han, Y. Matsui, N. Nagaosa, and Y. Tokura, *Nature* **465**, 901 (2010).
- [127] A. Nogaret, *J. Phys.: Condens. Matter* **22**, 253201 (2010).
- [128] I. S. Ibrahim and F. M. Peeters, *Phys. Rev. B* **52**, 17321 (1995).
- [129] A. Matulis and F. M. Peeters, *Phys. Rev. B* **62**, 91 (2000).
- [130] L. Radzihovsky and T. C. Lubensky, *Phys. Rev. E* **83**, 051701 (2011).
- [131] M. C. Chang and Q. Niu, *Phys. Rev. B* **50**, 10843 (1994).
- [132] F. D. M. Haldane, *Phys. Rev. Lett.* **61**, 2015 (1988).
- [133] O. Petrova and O. Tchernyshyov, *Phys. Rev. B* **84**, 214433 (2011).
- [134] M.-C. Chang and Q. Niu, *Phys. Rev. B* **53**, 7010 (1996).

- [135] D. J. Thouless, M. Kohmoto, M. P. Nightingale, and M. den Nijs, *Phys. Rev. Lett.* **49**, 405 (1982).
- [136] R. Matsumoto and S. Murakami, *Phys. Rev. Lett.* **106**, 197202 (2011).
- [137] Y. Onose, Y. Okamura, S. Seki, S. Ishiwata, and Y. Tokura, *Phys. Rev. Lett.* **109**, 037603 (2012).
- [138] M. Mochizuki, *Phys. Rev. Lett.* **108**, 017601 (2012).
- [139] F. D. M. Haldane and S. Raghu, *Phys. Rev. Lett.* **100**, 013904 (2008).
- [140] R. Shindou, R. Matsumoto, and S. Murakami, arXiv:1204.3349v1 [cond-mat.mes-hall].
- [141] S. Allen and D. Loss, *Physica A* **239**, 47 (1997).
- [142] P.M. Chaikin and T.C. Lubensky, *Principles of Condensed Matter Physics* (Cambridge University Press, Cambridge, England, 1995).
- [143] A. Altland and B. Simons, *Condensed Matter Field Theory* (Cambridge University Press, Cambridge, England, 2006).

Curriculum Vitae

Kevin Alexander van Hoogdalem

Date of birth: 7 May 1984

Place of birth: 's-Gravenhage, the Netherlands

Education

- 2008 - 2012 *PhD in Theoretical Physics*
University of Basel, Switzerland
Advisor: Prof. Dr. Daniel Loss
Thesis: Transport phenomena in nonitinerant magnets
- 2006 - 2008 *MSc in Applied Physics*
Delft University of Technology, the Netherlands
Advisor: Prof. Dr. Miriam Blaauboer
Thesis: Quantum random walks in lateral quantum dots
- 2001 - 2006 *BSc in Applied Physics*
Delft University of Technology, the Netherlands
Advisor: Dr. Bob van Someren
Thesis: Variable mesh finite difference methods
in charged particle optics
- 1995 - 2001 *VWO (Dutch highschool diploma)*
Alfrink College, the Netherlands

List of publications

An asterisk denotes a publication covered in this thesis.

- * K. A. van Hoogdalem and D. Loss, “*Ultrafast magnon transistor at room temperature*”, Phys. Rev. B **88**, 024420 (2013).
 - * K. A. van Hoogdalem, Y. Tserkovnyak, and D. Loss, “*Magnetic texture-induced thermal Hall effects*”, Phys. Rev. B **87**, 024402 (2013).
 - * K. A. van Hoogdalem and D. Loss, “*Frequency-dependent transport through a spin chain*”, Phys. Rev. B **85**, 054413 (2012).
 - * K. A. van Hoogdalem and D. Loss, “*Rectification of spin currents in spin chains*”, Phys. Rev. B **84**, 024402 (2011).
- K.A. van Hoogdalem and M. Blaauboer, *Implementation of the quantum walk step operator in lateral quantum dots*, Phys. Rev. B **80**, 125309 (2009).

